https://doi.org/10.59761/RCR5208

Metal sulfide quantum dots for photothermal and photodynamic cancer therapy

Cui Li,[a] Le Yu,[b] Guirong Shi,[a]* Ying Zhou,[b]* Kezhen Qi[a]*

[a] *College of Pharmacy, Dali University, Dali 671000, People's Republic of China*
[b] *College of Chemical Science and Technology, Yunnan University, Kunming 650500, People's Republic of China*

Cancer remains a leading cause of global mortality, highlighting the urgent need for safe and effective therapeutic strategies. Photothermal therapy (PTT) and photodynamic therapy (PDT) have emerged as promising approaches for tumour treatment. Quantum dots (QDs), semiconductor nanocrystals with unique quantum effects, offer significant potential in these therapies. Among them, metal sulfide quantum dots (MS QDs), with particle sizes ranging from 1 to 10 nm, stand out due to their excellent fluorescence, chemical stability, photophysical properties, and biocompatibility. These attributes make MS QDs particularly suitable for combined PTT/PDT in cancer therapy. This review systematically discusses the synthesis methods of MS QDs and highlights recent advancements in their application for PTT/PDT combination therapy. Finally, we provide perspectives on the future development of MS QDs in phototherapeutic applications. The bibliography includes 275 references.

Keywords: metal sulfide quantum dots, photothermal therapy, photodynamic therapy, tumour treatment, combination therapy.

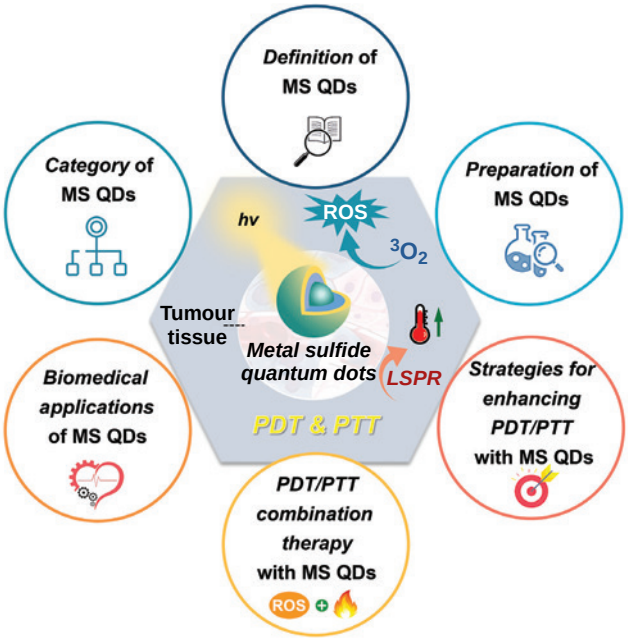

Contents

1. Introduction

Malignant tumours are a serious illness that presents a significant danger to human life and well-being. As a result, the urgent and vital issue in the field of global public health is the advancement of new technologies to improve the current clinical effectiveness of tumour therapy.[1] Traditional methods of treating tumours, such as surgery, radiation therapy (RT), and chemotherapy

Received 25 October 2025

(CHT), can cause various negative reactions like radiation-induced harm, toxic effects of CHT drugs, or multidrug resistance, significantly restricting their efficiency.[2,3] Novel techniques such as gene therapy (GT), immunotherapy, and thermotherapy offer patients more encouraging results compared to conventional tumour treatment methods.[4–6] However, extended use of these therapy options may weaken the immune system and potentially lead to reactions like organ dysfunction.[7,8] The pursuit of a tumour therapy method with minimal toxicity to healthy tissues and precise targeting to tumours is a pressing and daunting challenge. Currently, advances in diagnostic and therapeutic technologies for tumorus are rapidly expanding, with photothermal therapy (PTT) and photodynamic therapy (PDT) emerging as appealing choices within the field.[9] Compared to traditional cancer treatment methods, PTT and PDT offer unique advantages such as low toxicity, precise targeting abilities, and non-invasiveness.[10–12] PTT utilizes hyperthermia to eradicate cancer cells, while PDT relies on reactive oxygen species (ROS) to destroy tumour cells. Despite their distinct mechanisms, PTT and PDT both rely on light for activation. It is hoped that when exposed to near-infrared (NIR) laser irradiation, PTT and PDT can be used separately or in conjunction with each other. This dual approach has the potential to enhance treatment outcomes for tumours by combining the benefits of both therapies.[13,14] However, current photothermal agents (PTAs)/photosensitizers (PSs) used in these therapies face challenges such as low heat conversion rates, suboptimal tumour targeting, limited bioavailability, and inadequate tissue penetration of the light beam. To address these issues, researchers are actively exploring new PSs to improve the overall efficacy.[15–17]

In recent years, the increasing attention has focused on the research and utilization of nanomaterials, owing to the progress in nanoscience and nanotechnology. Nanomaterials may be classified according to their dimensions: zero-dimensional, one-dimensional, *e.g.*, nanorods and nanowires, two-dimensional, *e.g.*, graphene and metal chalcogenides, and three-dimensional, *e.g.*, nanoflowers and porous spheres. Quantum dots (QDs), which are semiconductor nanocrystals, are considered as the quasi-zero-dimensional nanomaterials and are renowned for their quantum size effect, surface effect, and quantum confinement effect. These unique qualities make them valuable in the fields of optics, electronics, biomedicine, and environmental conservation.[18–21] Among these, semiconductor QDs, particularly metal sulfide quantum dots (MS QDs) such as Ag_2S, CuS, and $CuInS_2$, have emerged as highly promising nanomaterials due to their size-tunable optical properties, excellent photostability, and good biocompatibility. These characteristics have enabled their widespread use in electronics, catalysis, and bioimaging, as highlighted in recent reviews focusing on specific MS QDs like $CuInS_2$ QDs[22] and ZnS QDs.[23] In particular, their potential in biomedicine has attracted growing interest, given their ability to serve not only as imaging agents but also as therapeutic platforms, especially in cancer treatment.

Building on this potential, the development of an ideal nanoplatform for PTT/PDT requires a careful balance of deep-tissue penetration, high therapeutic efficacy, and minimal toxicity. While various QDs have been explored, significant limitations persist. Conventional II-VI QDs (*e.g.*, CdSe QDs), despite their excellent optical tunability, pose considerable toxicity risks due to heavy metal ion leaching.[24] Conversely, highly biocompatible nanomaterials like silicon QDs or carbon QDs often lack the potent photothermal conversion efficiency (PCE) or robust ROS generation capacity required for effective tumour ablation.[25–27] MS QDs emerge as a superior class of materials that uniquely bridge this performance-biosafety gap. Their composition-dependent bandgap allows for strong absorption in the biologically transparent NIR-I/II windows, enabling deeper light penetration for both treatment and imaging.[28] More importantly, MS QDs such as CuS and Ag_2S exhibit exceptionally high PCE, while their semiconductor nature and the presence of catalytic metal ions (*e.g.*, Cu^+, Mo^{4+}, Mo^{6+}) facilitate multi-mechanistic ROS generation through both photocatalytic processes and Fenton-like reactions, enabling synergistic PDT/chemodynamic therapy (CDT).[29] Crucially, these high-performance features are coupled with favorable biocompatibility, as many constituent elements (Cu, Mo) are essential trace metals, and others (*e.g.*, Ag in Ag_2S) are effectively sequestered in a low-solubility sulfide matrix. This rare combination of properties positions MS QDs as a particularly promising and versatile platform for developing next-generation, image-guided combination therapies. Beyond serving as effective photothermal and photodynamic agents, MS QDs have a wide range of other applications including fluorescence imaging, biomarkers, and drug delivery, expanding the potential uses of these nanoparticles in tumour therapy. Their role in building sensitive fluorescent biosensors has been comprehensively overviewed as well.[30] In conclusion, MS QDs offer numerous advantages such as high efficiency, selectivity, controllability, low toxicity, and multifunctionality when used in combined with PTT/PDT tumour treatment. These qualities position MS QDs as one of the promising materials in the field of cancer therapy, demonstrating their potential to significantly improve treatment outcomes and provide new opportunities for personalized medicine approaches in fight against cancer.

This review highlights the progress in using MS QDs for both PTT and PDT in the treatment of tumours. It starts by discussing

C.Li. MS student in Pharmacy at Dali University.
E-mail: cc110100@outlook.com
Current research interests: use of functional nanomaterials for photocatalytic production H_2O_2 and H_2.
L.Yu. Ph.D. in Organic Chemistry from Korea University (2024) under the supervision of Prof. Jong Seung Kim. Lecturer at Yunnan University.
E-mail: yule19931115@163.com
Current research interests: fluorescence probes, photoacoustic imaging, photodynamic therapy, photothermal therapy.
G.Shi. Master of Medicine from Dali University (2013). Senior Laboratory Technician at the same University.
E-mail: shiguirong2008@163.com
Current research interests: pharmacology of traditional Chinese medicine.
Y.Zhou. Ph.D. from Dalian University of Science and Technology under the supervision of Prof Xuhong Qian (2008). Postdoctoral Fellow in the group of Juyoung Yoon at Ewha Womans University (2008–2011). Professor at College of Chemical Science and Technology of Yunnan University.
E-mail: yingzhou@ynu.edu.cn
Current research interests: fluorescence chemosensors and development of organic functional molecules.
K.Qi. PhD in Material Chemistry from Nankai University (2013). Postdoctoral Fellow in Prof. Wojciech Macyk's group, Jagiellonian University, Poland (2014–2015). Professor at Dali University.
E-mail: qkzh2003@aliyun.com
Current research interests: synthesis of nanomaterials and their applications in environmental chemistry and energy conversion, with particular focus on photocatalysis.

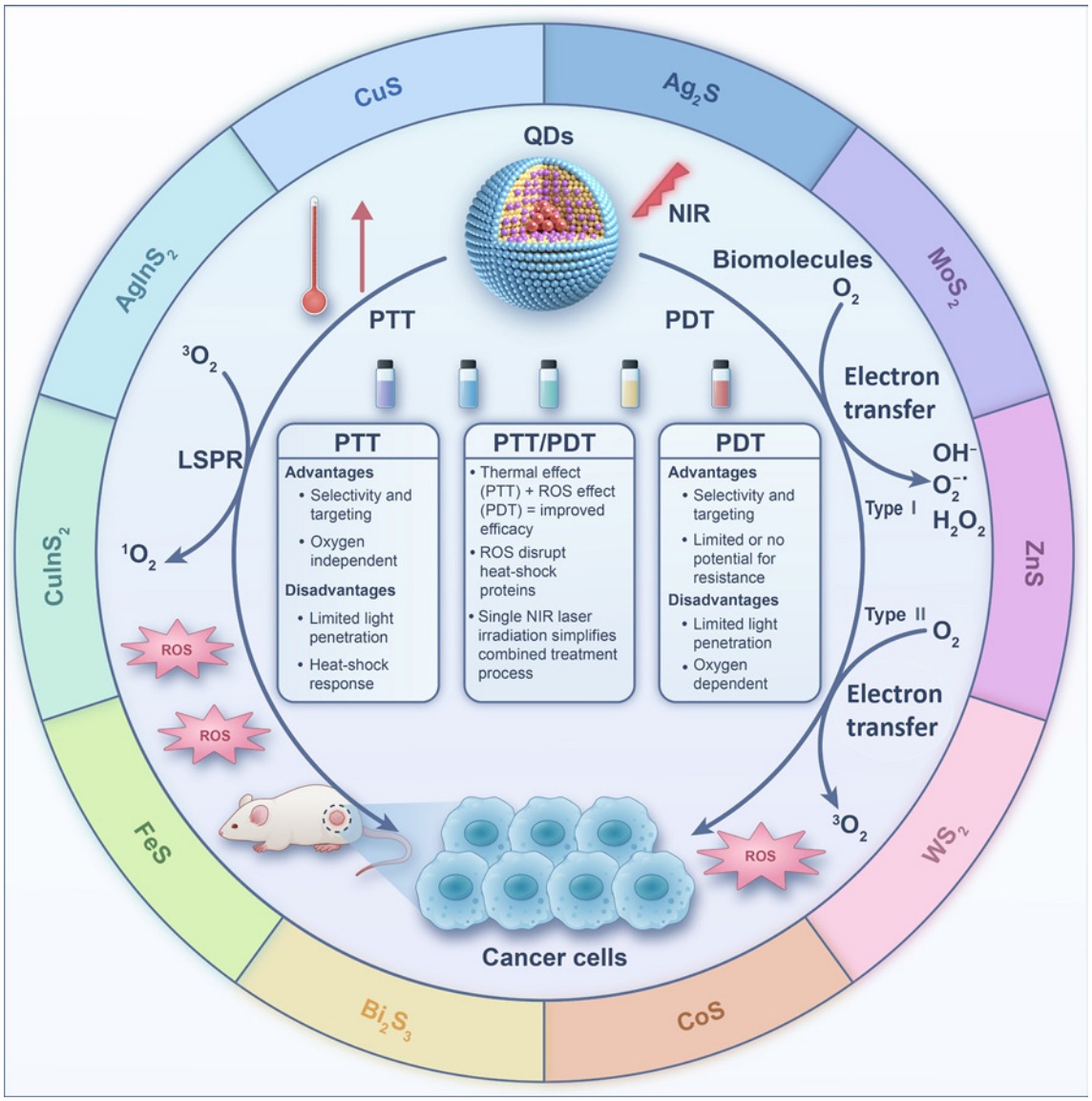

Figure 1. Progress in metal sulfide quantum dots in the photothermal/photodynamic treatment of tumours.

the basic concepts, advantages, and challenges of PTT/PDT. Next, it presents a summary for MS QDs: the method for their preparation, and the research progress in their combined treatment of tumours with PTT/PDT. Finally, it explores the difficulties and potential future pathways of the latter (Fig. 1).

2. Photothermal therapy (PTT) and photodynamic therapy (PDT)

2.1. Photothermal therapy

PTT employs PTAs to absorb NIR laser irradiation and convert it into heat, inducing tumour cell death due to their sensitivity to elevated temperatures.[31,32] When PTAs accumulate at tumour sites and are irradiated with NIR laser irradiation, localized temperatures can exceed 45°C, leading to immediate cancer cell necrosis. Mild-temperature PTT (42–43°C) can further enhance treatment by increasing tumour vascular permeability and improving the efficacy of adjunct therapies like CHT and RT.[33,34] On the other hand, localized surface plasmon resonance (LSPR), caused by light-induced oscillations of conduction electrons in nanoparticles, plays a key role in enhancing photothermal effects. LSPR characteristics depend on the nanoparticle's size, shape, composition, and environment, and enable efficient NIR-II mediated PTT.[35] Ideal PTAs exhibit strong NIR absorption, low fluorescence quantum yield, and high PCE. Both inorganic and organic PTAs are being utilized in the treatment of tumours. Inorganic photothermal nanomaterials, including noble metal materials (*e.g.*, gold, silver, platinum), carbon-based nanomaterials (*e.g.*, nanotubes, graphene, fullerenes), metal sulfide materials (*e.g.*, CuS, MoS_2, WS_2) and other QDs, have shown promise in tumour treatment. The research group led by Valery Tuchin and Elena Tuchina from the Prokhorov General Physics Institute of the Russian Academy of Sciences is internationally recognized for their pioneering work at the intersection of biophotonics and nanotechnology. Their primary focus is on developing and optimizing plasmonic nanoparticle-based strategies for combined cancer therapy.[36,37] Organic PTAs, such as small-molecule dyes and polymers, offer good biocompatibility, biodegradability, and NIR photothermal activity. They are classified into Zone I and Zone II agents and are valuable for both PTT and photothermal imaging.[38]

2.2. Photodynamic therapy

PDT is an emerging approach for treating tumours, leveraging PSs that generate cytotoxic ROS, such as singlet oxygen and free radicals, upon activation by specific wavelengths of light, ultimately leading to apoptosis of cancer cells.[39,40] During PDT, PSs produce cytotoxic ROSs under light irradiation at specific wavelengths, namely reactive oxygen radicals (Type I) and single-linear oxygen species (Type II), respectively. In Type I PDT, PSs interact directly with intracellular substrates and molecular oxygen through hydrogen or electron transfer, producing ROS such as superoxide anions ($O_2^{-\bullet}$), hydroxyl radicals ($^{\bullet}OH$), and hydrogen peroxide (H_2O_2). In contrast, Type II PDT involves energy transfer from PSs to triplet-state oxygen ($^3O_2$), generating highly cytotoxic singlet oxygen ($^1O_2$). However, the efficacy of Type II PDT is limited by its reliance on oxygen availability. In comparison, Type I PDT is more effective in hypoxic tumour environments due to its lower oxygen dependence and ability to produce ROS even under reduced oxygen conditions.[41,42]

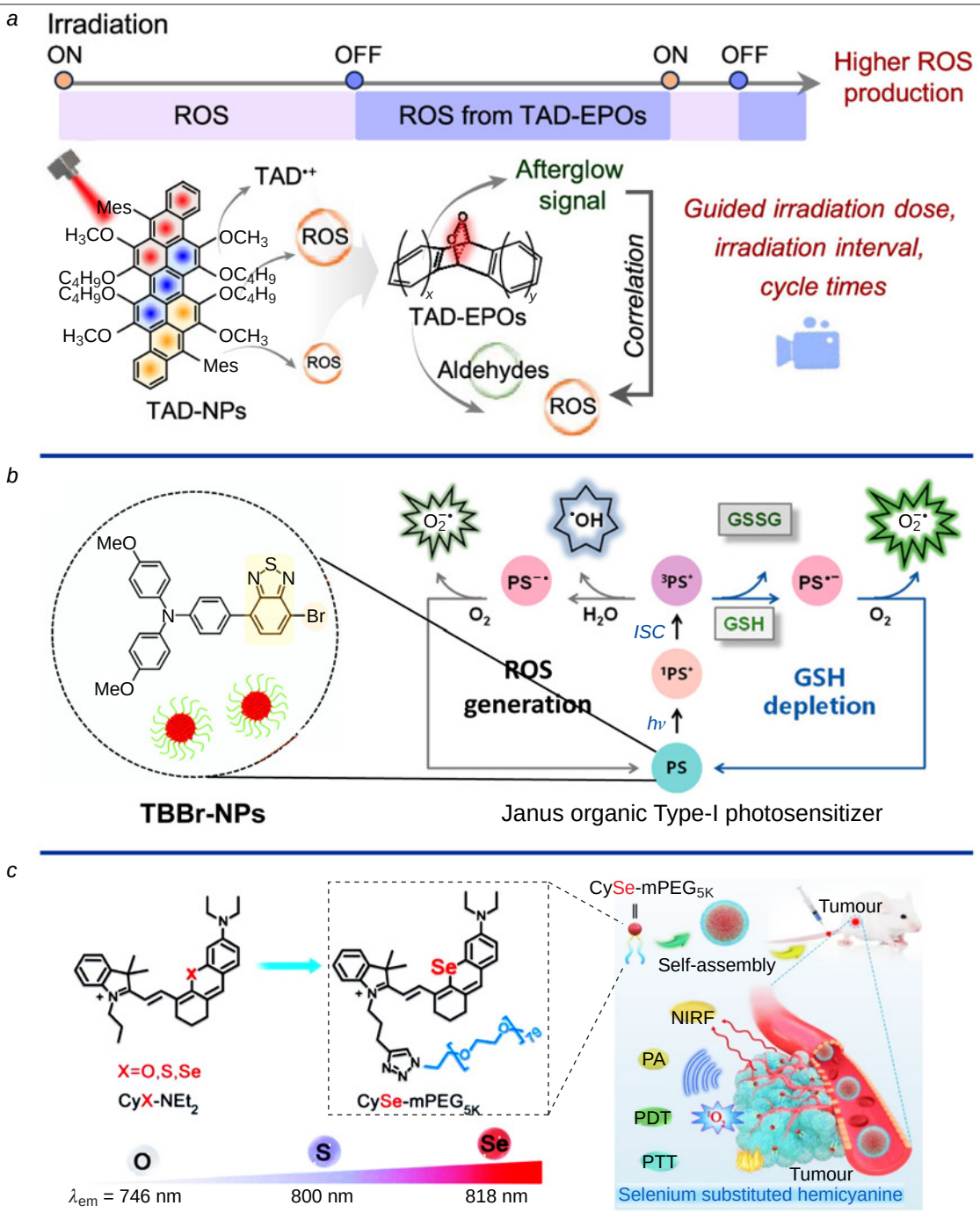

Figure 2. (*a*) Long-persistent photodynamic efficacy for enhancing fractionated therapy irradiation. TAD EPOs tri-anthracene derivative nanoparticles (TAD-NPs). Reproduced from Y.Wang *et al.*[48] with the permission from the American Chemical Society. (*b*) Schematic illustration of the Janus-PS of TBBr for hypoxia-tolerant PDT. Reproduced from H.Wang *et al.*[49] with the permission from the American Chemical Society. (*c*) Chemical structures of C_yX-NEt_2 (X = O, S, Se) and C_ySe-mPEG5K, and the schematic illustration of tumour targeting imaging-guided phototherapy. Reproduced from Yao *et al.*[50] under the CC BY 3.0 license.

The concept of PDT dates back to 1900, when Tappeiner[43] first introduced red light irradiation for skin tumour treatment — marking a foundational milestone. Since the 1950s, research into PDT's anticancer potential has significantly expanded. The therapeutic success of PDT hinges on the properties of the PSs, which should ideally exhibit low toxicity, high triplet quantum yield, and suitable triplet-state lifetimes to efficiently convert light energy into ROS. Early-generation PSs, such as hematoporphyrin derivatives and PS II, were limited by short-wavelength absorption, poor tumour selectivity, and phototoxicity affecting healthy skin.[44] To overcome these limitations, second-generation PSs including porphyrin and dihydroxybenzene derivatives, phthalocyanines, and anthraquinone-based compounds, were developed. These agents offer improved chemical purity, longer wavelength absorption for deeper tissue penetration, and enhanced photodynamic effects.[45] However, challenges such as hydrophobicity and lack of tumour specificity remain.[46] Third-generation PSs aim to address these shortcomings by incorporating targeting moieties such as polymers, liposomes, sugars, and antibodies, or by structural modifications including glycosylated porphyrins, porphyrin–fullerene complexes, and nanoparticle-based conjugates. These advances enhance tumour targeting, improve bioavailability, and reduce off-target effects, marking a significant step forward in PDT.[47] Recent developments have focused on optimizing PS functionality and biocompatibility. For instance, tri-anthracene derivative nanoparticles (TAD-NPs) facilitate enhanced ROS generation and spatially precise graded PDT for pancreatic tumours (Fig. 2 *a*).[48] Janus-type organic PSs (*e.g.*, TBBr-NPs) have demonstrated sustained ROS production while depleting intracellular glutathione (GSH), with one study reporting 96.3% tumour growth inhibition in mice after a 60-day regimen (Fig. 2 *b*).[49] Another breakthrough involves replacing oxygen with selenium in hemi-carbocyanine dyes, leading to CySe-mPEG5K — a dye with improved ROS generation, controlled phototoxicity, and extended optical activation profiles. This dye has shown potent efficacy in eliminating both cancer cells and bacteria under 750 nm laser irradiation (Fig. 2 *c*).[50] Together, these innovations reflect substantial progress in PDT, promising safer and more effective strategies for cancer treatment through enhanced PS design and functionality.

2.3. Advantages and challenges of PTT/PDT combination therapy

PTT presents a promising strategy for tumour treatment by converting NIR light into heat through PTAs, leading to localized hyperthermia and subsequent tumour cell ablation. However, its effectiveness can be hindered by factors such as attenuation of light intensity and uneven PTA distribution within tumour tissues. These limitations can result in irregular heat dispersion, reducing therapeutic efficacy. Moreover, while PTT effectively eradicates tumour cells, it poses a risk of collateral damage to surrounding healthy tissues due to excessive heat generation. In contrast, PDT utilizes PSs to convert molecular oxygen into cytotoxic ROS, which induce irreversible damage to tumour cells and microvasculature. PDT also initiates inflammatory and immune responses that contribute to long-term tumour control. Although PDT is a milder and more controlled approach compared to PTT, it typically acts over a prolonged period and is often limited by the hypoxic conditions prevalent in tumour microenvironments, which restrict ROS generation and thus reduce treatment efficacy. The combination of PTT and PDT capitalizes on the complementary advantages of each modality, offering a synergistic therapeutic effect. This integrated strategy enhances tumour eradication efficiency while potentially minimizing adverse effects on normal tissues (Fig. 3).[14,51] In current biotherapeutic research, this dual approach extends beyond MS QDs, incorporating various materials with high PCE-such as gold nanoparticles, sulfide-based nanomaterials, carbon-based nanoparticles, and quantum dots-coupled with PSs.[52–55] Functionalization of these nanomaterials further improves pharmacokinetics, targeted delivery, and PCE. This non-invasive therapy boasts multiple advantages: selective tumour destruction, reduced off-target effects, and controllability through tuning of photosensitive materials and light exposure parameters.[56–59] Additional benefits include repeatability, patient-specific treatment customization, and lower risk of drug resistance.[60,61] PTT/PDT has demonstrated effectiveness across a range of tumour types, including solid tumours (*e.g.*, breast, liver, and gastric cancers)[62–64] and hematologic malignancies (*e.g.*, lymphoma, myeloma, leukemia).[65–67] Furthermore, the combination approach enables reduced dosages and laser intensities, yielding more tolerable and effective treatments[68] and it can be synergistically integrated with other therapies such as CHT, RT, and sonodynamic therapy (SDT).[69–71] Despite these promising

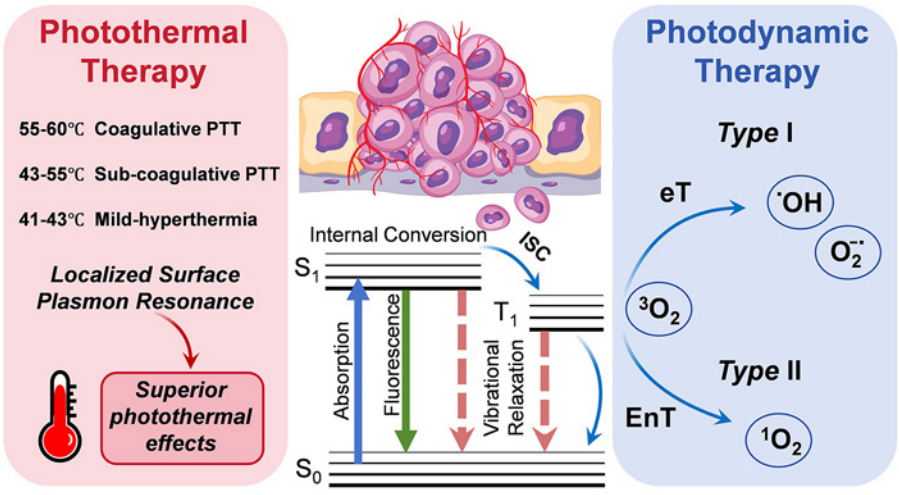

Figure 3. The antitumour mechanism of PDT and PTT of nanomaterials. ISC is intersystem crossing; eT is electron transfer; EnT is energy transfer.

outcomes, several challenges persist. PDT is constrained by tumour hypoxia, which impedes ROS production, while PTT may induce heat shock responses that limit its effectiveness.[72–74] In addition, the performance of PTAs and PSs can vary due to tumour heterogeneity, light penetration limitations, potential toxicity, and stability issues. These factors underscore the urgent need for the development of novel, more efficient PTAs/PSs with enhanced targeting, stability, and light responsiveness. Another critical limitation is the poor penetration depth of light, especially in deep-seated tumours, which calls for improved photo-irradiation technologies or alternative treatment strategies.[75] Moreover, patients undergoing PTT/PDT may experience discomfort, including pain and burning sensations, necessitating effective clinical management.[76] Future technological advancements are essential to address these obstacles and to further optimize the efficacy and safety of PTT/PDT in clinical oncology.

3. Quantum dots (QDs)

Quantum dots, as quasi-zero-dimensional nanomaterials, are a type of semiconductor nanoparticles characterized by particle sizes smaller than or near the exciton Bohr radius of the corresponding semiconductor material.[77,78] The investigation of QDs officially commenced in 1983 with the groundbreaking work of Brus and co-workers,[79] who introduced cadmium sulfide nanocrystals that exhibited distinct characteristic such as the size effect. Following this, in 1993, Bawendi co-workers[80] achieved a major breakthrough by successfully dispersing nanocrystals of CdE (E = S, Se, Te), which marked a pivotal moment in the organized exploration of QDs during the rapid expansion phase of semiconductor nanocrystal research. In 2004, Nie and co-workers[81] made significant progress in the field of QDs disease detection with their milestone tumour targeting and imaging studies conducted on live animals. The prestigious Nobel Prize in Chemistry was bestowed upon Moungi Bawendi, Louis Brus, and Alexei Ekimov[82,83] in 2023 for their innovative contributions to the discovery and synthesis of QDs, emphasizing the crucial role of fundamental science at the nanoscale. The present review article focuses on a brief introduction to the classification, optical properties and biomedical applications of QDs.

3.1. Optical properties of QDs

The luminescence principle of QD is similar to that of conventional semiconductor material, where an energy of excitation higher than its forbidden bandwidth causes electrons in the ground state to jump to the excited state, forming an 'electron–hole' pair (Fig. 4 *a*).[84] Electrons in the conduction band (CB) are able to move freely within the states, and can lose energy through thermal processes or other mechanisms as they move towards the bottom of the CB where they may eventually combine with holes, leading to photon emission. However, electrons may also get trapped in semiconductor, resulting in a decrease in quantum yield (QY). In defect-free QDs, a blue shift in the fluorescence spectrum of QDs appears as their size decreases, resulting in broader absorption bands. Generally, excited QDs generate electron–hole pairs (excitons), which can either emit light through direct recombination of electrons and holes, or react with surface defects and the reactants.

The unique properties of QDs arise from their quantum effects, particularly when their size enters the nanometer scale. When the physical size is comparable to the De Broglie wavelength, the energy level spacing is split, leading to the occurrence of the quantum size effect.[85] Indeed, this results in quantum limiting effects, quantum size effects, dielectric limiting effects, and surface effects that distinguish nanometer systems from macroscopic and microscopic systems. Fine-tuning the shape, structure, and dimensions of QDs allows for easy manipulation of properties like the bandgap width, the exciton binding energy, and the energy blue shift. Smaller dots display a more prominent blue shift in their absorption and emission spectra (Fig. 4 *b*). The principal consequence of quantum confinement is the size-specific bandgap of semiconductor QDs, facilitating precise adjustment of the energy gap based on the dimensions.[86] The dielectric confinement effect leads to the enhanced dielectric characteristics at the nanoparticle-matrix interface. This effect materializes when there is a notable variance in refractive indexes between the matrix and the particle, inducing the establishment of a refractive index boundary. When the intensity of the local field at the particle periphery surpasses that of the incident field, a phenomenon termed the medium-limited field effect will appear. Transition metal oxide QDs and other semiconductor QDs exhibiting dielectric-limited domain effects will affect their various properties such as light absorption and photochemistry. The surface effect is a result of the atom concentration on the surface of QDs.[87] As the size of the QDs decreases, the specific surface area will be larger. The increase in surface area causes an insufficient coordination of surface atoms, resulting in an abundance of unsaturated and

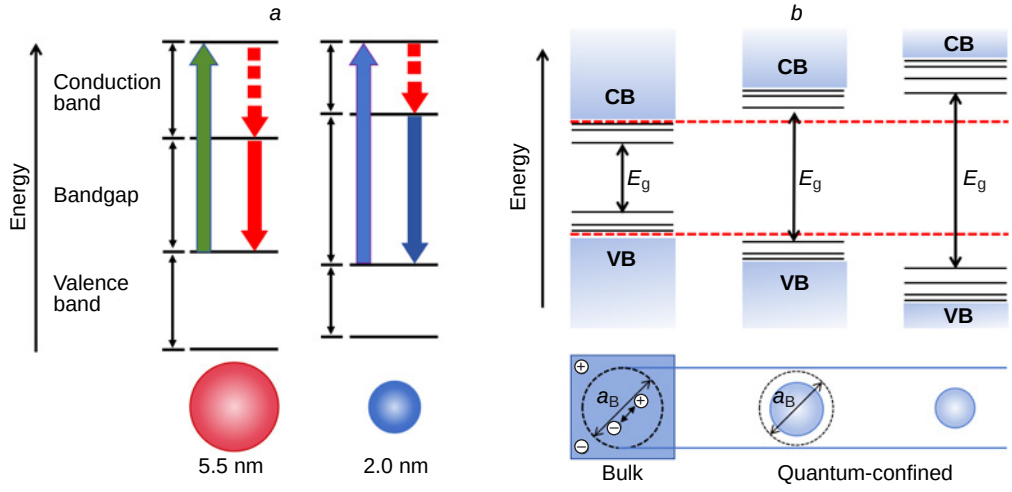

Figure 4. (*a*) Schematic diagram of the principle of quantum dot photoluminescence (solid lines are radiative leaps; dashed lines are non-radiative leaps), (*b*) Quantum confinement occurs when the spatial extent of electronic wave functions is smaller than the Bohr exciton diameter (aB), leading to size-dependent optical and electrical properties distinct from those of parental bulk solids. The emission wavelengths of QDs vary depending on their size.

dangling bonds that increase reactivity. The reactive surface atoms easily bond with other atoms or molecules, altering the atomic configuration and electronic energy levels of the nanoparticle surface. Surface defects create trapping states for electrons or holes, which in turn impact the absorption and luminescence properties of QDs and lead to the generation of nonlinear optical effects. Due to the diverse physical phenomena associated with these surface effects, QDs show promise for a range of applications in various fields. These applications include solar energy conversion, light-emitting devices, photodetection, catalysis, molecular and cellular labeling, as well as cancer therapy. The unique properties of QDs make them highly versatile and valuable in the development of new technologies and advancements in different areas of science and technology.

The fluorescence mechanisms and optical properties of MS QDs cannot be adequately described by the single framework of the quantum size effect alone. For classic binary QDs, such as CdSe, emission originates from the radiative recombination of band-edge excitons, with the emission peak position being highly sensitive to nanocrystal size — a hallmark of the classic quantum confinement effect. In contrast, ternary (or multinary) sulfide QDs, represented by materials like $CuInS_2$ and $AgInS_2$, exhibit distinctly different optical characteristics: typically broad emission spectra, large Stokes shifts, and a notably weak dependence of the emission peak position on particle size. These features indicate that the dominant luminescence mechanism shifts from band-edge exciton recombination to a recombination process governed primarily by intrinsic defect states.[88] The broad emission and weak size dependence of ternary MS QDs stem from their inherent defect-assisted emission mechanism. In $CuInS_2$ QDs, the most widely accepted model involves the radiative recombination of a conduction band (or shallow donor state) electron with a hole localized at an acceptor defect level, where the acceptor state is commonly associated with copper vacancies. Statistical variations in the type, concentration, and spatial distribution of these defects among individual QDs lead to an in homogeneously broadened emission profile across the ensemble. More importantly, the energy levels of these defect states are determined primarily by the local lattice environment and chemical composition, rendering them relatively insensitive to changes in the overall QD dimensions. This explains the minimal shift in the emission peak with varying size and represents a fundamental departure from the classical quantum confinement paradigm, forming the core of understanding their optical properties. For photothermal and photodynamic therapy applications, this defect-physics-dominated nature carries dual implications. On one hand, the large Stokes shift effectively separates excitation and emission wavelengths, reducing self-absorption and facilitating deeper tissue optical imaging and treatment monitoring. On the other hand, defect states can also act as channels for nonradiative recombination, which typically results in a low intrinsic photoluminescence quantum yield. However, through precise composition tuning, surface passivation, and ligand engineering, it is possible to purify defect states, suppress nonradiative pathways, and significantly enhance emission efficiency. Studies show that optimized core/shell structured MS QDs can achieve photoluminescence quantum yields approaching 100%, laying the groundwork for developing high-brightness theranostic probes.[89] Surface functionalization has also proven to be an effective strategy for modulating their optical properties while enhancing biocompatibility and targeting specificity.[90]

3.2. Advantages of QDs in biomedical applications

Quantum dots possess several advantageous properties, such as high quantum yield, impressive brightness, elevated extinction coefficients, and remarkable stability against photobleaching. These properties make them excellent fluorescent probes for cellular-level imaging, enabling detailed visualization of intracellular structures. Unlike traditional fluorophores that emit continuous fluorescence, QDs exhibit scintillation-like properties, allowing for more precise detection of single cells and subcellular components. QDs have also shown great potential in *in vivo* imaging, particularly when functionalized with targeting ligands to enhance accumulation in specific organs or tissues.[91,92] Compared to organic dyes, QDs provide higher luminance and more stable fluorescence, which is critical for applications requiring long-term monitoring, such as tumour tracking. Their intrinsic fluorescence enables repeated excitation without significant signal loss, offering clear advantages over traditional dyes that may degrade under physiological conditions. In phototherapy, QDs function both as PSs and energy donors. They surpass organic PSs in terms of absorption strength, emission intensity, photostability, water solubility, and tissue accumulation. By adjusting their size and composition, QDs can be tuned to emit in the NIR range, enhancing tissue penetration and making them suitable for treating deep-seated tumours.[93] While many multifunctional nanomaterials have been developed for combined imaging and phototherapy, these often rely on complex assemblies of multiple components, which may degrade or disintegrate *in vivo*, reducing therapeutic efficacy. In contrast, QDs possess intrinsic optical and therapeutic properties, making them more stable and reliable for real-time image-guided cancer therapy. Additionally, QDs can serve as drug delivery vehicles due to their ease of functionalization, broad drug compatibility, and trackable optical signals after administration.[94]

Quantum dots are also being explored in fluorescence-activated cell sorting, biosensing, and tumour targeting applications.[95,96] These diverse functions highlight the versatility of QDs in both diagnostic and therapeutic settings, supporting their future clinical potential. Kontareva *et al*.[97] studied the uptake of Ag–In–S QDs by breast cancer cells with different metastatic tendencies, and discussed its potential in cancer diagnosis and treatment. Alsuraifi *et al*.[98] summarized the key role of QDs in photothermal and photodynamic therapy, and prospected the application prospect of QDs in biomedical field. Currently, clinical applications of PDT and PTT remain limited. For example, Lightdale *et al*.[99] demonstrated that PDT provided effective palliative care for esophageal cancer, with fewer side effects compared to laser therapies, Jethwa *et al*.[100] reported the use of laser-induced thermotherapy for treating intracranial tumours in patients unfit for surgery. The study showed promising results with high accuracy and minimal complications. In addition, researchers at Ningbo University Medical College Hospital compared indocyanine green (ICG)-enhanced laser thermocoagulation and PDT for treating choroidal hemangioma. ICG-laser therapy offered better visual outcomes and caused less damage to healthy tissues,[101] aminolevulinic acid (ALA)-based PDT has also been used with CO_2 lasers for treating skin and mucosal tumours. Cai *et al*.[102] reported high remission rates for Bowen's disease using PS with minimal side effects. Similarly, Hu *et al*.[103] found that combining 5-ALA-PDT with CO_2 laser therapy effectively treated vaginal intraepithelial neoplasia with minimal adverse effects. Zhang *et al*.[104] successfully treated seborrheic keratosis using a combination of

CO_2 laser and ALA-PDT, with complete lesion removal and no recurrence after four treatments. Despite these successes, the clinical use of PDT/PTT remains limited due to technical and biological challenges. Therefore, this paper emphasizes studies conducted at the cellular and animal levels to better understand the therapeutic potential of PDT and PTT.

4. Metal sulfide quantum dots (MS QDs)

4.1. Definition/classification of MS QDs

Sulfur is abundantly found on Earth, and metal sulfides act as active catalysts in semiconductor photocatalysis. The cations commonly employed in building sulfide semiconductors are metals with a d10 configuration, including zinc, cadmium, copper, silver, indium, and tin. Binary metal–sulfur compounds are usually represented by the general formula M_xS_y (M = Zn, Ag, Cu, Bi, *etc*.). Ternary and multisulfur compound semiconductors make up materials with a varied range of activities that can be synthesized from S and M *via* regulating the bandgap by adjusting their dimensions and components. In metal sulfides, the cations' atomic orbitals and S^{2-} orbital hybridize to create multiple dense molecular orbitals, leading to the formation of the CB and valence band (VB). Most metal sulfide semiconductors display negative CB, demonstrating a strong reducing capability akin to metal oxides. Additionally, due to the higher VB positions attributed to S 3p orbitals compared to O 2p orbitals, metal sulfides generally exhibit weaker oxidizing properties than metal oxides.[105] Consequently, metal sulfides are predominantly reducing and weakly oxidizing materials with narrower band gaps. Metal sulfides have been a subject of increasing interest in recent years due to their unique properties such as lower VB, narrower bandgap, and strong light-trapping abilities.

4.2. Light response mechanisms and applications of MS QDs

Among metal compound nanomaterials, metal sulfides stand out for their strong NIR absorption capabilities. If the LSPR absorption peak of metal sulfides falls in the NIR region, then the hot carriers generated through this process have higher heating energies compared to direct photoexcitation. These higher heating-energy carriers can freely move and dissipate their energy by heating the local environment, resulting in a photothermal effect on the material. This photothermal effect has various applications, including PTT in cancer treatment, optical imaging of tumours, pollutant degradation, and seawater desalination. For instance, ultra-small copper sulfide nanoparticles (CuS@BSA) prepared by Wan *et al*.[106] have been shown to be biocompatible, and to be showcasing their effectiveness in bio-imaging and PTT. The step-scheme (S-scheme) heterojunction, first conceptualized by Yu and co-workers[107] in 2019, represents an advanced charge transfer architecture designed to overcome the limitations of conventional heterojunctions. S-scheme heterojunction is a hybrid of reduced photocatalyst (RP) and oxidized photocatalyst (OP). Reduced photocatalyst has higher Fermi level (EF) and more negative CB potential than OP. When the two components are in contact, their EF difference leads to the transfer of electrons from RP to OP. Therefore, due to the accumulation of electrons, the EF and the band edge of OP bend upward and downward in the interface region, respectively. At the same time, after light excitation, the photogenerated electrons in the CB of OP will migrate to the VB of RP under the drive of Coulomb gravity. Finally, the photogenerated electrons with strong reduction ability remain in the CB of RP, while the holes with high oxidation ability remain in the VB of OP.[108] The existence of this S-scheme charge transfer pathway has been rigorously validated by sophisticated characterization techniques. *In situ* irradiated X-ray photoelectron spectroscopy can track interfacial charge flow, femtosecond transient absorption spectroscopy probes ultrafast carrier dynamics,[109] the detection of key radical species by electron paramagnetic resonance,[110] and Kelvin probe force microscopy visually maps the surface potential changes and the built-in electric field.[111,112] The carriers in the S-scheme heterojunction are effectively separated and have strong redox ability, thus giving the photocatalyst higher photocatalytic activity.[113] Highly efficient full-solar spectrum-driven photocatalysts (1D/1D $MoO_{3-x}/Mn_{0.3}Cd_{0.7}S$ (MO/MCS)) developed by Yao *et al*.[114] represent a new S-scheme heterojunction with dual effects of LSPR and photothermal effects. The incorporation of MO/MCS extends light absorption to the NIR region through the LSPR effect of MO and utilizes the significant photothermal effect to enhance the surface temperature of the photocatalyst particles. This, in turn, accelerates the photoreaction process. More critically, the established S-scheme heterojunction between MO and MCS drastically enhances the separation of photoinduced electron-hole pairs. This synergistic design leads to exceptional photocatalytic hydrogen evolution performance. Furthermore, the efficient separation of charge carriers in such heterojunctions also promotes the generation of ROS for applications like PDT, highlighting the versatile potential of S-scheme photocatalytic systems. Jiang *et al*.[115] created Bi_2S_3/Ti_3C_2 two-dimensional nanohybrid structures to improve the efficacy of PDT and PTT for tumorr treatment. By combining Bi_2S_3 with Ti_3C_2, they were able to enhance the separation of photogenerated $e^- – h^+$ carrier pairs, leading to improved photocatalytic activity, especially in the NIR region. This expanded absorption range allowed for the generation of O_2 through the reaction of VB holes of Bi_2S_3 with water, as well as the creation of $^1O_2$ through energy transfer. Additionally, the addition of triphenylphosphonium bromide on Bi_2S_3/Ti_3C_2 nanohybrid structures resulted in complete eradication of U251 tumour cells without recurrence when exposed to NIR laser irradiation. Furthermore, these nanohybrid structures showed strong X-ray attenuation ability for use in CT imaging. Through a combination of LSPR-induced photothermal effects and PDT therapy, these nanomaterials offer promising solutions for those addressed complex challenges like cancer treatment and pollution control.

4.3. Synthesis of MS QDs

To advance the research on QD performance, it is essential to obtain stable and high-quality QD materials. A recent review by Houtepen *et al*.,[116] published in Nature Reviews Methods Primers, provides a comprehensive overview of the preparation methods for QDs. Early QD synthesis relied on conventional chemical methods such as co-precipitation, microemulsions, and micelle-based techniques, which laid the foundation for the development of more advanced strategies. These improvements in synthesis techniques have significantly expanded the potential applications of QDs across various fields. Typical synthesis methods employ water-soluble metal salts as precursors, while sulfur-containing compounds, often dissolved in hydrophobic solvents such as acetic acid, propionic acid, amines, or alcohols, act as ligand stabilizers. MS QDs such as CdS, PbS, and ZnS can

be synthesized through heating and refluxing these precursors with the stabilizers. Among the most widely used preparation techniques are solvent or hydrothermal synthesis and thermal injection synthesis, both of which enable precise control over particle size and crystallinity. In addition to these, alternative approaches such as microwave-assisted and ultrasound-assisted methods utilize materials with high dipole moments that react under high-frequency electromagnetic radiation and elevated temperatures to form QDs. Other advanced techniques include successive ionic layer adsorption and reaction (SILAR), liquid-phase exfoliation, sonochemistry, and chemical vapor deposition, all of which offer unique advantages depending on the desired QD composition and application.

4.3.1. Hot-injection synthesis method

The hot-injection method, also known as the organometallic precursor method, is the use of the principle of solution supersaturation, in which the use of syringes is to rapidly inject the precursor solution into a hot reaction solution at a specific temperature, so that the rapid growth of the product crystals and the occurrence of uniform nucleation are achieved. This technique promotes the uniform growth of QDs, ensuring consistency in their state and achieving homogeneity and monodispersity without the need of high temperature or pressure. Moreover, the reaction conditions are easily manageable. LaMer and Dinegar [117] developed a model in 1950 to explain the process of nucleation and growth of monodisperse colloidal microspheres (Fig. 5). The model suggests that the reaction between metal and sulfur precursors results in the formation of monomers, which then come together to form larger nuclei. These nuclei eventually develop into QDs through the continuous addition of monomers. This model provides valuable insights into the mechanisms underlying the formation of monodisperse colloidal microspheres. The reaction can be divided into three stages: In the first stage, the monomer concentration is changed or becomes supersaturated by adding precursors or changing reaction parameters.[118] In the second stage, once the monomer reaches a supersaturated state, which is the critical concentration for the start of nucleation, the nucleation process continues until the monomer concentration falls below the critical concentration for nucleation when the stage is terminated. The third phase, in the later stages of the growth phase, ideally provides a balance between consumption and production of monomers and maintains a certain degree of monomer supersaturation. Conversely, solution growth may be accompanied by an Ostwald ripening process, a phenomenon caused by the greater solubility of small particles throughout the system, which can lead to a broader quantum dot size distribution.[119] This model contributes to the fundamental understanding of colloidal chemistry and nanoparticle synthesis, paving the way for further advancements in the field.

In 1993, Bawendi and co-workers [80] successfully synthesized CdE (E = S, Se, Te) QDs utilizing this approach. They introduced organometallic precursors into heated coordination solvents for decomposition to produce QDs with adjustable size (1.2–11.5 nm) and exceptional optical characteristics. The precursor chemicals used in the preliminary synthesis included dimethyl cadmium (Me_2Cd) and bis(trimethylsilyl) sulfide [$(TMS)_2S$] as sources of Cd and S respectively, along with tri-n-octylphosphine and tri-n-octylphosphine oxide as stabilizing agents. High-quality CdS QDs were obtained within a growth temperature range of 290–320°C. To synthesize CdSe and CdTe QDs, $(TMS)_2S$ and bis(*tert*-butyldimethylsilyl) tellurium were employed as Se and Te precursors, respectively. Minimal CdSe and CdTe QDs were achieved at a growth temperature of 100°C. However, due to the high cost and hazardous nature of certain reagents (*e.g.*, Me_2Cd), subsequent studies transitioned to safer options including CdO, S, oleylamine (OAm), oleic acid (OA), and 1-octadecene (ODE). This shift led to the development of the 'organometallic thermal injection method', which became a widely accepted technique for synthesizing uniform and high-quality QDs (Table 1). For example, in the study of Malankowska *et al.*[126] $AgInS_2$ QDs and Bi_2S_3 QDs were prepared by thermal hot-injection method. In the process of preparing $AgInS_2$ QDs, a mixture of $AgNO_3$, $In(acac)_3$, and OA was combined in a three-necked flask and then mixed before ODE was added. The solution was degassed with nitrogen, heated, and injected with DDT. Subsequently, sulfur solution was rapidly injected while stirring continued, and the resulting liquid product was cooled, centrifuged, washed, and dried to yield $AgInS_2$ QDs. The synthesis method for Bi_2S_3 QDs involved thermal injection using a starch capping agent. Ammonium bismuth citrate and DI were mixed and heated to a specific temperature, followed by the addition of soluble starch and stirring at that temperature for approximately 15 min. Na_2S solution was then added to the ammonium barium citrate solution and stirred at 100°C for 1 h to obtain Bi_2S_3 QDs post washing and drying. The average size of $AgInS_2$ QDs was approximately 12 nm, with difficulties in determining the exact size due to the presence of solvents like OA, ODE, dodecyl alcohol, and OAm on their surface. On the other hand, Bi_2S_3 QDs were spherical and ranged in size from 1–2 nm. Öberg *et al.*[152] synthesized Ag_2S colloidal quantum dots (Ag_2S CQDs) using a low temperature thermal injection method (Fig. 6*a*). Initially, $AgNO_3$ was dissolved in OA and oleylamine, followed by heating to the specified temperature. Subsequently, bis(trimethylsilyl) sulfide was injected into octadecene. The resulting dispersion was then cooled to room temperature and underwent washing with toluene and

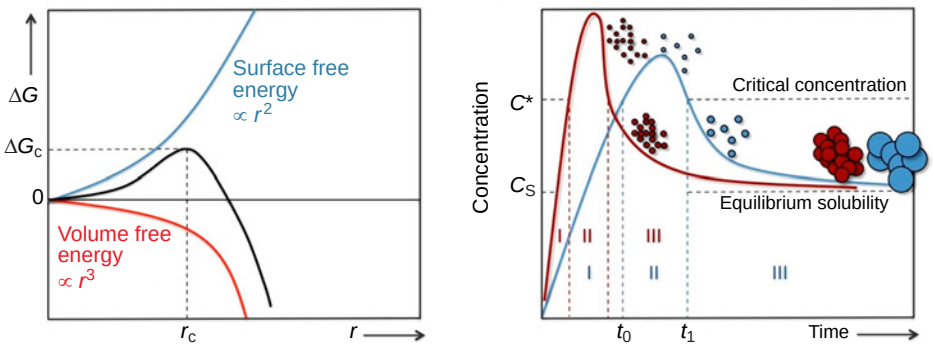

Figure 5. Schematic diagram of Lamer's theoretical growth mechanism. Reproduced from Reiss *et al.*[120] with permission from the American Chemical Society.

Table 1. Preparation of MS QDs by thermal injection method.

Complex	Crystal structure type	Reactants	Morphology	Size, nm	Ref.
ZnS	Sphalerite + Wurtzite	$Zn(OA)_2$, DDT, ODE	Spherical	2.9–3.5	121
ZnS	Sphalerite	$ZnCI_2$, DDT, ODE	Spherical	4.5	122
ZnS	–	$ZnCI_2$, S, DDT, OLA/OA	Spherical	9.5	123
Ag_2S	Monoclinic	AgAc, $C_8H_{18}S$, OLA, OA, ODE	Spherical	2.4±0.6, 3.5±1.3	124
Sb_2S_3	Stibnite	CTAB, SDS, DEA, EDTA, TAA	Spherical	3–5	125
Bi_2S_3	Orthorhombic	Na_2S, $Bi(NH_3)_2C_6H_7O_7$	Spherical	1–2	126
$CuFeS_2$	Chalcopyrite	$Cu[S_2CN(C_2H_5)_2]_2$, $Fe[S_2CN(C_2H_5)_2]_3$, S, TOP, OLA, OA, DCB	Spherical	12	127
$CuFeS_2$	Chalcopyrite	CuCI, Ga, S	–	35	128, 129
Cu_2SnS_3	Zinc stannate	CuCI, $SnCI_2$, $NaBH_4Se$/Se, TOPO, OLA, DDT/OA	Spherical	3–16	
Cu_3BiS_3	Orthorhombic	$Cu(acac)_2$, $Bi(NO)_3$, S, OLA	–	8–11	130
$AgInS_2$	Sphalerite	Ag(ac), $In(ac)_3$, Na_2S, 1-GSH	Aggregated	3	131, 132
$AgInS_2$	Orthorhombic	Ag(ac), $In(ac)_3$, S, OLA, DDT, ODE	Polyhedral	4	133
$AgInS_2$	Tetragonal	$AgNO_3$, $In(acac)_3$, S, OA, ODE, OLA, DDT	Amorphous	12	126
$ZnInS_4$	Hexagonal	$ZnCI_2$, $In(ac)_3$, $C_{18}H_{33}NaO_2$, S/Tu, OLA, ODE	Spherical	2–10	134
Cu_2ZnSnS_4	Wurtzite	$CuCI_2$, $SnCI_4$, $ZnCI_2$, Na(oI), S, DDT, OLA, ODE	Spherical	10–15	135
Cu_2ZnFeS_4	Chalcopyrite	CuCI, $ZnCI_2$, $Fe(acac)_3$, S, ODE, (OLA, OA)/(TDPA, TOPO)	Triangular	10–15	136
Cu_2FeSnS_4	Cassiterite	$Cu(acac)_2$, $Fe(acac)_2$, $SnCI_2$, S, OLA	Triangular or spherical	13	137
$ZnSe_xS_{1-x}$	Cubic	ZnO, $Mn(CH_3COO)_2$, Se, ODE, OA	Spherical	3.28–4.42	138
ZnSeS	Sphalerite	$NaBH_4$, $ZnSt_2$, Se, S, OLA, ODE	Spherical	4.1	139, 140
$CuInS_2$	Chalcopyrite	CuCl, $InCl_3$, $SC(NH_2)_2$, OLA, OA	Quadrilateral	25	141
$CuInS_2$	Chalcopyrite	CuI, $In(Oac)_3$, ODE, OLA	Spherical	4.25±0.2	142
$CuInS_2$	Sphalerite	CuI, $In(ac)_3$, DDT, OLA, OA	Pyramid	4.2–5.4	143
$CuInS_2$	Chalcopyrite + wurtzite	CuI, $In(ac)_3$, DDT, OLA, OA	Pyramid or hexagonal	10–15	143
Cs_2SnI_6	–	SnI_4, ODE, OLA, OA	Aggregated	5–10	144
Cs_2SnI_6	Cubic	Cs_2CO_3, ODE, OLA, OA	Spherical	2.5	145
Cs_2SnI_6	Perovskite	Cs_2CO_3, ODE, OLA, OA	Nanoribbon	30×8	145
CuGaS	Chalcopyrite	CuI, $C_{15}H_{21}GaO_6$, DDT	Triangular	2.2	146
$Zn(Te_{1-x}S_x)$	Sphalerite	$ZnEt_2$, Te, TOP, DDT, ODE, OLA	Spherical	2.8–3.0	147
CdZnSeS	–	CdO, $Zn(CH_3COO)_2$, S, Se, OA, ODE, TOP	Spherical	5.5–7.5	148
$Cu_2AgInS_2Se_2$	Tetragonal	AgCl, $CuCl_2$, $InCl_3$, Se, S, OLA, DDT	Ring-shaped	6.4	149
$Ag_xCu_yInS_2$	Wurtzite + chalcopyrite	$C_{10}H_2CuF_{12}O_4$, $C_5H_{10}NNaS_2$, $C_5H_{10}AgNS_2$, $InCl_3$, THF, DDT, ODE	Spherical or hexagonal	4.9±0.6	150
Cu_2AgInS_4	Zinc stannate	$CuCl_2$, AgCl, S, OLA, DDT	Cubic shapes	6.18	151

Notes. ac is acetate, acac is acetylacetate, CTAB is cetyltrimethylammonium bromide, DEA is *N*-alkylalkanolamide, DCB is dichlorobenzene, DDT is dodecanethiol, EDTA is ethylenediaminetetraacetic acid, OA is oleic acid, ODE is 1-octadecene, OLA is oleylamine, SDS is sodium dodecyl sulfate, TAA is thioacetamide, TDPA is tetradecylphosphonic acid, TOP is trioctylphosphine, TOPO is trioctylphosphine oxide, Tu is thiourea. A dash indicates that no data is available.

methanol. The synthesized Ag_2S CQDs particles have a relatively broad particle size distribution with diameters ranging from 3–10 nm with broad photon absorption in the UV-visible region (Fig. 6 *b*). The thermal injection method has the advantages of fast preparation speed, narrow size distribution of nanoparticles, and suitable for large-scale production. However, the disadvantages of this method include high requirements for solution composition and injection process conditions, and some materials may form amorphous structures due to rapid cooling. Numerous researchers are also trying to solve these existential problems in order to obtain better synthetic conditions and synthetic routes.

4.3.2. Solvent- or hydrothermal synthesis methods

Solvent- or hydrothermal synthesis refers to the formation of QDs in a liquid-phase medium through chemical reactions conducted under elevated temperatures and pressures. This method typically employs metal salts or organometallic compounds as precursors. The process consists of several key stages: pre-treatment of reactants, mixing in an appropriate solvent, conducting the reaction under controlled conditions, and subsequent separation and purification of the resulting nanocrystals. Careful adjustment of parameters such as pH and temperature is critical, as these factors directly influence the reaction kinetics and nucleation processes, thereby impacting

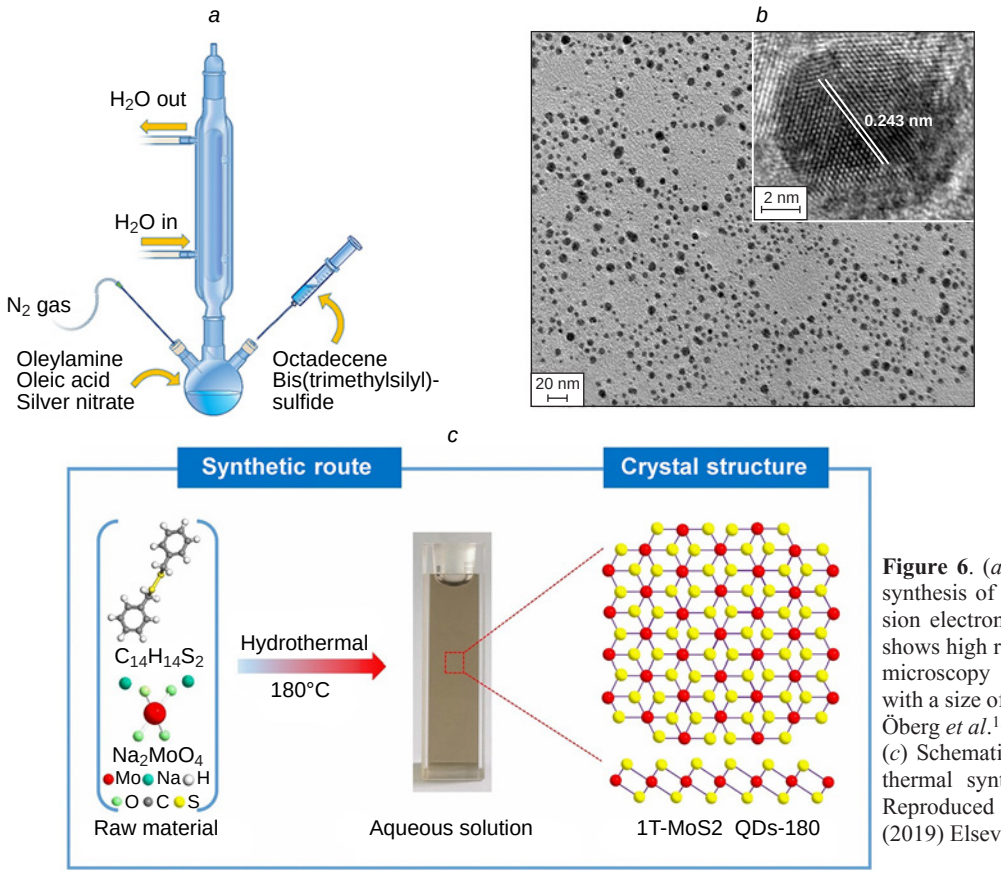

Figure 6. (*a*) Schematic illustration of the synthesis of Ag_2S CQDs and (*b*) transmission electron microscope image. The inset shows high resolution transmission electron microscopy image of a single crystal QD with a size of about 5 nm. Reproduced from Öberg *et al*.[152] with permission from Wiley. (*c*) Schematic process route for the hydrothermal synthesis of 1T-MoS_2 QDs-180. Reproduced from Li *et al*.,[154] copyright (2019) Elsevier.

the size, morphology, and crystalline structure of the QDs. Once the precursor solution is prepared and mixed, it is sealed in a high-pressure reaction vessel, such as a Teflon-lined autoclave and subjected to the desired temperature and pressure conditions. Upon completion of the reaction, the products are isolated through standard techniques such as precipitation, centrifugation, filtration, and repeated washing to remove residual byproducts and unreacted precursors. As a representative example, Srivastava *et al*.[153] demonstrated a one-step hydrothermal synthesis of WS_2 QDs. In this procedure, sodium tungstate and L-cysteine served as the tungsten and sulfur sources, respectively. The hydrothermal reaction yielded a yellow colloidal solution, from which WS_2 QDs were obtained following purification *via* dialysis. Transmission electron microscopy analysis confirmed the formation of well-dispersed, uniformly shaped QDs. Moreover, selected area electron diffraction patterns validated their crystalline nature and granular morphology. This synthesis approach offers significant advantages, including straightforward operation, relatively low-cost equipment requirements, and potential for scale-up. However, its effectiveness hinges on the precise optimization of multiple reaction variables, which can pose challenges in reproducibility and control over final product quality.

Molybdenum disulfide (MoS_2), a typical transition metal sulfide compound, exists in three main thermodynamic phases: 1T, 2H, and 3R. These phases differ based on the stacking arrangements of molybdenum atoms. The 1T phase represents a metastable metallic form characterized by excellent electrical conductivity, whereas the 2H and 3R phases are stable semiconductors. Li *et al*.[154] successfully synthesized water-dispersible 1T-MoS_2 QDs (designated as 1T-MoS_2 QDs-180) through precise control of the hydrothermal reaction temperature (Fig. 6*c*). Sodium molybdate (Na_2MoO_4) and diphenyldisulfide ($C_{14}H_{14}S_2$) were used as molybdenum and sulfur sources, respectively. These precursors were dissolved in a mixed solvent of water and ethanol and then reacted in a Teflon-lined stainless-steel autoclave at 180°C for 20 hours. The resulting dispersion was centrifuged to remove insoluble residues, and the supernatant was subsequently freeze-dried to obtain solid 1T-MoS_2 QDs-180. The as-synthesized QDs exhibited ultra-small, well-dispersed particle sizes averaging approximately 3.3 nm, along with a high 1T phase purity exceeding 82%. The hydrothermal method employed for synthesis offers several practical advantages, including simplicity, low equipment costs, and scalability for large-scale production. Furthermore, it allows for the formation of highly structured QDs under relatively mild conditions (typically <200°C), with good control over size and morphology. However, certain limitations remain. The method requires stringent control over multiple reaction parameters-including precursor type and concentration, solvent system, temperature, duration, and pH. Additionally, achieving uniform dispersity of the final products can be challenging, and the chemical treatments involved may generate hazardous byproducts that require careful handling and disposal. A comprehensive summary of the synthesis conditions and characterization results of various MS QDs is presented in Table 2.

4.3.3. Synthesis with successive ion layer adsorption and the reaction procedure

SILAR is a process for liquid-phase thin film fabrication. Its principle is to use a semiconductor photoanode to sequentially adsorb the anions and cations from the precursor solution, thereby forming the film of QDs covering the photoanode. In 1985, Nicolau[182] first proposed the use of SILAR to prepare sulfide films. Because of its affordable cost and straightforward

Table 2. Synthesis of metal sulfide QDs by solvent or hydrothermal methods.

Complex	Crystal structure type	Reactants	Morphology	Size/nm	Ref.
ZnS	Sphalerite	$ZnCI_2$, S, OLA	Spherical	8–11	155
ZnS	Wurtzite	n-$(DDTC)_2$, OA, OLA, ODE	Spherical	7–10	156
ZnS	Hexagonal	Zn-(PhDTC)-Phen/Pyr, TOP, HDA	Spherical	9.5	123
ZnS	Sphalerite	Zn-$(HTC/HDX)_2$, HDA	Filamentous	300×4.4	123
MnS	Wurtzite	$MnCI_2$, S, OLA	Rod-shaped	20×37–20×60	155
CuS	Monoclinic	$Cu(acac)_2$, S, OLA	Spherical	12	157
Cu_7S_4	Monoclinic	Cu-(DTTC), OA	Spherical	26	123
Ag_2S	Face-centered cubic	$Ag(NO_3/OAc)$, DDT	Spherical	3–18	158, 159
Bi_2S_3	Orthorhombic (bismuthinite)	$Bi(OctA)_2$, DDT	Rod-shaped	11×74	160
SnS	Orthorhombic	Sn-$(DDTC)_3$, OLA, ODE	Plate-like	7000×3000×20	123
SnS_2	Hexagonal	Sn-$(DDTC)_3$, OA, OLA, ODE	Plate-like	150×6	123
SnS_2	Hexagonal	$SnCI_4$, Cys	Plate-like	5.2	161
EuS	Cubic	Eu(DTC)biPy, OLA, TOP	Spherical	5	162
FeS_2	–	$FeCl_2$, Na_2S, DMSO	Spherical	2.5–5	163
MoS_2	Hexagonal	$(NH_4)_2MoS_4$, N_2H_4	–	2.8	164
MoS_2	–	Na_2MoO_4, GSH	Spherical	2.7±0.3	165
MoS_2	–	$(NH_4)_2MoS_4$, CH_4N_2S, NAC	Hexagonal	2.1	166
MoS_2	–	$(NH_4)_6Mo_7O_{24}$, 6-MP	Spherical	2.2±0.6	167
$CuInS_2$	Chalcopyrite	$CuCl_2$, $InCl_3$, MPA	Quadrilateral	2–4	168
$CuInS_2$	Chalcopyrite	Cu(OAc), $In(OAc)_3$, DDT, ODE, OA	Spherical	3	169
$CuInS_2$	Wurtzite	CuI, $In(ac)_3$, ODE, DDT	Plate-like	10–20	170
$CuInS_2$	Sphalerite	CuI, $In(ac)_3$, ODE, DDT	Pyramid	10	170
$AgInS_2$	Orthorhombic	AgCl, S, In	Clustered	20–30	171
$CuInFe_{1-x}S_2$	–	CuCI, $InCI_3$, $FeCI_3$, Tu, OLA, ODE, OA	Plate-like	20	172
$AgGaS_2$	Orthorhombic	$Ag(S_2CNEt_2)$, $Ga(S_2CNEt_2)_3$, DDT/HDT, OLA/HDA	Polyhedral	16	173
$AgSbS_2$	Monoclinic	$AgNO_3$, $SbCI_3$, TMS, OLA, OA	–	5–20	174
Cu_2ZnSnS_4	Orthorhombic	$CuCI_2$, $ZnCI_2$, $SnCI_2$, TCA, EDA	Plate-like	20–50	175
$CuInZnS_3$	Sphalerite	$Cu(ac)_2$, $In(ac)_3$, $Zn(ac)_2$, S, DDT, OLA, OA, $Mn(ac)_2$(dopant)	–	2–5	176
CuInZnS	Chalcopyrite	CuI, $In(OAc)_3$, $Zn(OAc)_2$, DDT, ODE	Narrow ring-shaped	7±0.6, 3.2±0.5, 4.1±0.4	177
CuInZnS	Chalcopyrite	TAA, $Zn(OAc)_2$, $In(NO_3)_3$, $HSCH_2CH(NH_2)CO_2H$	Spherical	3–5	178
CuInZnS	Cubic	$Cu(NO_3)_2$, $In(NO_3)_3$, $Zn(NO_3)_2$, GSH, Na_2S	Spherical	3.76	179
ZnCuInS	Chalcopyrite	$Zn(OAc)_2$, Cu(OAc), S, $In(OAc)_3$, DDT, OA	Spherical	3	180
Ag_2ZnSnS_4	Tetragonal	$AgNO_3$, $ZnCl_2$, $SnCl_2$, CH_4N_2S	Spherical or quadrilateral	1.6–4.5	181
AgInZnS	Hexagonal	$AgNO_3$, $In(NO_3)_3$, $Zn(NO_3)_2$, GSH, Na_2S	Spherical	3.51	133

Notes. Bipy is 2,2′-bipyridine, DDTC is metal diethyldithiocarbamate, DTC is dithiocarbamate, EDA is ethylenediamine, HDA is hexadecylamine, HDT is hexadecanethiol, HDX is hexyl dithioxanthate; HTC is hexylthiocarbamate, 6-MP is 6-mercaptopurine, MPA is mercaptopropionic acid, NAC is *N*-acetyl-*L*-cysteine, Phen is1,10-phenanthroline, TCA is thioacetamide. A dash indicates that no data is available.

experimental procedure, which does not necessitate high temperature or pressure, it is frequently utilized in producing different types of QDs. Kumar *et al*.[183] and colleagues utilized the continuous ion layer adsorption technique for fabricating QDs films composed of binary metal sulfides (PbS) and ternary metal sulfides (PbSbS) (Fig. 7 *a*). This method allowed for precise control over the thickness and composition of the films, resulting in materials with unique optical and electronic properties. The QDs were attached to the TiO_2 film through the steps of soaking, washing and drying, and after several cycles, the Pb–S/Sb–S bilayer structure forming on the TiO_2 film was transformed into $Pb_5Sb_8S_{17}$. The chemical reaction responsible for the development of PbSbS is illustrated as follows (see Eq. (1)–(5) below). Similarly, Suchikova *et al*.[184] used SILAR to synthesize $Cd_xTe_yO_z$/CdS/ZnO heterostructures. Achieving control on growth rate at the atomic level is through different cycles of the continuous ion layer adsorption method, which only requires compatibility with low temperatures to provide uniform coatings. However, the SILAR method also presents certain limitations, including a relatively slow growth rate and restrictions on the types of materials it can be applied to.

$$Pb(NO_3)_2 \longrightarrow Pb^{2+} + 2\,NO_3^- \text{ (aq.)} \quad (1)$$

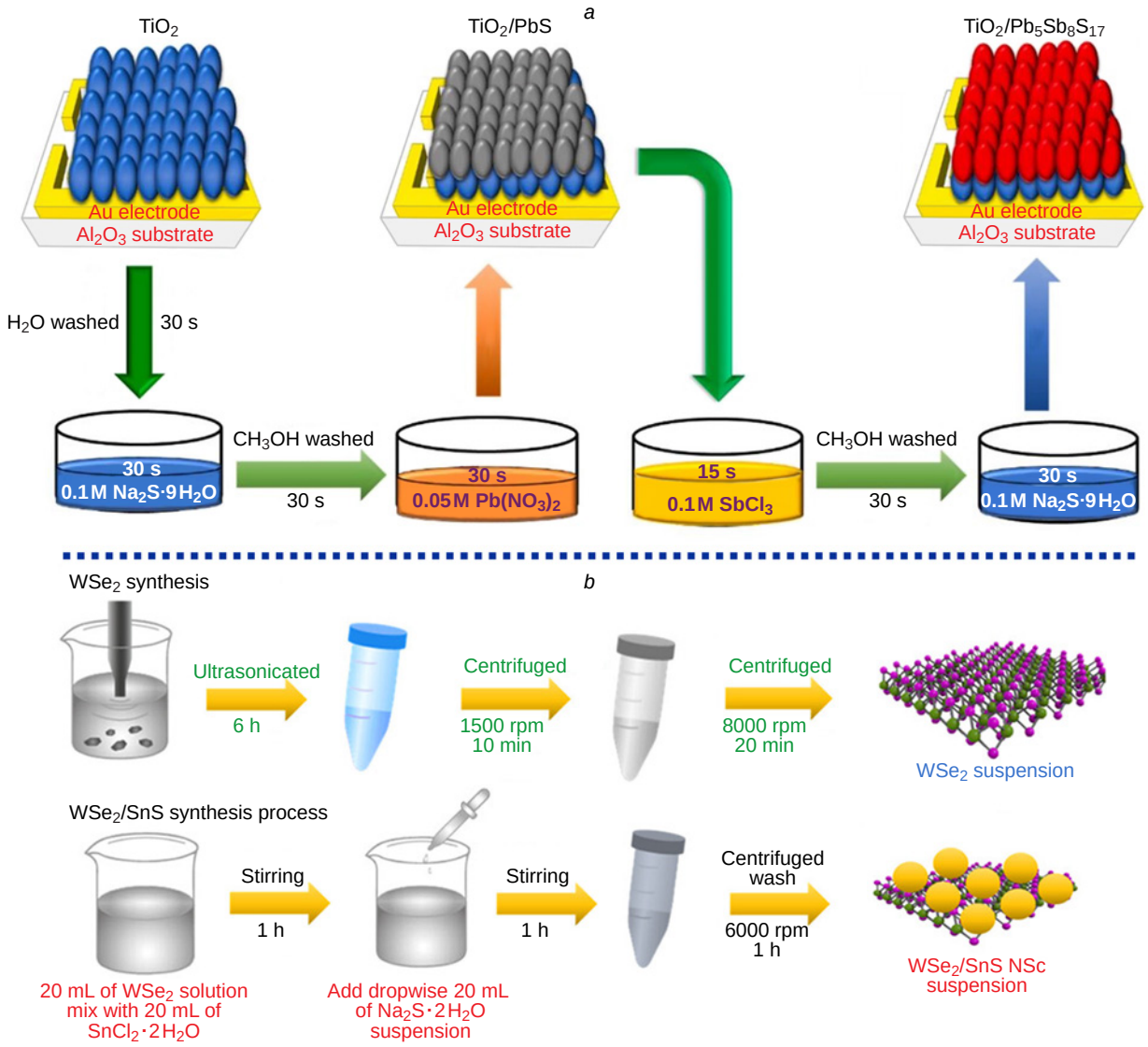

Figure 7. (*a*) Diagram illustrating the fabrication of gas sensor device and the synthesis of PbSbS QDs using SILAR technique. Reproduced from Kumar *et al.*[183] with permission from Elsevier. (*b*) Schematic of the preparation of WSe_2/SnS by liquid-phase exfoliation combined with wet chemical synthesis methods. Reproduced from Cheng *et al.*[186] with permission from the American Chemical Society.

$$Pb^{2+} + 2\,NO_3^-(ag) + Na_2S\cdot 9\,H_2O \longrightarrow \longrightarrow PbS + 2NaNO_3 + 9H_2O \quad (2)$$

$$PbS + SbCl_2 \longrightarrow PbS/Sb^+ \quad (3)$$

$$PbS/Sb^+ + Na_2S\cdot 9\,H_2O \longrightarrow PbS/SbS + 6\,NaCl + 9\,H_2O \quad (4)$$

$$Pb-S/Sb-S \longrightarrow Pb_5Sb_8S_{17} \quad (5)$$

4.3.4. Synthesis *via* liquid-phase exfoliation method

Many QDs (such as MoS_2, SnS_2, and WS_2) have layered crystal structures, which can be obtained as single-layer or multi-layer QDs using liquid-phase exfoliation. This method is cost-effective and can be performed at room temperature. The size of the QDs can be controlled to adjust their bandgap and absorption range. WS_2 QDs were synthesized by Bora *et al.*[185] using a straightforward liquid-phase exfoliation method. WS_2 powder was mixed with *N*-methyl-2-pyrrolidone (NMP) and subjected to continuous ultrasound treatment with an ultrasonic homogenizer for 15 h. The resulting solution was centrifuged at low temperature, yielding a colorless supernatant containing WS_2 QDs. The excess solvent was evaporated, and the WS_2 QDs were re-dissolved in NMP at a concentration of 1.0 mg mL^{-1} for further analysis. Ultimately, WS_2 QDs were obtained with an average diameter of 2.4±0.1 nm. Cheng *et al.*[186] synthesized WSe_2/SnS nanocomposites using a combination of liquid-phase stripping and wet chemical synthesis (Fig. 7*b*). NMP solvent was used as the best dispersing solvent, and WSe_2 nanosheets were obtained by ultrasonication and centrifugation at room temperature, and then $SnCl_2\cdot 2\,H_2O$, $Na_2S\cdot 2\,H_2O$, and WSe_2 were co-dissolved in an appropriate amount of ethanol, and the stirring with an appropriate period of time could lead to the ionised Sn^{2+} and S^{2-} were adsorbed on the surface of WSe_2 nanosheets, and finally the WSe_2/SnS nanocomposites were obtained after centrifugal washing. Similarly, Fu *et al.*[187] used a combination of ultrasound treatment and liquid-phase exfoliation to synthesize SnS_2 QDs. Initially, tin(II) chloride pentahydrate and thioacetamide were dissolved in deionized water, and the resulting solution was heated and centrifuged to yield yellow SnS_2 crystals. These crystals were then dispersed in ethanol, subjected to sonication and liquid-phase exfoliation, and finally centrifuged to obtain nanocrystals with a uniform hexagonal morphology. The synthesized SnS_2 QDs exhibited a diameter of approximately 50 nm and could be

dispersed in ethanol to form stable colloidal solutions. The size of the dispersed SnS_2 QDs ranged from 2 to 4 nm. The study demonstrates that the layered QDs produced through liquid-phase exfoliation offer themselves a wide range of tunable and precise controllable absorption over bandgaps.

4.3.5. Microwave-assisted synthesis method

The microwave-assisted method is a speedy, energy-efficient, and high-quality process that uses microwave radiation energy to facilitate chemical reactions and material transformations, particularly in the creation of nanomaterials. Chen *et al*.[188] produced photoluminescent CuInZnS QDs (CIZS QDs) using a room temperature ionic liquid (RTIL) under microwave irradiation. This RTIL, known for its high polarizability, serves as a microwave absorber, resulting in an increased instantaneous nucleation rate and enabling the rapid synthesis of CIZS QDs at lower temperatures. Furthermore, the surface modification of these QDs with RTIL has proven to be effective in passivating surface defects, ultimately enhancing the quality of the nanomaterials produced. Analysis by X-ray diffraction of multiple CIZS QDs with different levels of $[Bmim]BF_4$ addition exhibited almost indistinguishable results. The research revealed that the morphology of CIZS QDs was influenced by the quantity of $[Bmim]BF_4$ added. An increase in $[Bmim]BF_4$ led to a decrease in the sample peak intensity, indicating a notable impact on crystallinity and particle size. The CIZS QDs displayed nearly spherical shapes with average sizes of 4.11, 3.99, 3.70, 3.12, and 2.67 nm, respectively. Larger amounts of $[Bmim]BF_4$ resulted in smaller quantum dot sizes, attributed to reduced surface tension of the precursor due to higher RTIL concentration, promoting quicker nucleation of the QDs. In comparison to conventional methods utilizing mixed raw materials, shape-controlled CIZS QDs showed tunable emission peaks ranging from 677 to 579 nm, *i.e.* expanding the emission wavelength. This efficient approach is expected to be a valuable tool for rapid synthesis of CIZS QDs and with the flexibility over a wider range of emission wavelengths. In recent years, researchers have investigated various methods for synthesizing materials that are more efficient and environmentally friendly. One promising approach is the use of water as a solvent in a process known as green synthesis. This method holds potential for reducing the environmental impact of chemical reactions by replacing conventional solvents with water, which is a more sustainable and less toxic alternative. By utilizing water as a solvent, researchers can potentially reduce the use of hazardous chemicals and minimize waste generation during the synthesis process. This innovative strategy not only advances sustainable practices in chemical manufacturing but also underscores the growing importance of developing greener technologies within the field of materials science.

5. Metal sulfide QDs for PTT/PDT combination therapy in tumours

Significant advancements have been made in tumour PTT and PDT by designing and utilizing proper MS QDs. In addition to using standalone MS QDs, some researchers have modified QDs with folate (FA), hemi-branched cysteine bromide (Hemi-Br), GSH, bovine serum albumin (BSA), among others, to improve therapeutic outcomes. Moreover, incorporating anticancer drugs and PSs into the same delivery nano-system has demonstrated high treatment efficacy against cancer cells, further highlighting the potential for synergistic and multistage tumour-targeted therapy. Beyond tumour treatment, MS QD materials can also be utilized for early tumour diagnosis, tumour fluorescence imaging, and other applications, showcasing the versatility of these materials. This summary provides an overview of the research progress on various types of MS QDs that are employed in PTT/PDT for tumour treatment.

5.1. CuS QDs

Copper sulfide is known for its ideal visible light modulation capabilities and biocompatibility, which make it a promising material in the field of semiconductor selection. In particular, CuS QDs have garnered significant attention for their NIR absorption, low biotoxicity, superior photothermal conversion performance, and ease of surface modification. These unique properties have positioned CuS QDs as a valuable tool in the realm of tumour diagnosis and treatment, with potential applications as nuclear tracers, contrast agents, and in therapeutic diagnostics. Furthermore, CuS QDs offer the capability to effectively kill cancer cells through PDT and PTT effects, as well as responding to external stimuli for the controlled drug release. By integrating these diverse functionalities into a single system, CuS QDs have the potential to achieve material multi-functionalization to meet the complex requirements for both diagnostic and therapeutic applications.

In 2016, Tan *et al*.[189] developed thermo sensitive liposomes (TSL) modified with FA and polyethylene glycol (PEG) to serve as versatile nanocarriers for enhancing the solubility, stability, and biocompatibility of chlorine E6 (Ce6). For the first time, they utilized a combination of Ce6 and CuS (Ce6–CuS–TSL) for synergistic PDT and PTT therapy. Upon delivery of Ce6–CuS–TSL to tumour cells, the enclosed CuS was activated through 808 nm NIR laser exposure (1.5 W cm^{-2}, 5 min), causing PTT-induced cell damage and TSL breakdown as well. Subsequent release of Ce6 from the nanocarriers TSL, followed by irradiation with a 660 nm laser (1.0 W cm^{-2}, 3 min) in the presence of oxygen, resulted in the fulfillment of PDT-mediated cancer cell destruction. Ce6–CuS–TSL exhibited minimal dark toxicity while demonstrating potent phototoxicity when exposed to combined 660 and 808 nm laser irradiation, effectively suppressing tumour growth without observable adverse effects. The potential of Ce6–CuS–TSL as a reliable carrier for the dual therapy of cancer cells involving photothermal and photodynamic treatments is apparent. In the same year, Zhong *et al*.[190] creatively utilized chicken egg white (CEW) as a surface ligand to synthesize CuS QDs with a narrow size distribution of 7.1 ± 0.6 nm at body temperature (37°C). When subjected to 980 nm laser irradiation at 0.44 W cm^{-2}, the water-soluble CuS QDs achieved an impressive PCE of 47.2%. Additionally, these CuS QDs were found to have minimal cytotoxicity and exhibited a remarkable photothermal effect, effectively eradicating cancer cells both in laboratory experiments and animal studies. The biocompatibility and efficiency demonstrated by these CuS QDs make them promising candidates for PTT to eliminate tumour cells in living organisms. In the study carried out between 2020 and 2023, scientists made significant progress in the development and examination of CuS QDs. For instance, Zhao *et al*.[191] formulated and synthesized non-harmful and non-crystalline $Ag_{2-x}Cu_xS$ QDs. These particular $Ag_{2-x}Cu_xS$ QDs achieved efficient eradication of tumours through a strong photothermal impact guided by dual-mode imaging of NIR fluorescence/photoacoustic (PA), without inducing substantial pathological alterations in vital organ tissues. In the departure from traditional liver and breast cancer models, Zhang *et al*.[192] selected cutaneous

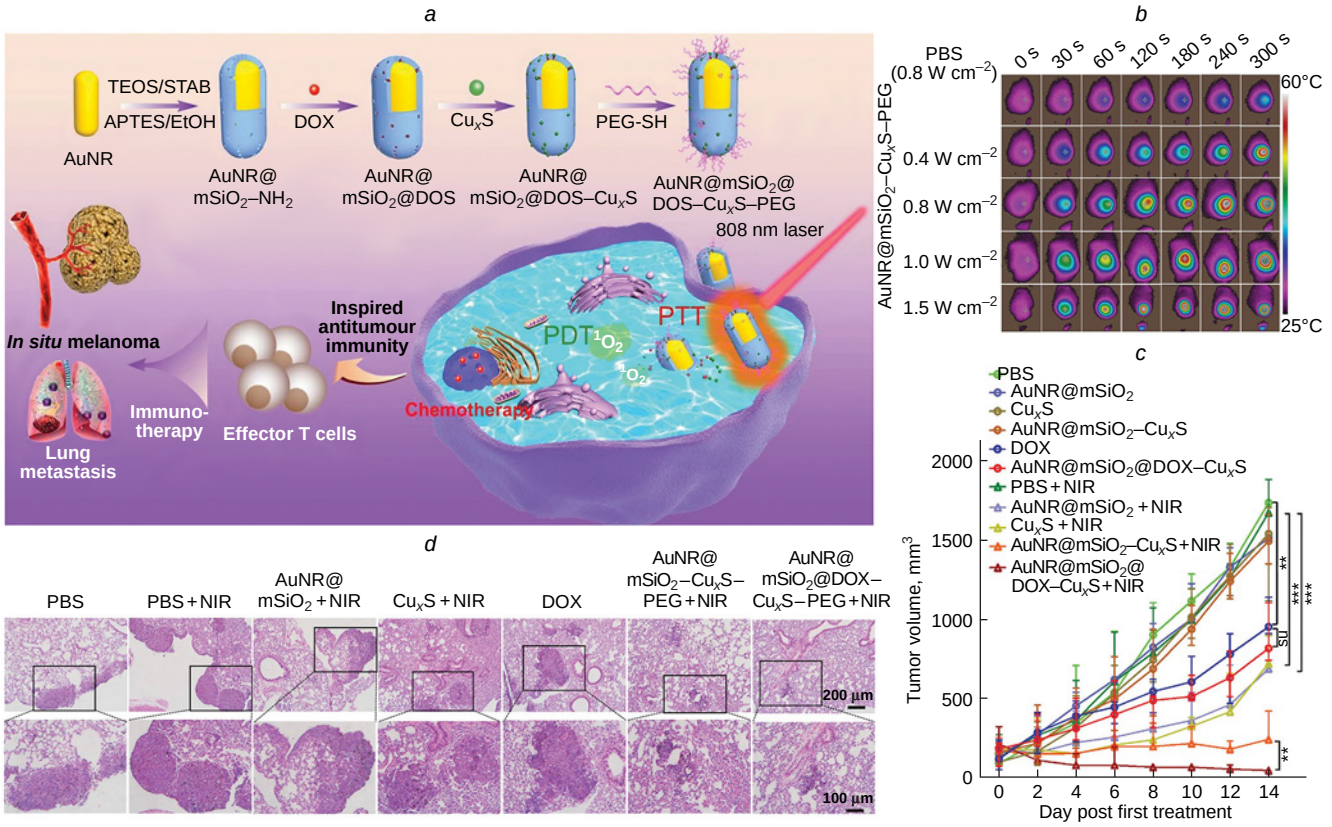

Figure 8. (*a*) The schematic illustration depicts the mechanism of the multifunctional Cu_xS- and DOX-loaded AuNR@$mSiO_2$ platform, which is triggered by NIR light for combined PTT, PDT, and CHT. (*b*) Thermographic images of tumour-bearing mice treated with either phosphate-buffered saline or AuNR@$mSiO_2$–Cu_xS and subjected to NIR irradiation at different times and power densities are displayed. (*c*) Measurements of tumour volume in mice following various treatments show significant differences. (*d*) Histological examination of lung metastatic nodules with H&E staining is presented for analysis. Reproduced (*a*–*d*) from Zhang *et al*.,[192] copyright (2021) the Royal Society of Chemistry.

melanoma for treatment and developed a multifunctional platform that could be activated by NIR light (AuNR@$mSiO_2$@DOX–Cu_xS–PEG) (Fig. 8). The PCE of the AuNR@$mSiO_2$–Cu_xS–PEG composite material was measured at 69.7%, significantly outperforming AuNR@$mSiO_2$ (36.8%) and Cu_xS (14.5%) alone. Moreover, the AuNR@$mSiO_2$@DOX–Cu_xS–PEG composite has exhibited potent tumour-killing capabilities and could simultaneously trigger CHT, PTT, and PDT effects *in vivo*. It also demonstrated notable efficacy in suppressing lung metastasis and eliciting a robust antitumour immune response. These findings highlight the potential clinical utility of AuNR@$mSiO_2$@DOX–Cu_xS–PEG for the treatment of cutaneous melanoma and metastatic lung cancer.

5.2. Ag_2S QDs

Silver sulfide QDs, known as NIR QD materials, are characterized by their low-toxic or non-toxic nature. Specifically, Ag_2S QDs are distinguished by their high biocompatibility, minimal cytotoxicity, excellent stability in aqueous solutions, and a narrow bandgap. These QDs emit photoluminescence in the NIR-II (1000–1700 nm), contrasting with those that emit in the NIR-I (700–900 nm).[193] Therefore, with Ag_2S QDs, there is a capability for enhanced penetration depth of photon energy exceeding 5 mm and a superior signal-to-noise ratio exceeding 100 during practice treatment. Their utilization has grown rapidly, extending to various biological and cellular imaging applications. Ag_2S QDs have showcased the ability to generate ROS effectively under NIR light, offering potential for combined delivery with anticancer medications to target tumour tissues.[194] Their potential as outstanding agents for tumour PTT holds promise.

In 2016, Gao *et al*.[195] utilized a custom-designed aptamer to directly produce water-soluble Ag_2S QDs with NIR fluorescence for targeted tumour imaging and PTT at ambient temperature. This synthesis process omits any harmful chemical reducing agents, thus diminishing potential biological hazards in live cells during the application practice, rendering the QDs an optimal tool in biological applications. In 2018, Zhao *et al*.[196] introduced an innovative hybrid nanogel structure incorporating Ag_2S QD@PC10ARGD for precise NIR-II fluorescence imaging, PA, and PTT of tumours. These hybrid nanogels possess substantial promise for early tumour diagnosis and therapy. In the follow-up study,[197] the authors fabricated Ag_2S QDs (CPCC-Ag_2S QDs) coated with genetically engineered peptides (RGDPC10A) for NIR-II fluorescence imaging, PA, and PTT of tumours. These QDs demonstrated remarkable stability, resistance to photobleaching, and a QY reaching 3.78% in the NIR-II biological window. This investigation introduced a novel strategy for constructing therapeutic platforms for early tumour diagnosis and therapy. In 2021, Gao *et al*.[198] synthesized GSH-Ag_2S QDs through an aqueous precipitation approach to serve as both a fluorescent imaging tool and a water-phase synchronous PTT probe. By adjusting the duration of heating, the size of GSH-Ag_2S QDs could be precisely modulated within the 2.0–5.8 nm range. These QDs boasted their wide absorption spectra and narrow fluorescence emission spectra in the NIR region, showcasing a distinct emission peak between

808–815 nm, rendering them suitable for cellular imaging applications. With their intrinsic fluorescence properties, GSH-Ag_2S QDs present significant potential for PTT cancer therapy, obviating the necessity for supplementary tracking agents through the fluorescence-guided imaging. Hashemkhani *et al.*[199] integrated therapeutically active AS-2MPA Ag_2S QDs, optically trackable in the NIR spectrum, with cetuximab aimed at the epidermal growth factor receptor (EGFR) and loaded with 5-aminolevulinic acid for PDT. This combination therapy, used alone or with 5-fluorouracil, aimed to enhance therapeutic outcomes in EGFR-positive colorectal cancer. In 2025, Kim *et al.*[200] reported a biosynthetic protein Ag_2S QD (mussel-protein-mineralized silver nanodots; MSND) *via* specific motif-mediated silver biomineralization (Fig. 9). This MSND represents a biosafe, high-performance PS that enables near-infrared-triggered theranostics for localized cancer therapy. *In vitro* phototherapy experiments demonstrated that MSNDs can generate ROS with remarkable efficacy under NIR irradiation and exhibit a substantial PCE (~59%). Furthermore, the outstanding photochemical functionality of MSNDs allows for direct cancer cell eradication through potent photodynamic and photothermal actions in the presence of an 808 nm NIR laser. Long-term safety assessments indicated that MSNDs undergo effective biodegradation and clearance, demonstrating excellent biocompatibility and addressing a key regulatory concern for clinical translation. Most importantly, the significant therapeutic efficacy observed in both small and large animal tumour models, without compromising long-term systemic safety, renders MSNDs highly promising for clinical cancer therapy applications. This platform overcomes the major limitations of traditional PSs, offering a clinically translatable theranostic strategy for precise and complete cancer ablation in a minimally invasive manner.

5.3. MoS_2 QDs

In recent years, with the vigorous development of nanotechnology, molybdenum-based nanomaterials have gradually attracted extensive attention in the biomedical field because of their excellent biocompatibility, high catalytic activity, redox chemistry and strong light heat conversion efficiency, which greatly promoted the diversified application of molybdenum-based nanomaterials in the biomedical field.[201] Molybdenum sulfide (MoS_2) is a substance from the family of

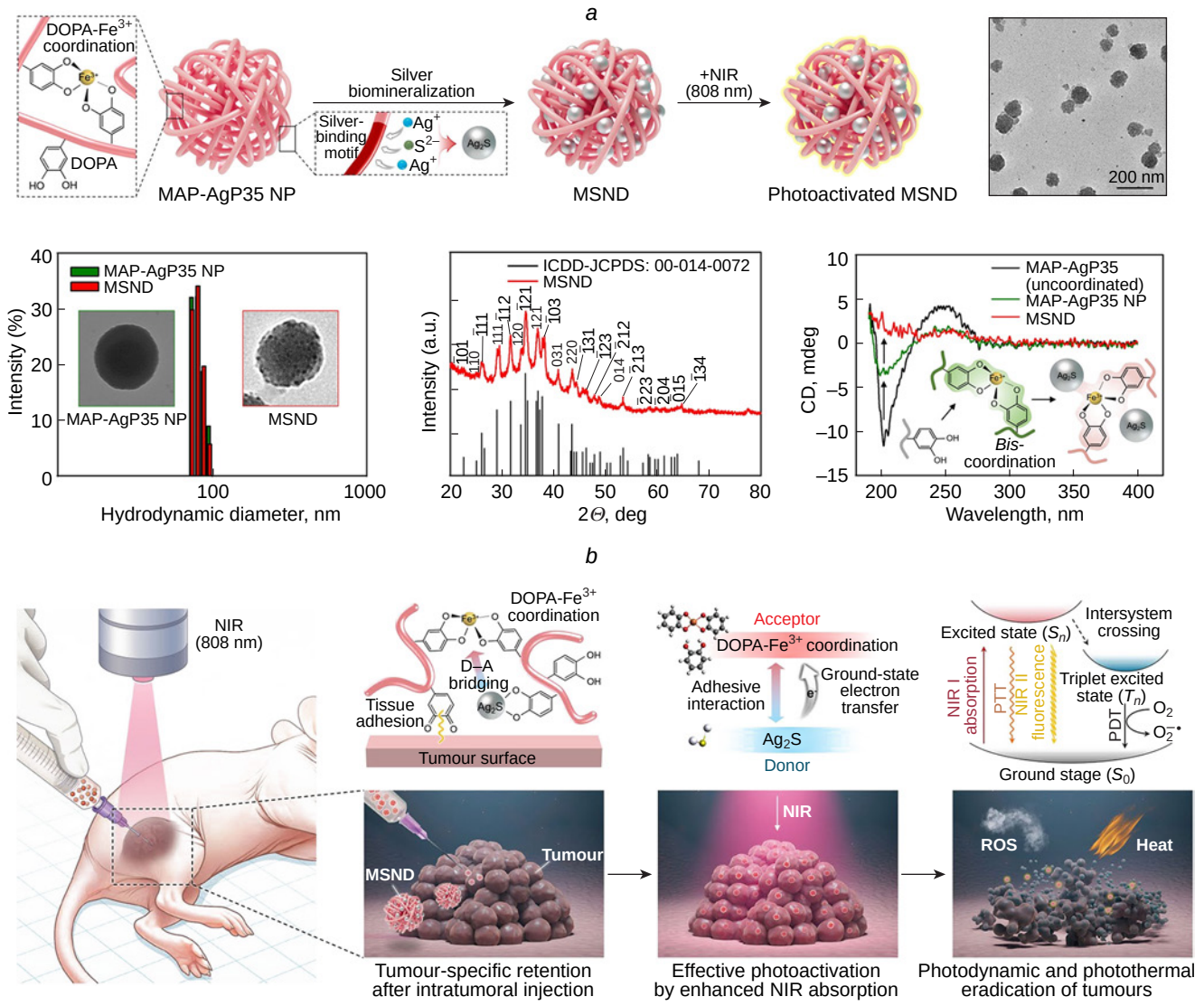

Figure 9. (*a*) Synthesis and characterization of the MSNDs. (*b*) MSNDs as NIR theranostics enable externally controlled, localized cancer therapy. Reproduced from Kim *et al.*[200] under CC BY-NC-ND 4.0. License.

transition metal dichalcogenides, featuring a layered structure similar to graphene. MoS_2 QDs exhibit certain catalytic activity and excellent fluorescence properties. Moreover, compared with other QDs such as CuS QDs or PbS QDs, MoS_2 QDs have shown low cytotoxicity, making them a popular material for quantum dot research in recent years.

Dong *et al.*[202] utilized tetrabutylammonium-assisted ultrasonication to trigger OH-mediated chain-like Mo–S bond dissociation in multilayer MoS_2 powder, affording small-sized MoS_2 QDs with desired optical properties. These MoS_2 QDs displayed exceptional downconversion photoluminescence behaviour and showed a superior ability to generate toxic $O_2^{-\bullet}$ in the presence of the commercial PS Protoporphyrin IX disodium salt, making them extremely promising for use in PDT. On the other hand, Wang *et al.*[203] developed a multifunctional nanomaterial comprising MoS_2QDs@polyaniline (MoS_2@PANI) inorganic-organic nanohybrids, which demonstrated impressive PA/CT imaging capabilities and a significant tumour homing effect. Moreover, this nanomaterial effectively treated cancer through a combination of RT and PTT, achieving a PCE of 31.6%. The intravenous injection of MoS_2@PANI hybrid nanoparticles followed by localized laser irradiation resulted in notable cell death rates of 62.3% for PTT, 51.1% for RT, and 78.4% for PTT/RT in 4T1 cells. The synergy of photothermal and radiotherapy guided by PA/computerized tomographic (CT) imaging using MoS_2@PANI has enabled precise tumour targeting and complete tumour eradication, demonstrating the immense potential of this versatile nanohybrid material. Liu *et al.*[204] developed a composite material (PEG-MoS_2-Au-Ce6) for visual-guided PTT/PDT in anti-tumour applications. Exposed to 808 nm laser (1.5 W cm^{-2}) for 10 min, PEG-MoS_2-Au-Ce6 reached a peak temperature of 59.2°C. The PEG-MoS_2-Au-Ce6 treatment led to a 72.3% cell death rate, indicating a significant inhibitory action on cancer cells through PTT/PDT combination therapy. In addition, PEG-MoS_2-Au-Ce6 showed a preference for its accumulation at the tumour sites, achieving peak uptake at 6 h. Administering PEG-MoS_2-Au-Ce6 to the female BALB/c nude mice resulted in a swift rise in tumour surface temperature from 25 to 57°C within 5 min, triggering cancer cell death *via* thermal therapy. The survival rate of the treated mice remained at approximately 100% after 30 days. Therefore, this dual-modal nano-system displays encouraging synergistic effects in PTT/PDT-based antitumour therapy. Li *et al.*[205] created ultra-small MoS_2 QDs designed for PTT that was guided by CT and multispectral optoacoustic tomography imaging techniques. By embedding the MoS_2 QDs into removable nanoparticles of SiO_2, this nanoparticle not only broke down and exited the body within an appropriate timeframe through the influence of GSH redox reaction but also displayed significant tumour uptake because of

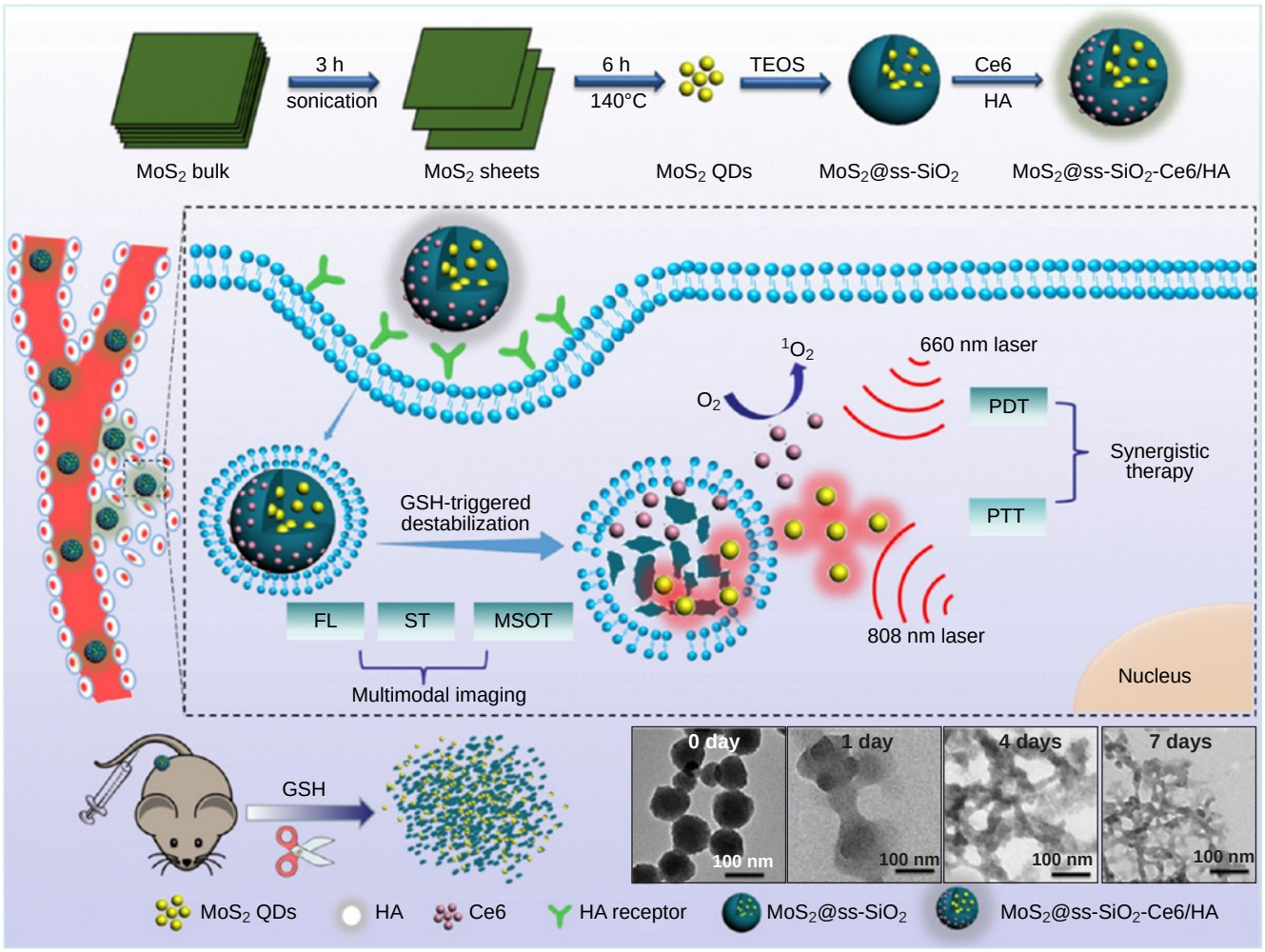

Figure 10. Formation and operation of MoS_2@ss-SiO_2-Ce6/HA nanocomposites and GSH-responsive degradation mechanism leading to efficient removal from the body. Reproduced from Li *et al.*[205] with permission from the American Chemical Society.

its prolonged circulation in the blood. In addition, hyaluronic acid and Ce6 were attached to the surface, offering tumour-targeting and PDT abilities (Fig. 10). In the experiment with 4T1 tumour-bearing mice, the MoS_2@ss−SiO_2−Ce6/HA+808/660 nm treated group exhibited slight weight loss by day 21, notable tumour inhibition, and minimal adverse effects. The survival rate after 35 days was close to 100%, with the mice having the smallest tumour size, showcasing the superior effectiveness of the combined treatment in comparison to individual therapies. Thus, the MoS_2@ss-SiO_2-Ce6/HA nanostructure, combined with the 808 nm/660 nm laser, displayed improved anti-tumour properties in PTT/PDT therapy.

5.4. ZnS QDs

Zinc sulfide QDs have various benefits including excellent luminescence efficacy, extended fluorescence longevity, and adjustable emission ranges. They have the potential to act as emitters in electrochemiluminescence processes or engage in energy resonance transfer as both acceptors and donors of energy. The utilization of ZnS QDs is prevalent in fields like biosensing and medical diagnostics.

Combining commercialized magnetic resonance imaging (MRI) contrast agents with emerging tumour treatment methods enables precise tumour information, facilitating clear image-guided therapies. Irmania *et al*.[206] synthesized CuInSe QDs doped with Mn and coated with a ZnS passivation layer. They utilized GSH as a stabilizer in a one-pot microwave-assisted hydrothermal reaction. The resulting MnCuInSe/ZnS core-shell QDs can improve MRI capabilities, red emission efficiency, and ability to generate ROS. These QDs display a QY of 40%. When exposed to 671 nm (1.0 W cm^{-2}) laser for 5 min, MnCuInSe/ZnS QDs can eradicate over 80% of B16 cells, demonstrating minimal cytotoxicity and efficient singlet oxygen production for PDT in cancer therapy. Furthermore, they are suitable for fluorescence imaging and assessing cellular uptake, visualizing uptake and ROS production within cells. As a result, MnCuInSe/ZnS QDs offer a promise as cutting-edge therapeutic nanomaterials and versatile imaging and PDT agents for biomedical purposes. Choi *et al*.[207] fabricated QDs with a core/shell structure containing cadmium selenide/zinc sulfide. When these CdSe/ZnS QDs were used independently, a slight increase of 17% in ROS production was observed. Nonetheless, upon exposure to the presence and absence of ultraviolet A/B (UVA/UVB) irradiation, ROS levels rose significantly to 32% and 64% correspondingly, demonstrating the ability of CdSe/ZnS QDs to generate ROS, as the light sensitizers, when exposed to UV light. Experiments were conducted on A549 lung adenocarcinoma cells to assess the impact of CdSe/ZnS QDs in conjunction with UVA/UVB radiation. The findings revealed a more pronounced effect on A549 cells as exposed to CdSe/ZnS QDs combined with UVB radiation (cell viability of 68.81%) compared to CdSe/ZnS QDs combined with UVA irradiation (cell viability of 82.01%) or CdSe/ZnS QDs alone (cell viability of 89.2%), indicating the potent phototoxic properties of CdSe/ZnS QDs on A549 cells under UVB exposure. The level of apoptosis in A549 cells treated with CdSe/ZnS QDs+UVB was notably elevated (four times higher than the untreated control) compared to cells treated solely with QDs or UVA (both two times higher than the untreated control), suggesting that UVB irradiation effectively enhances the therapeutic efficacy of QDs in photodynamic cancer treatment. Normally, due to the limited ability of tissues to light penetration, the use of PDT in chondrosarcoma cases is infrequent. To tackle this obstacle, Mohsenian *et al*.[208] developed manganese-doped zinc sulfide QDs (Mn-doped ZnS QDs) and attached the PS Ce6 onto them using both covalent and non-covalent bonding techniques. The Mn-doped ZnS QDs-chlorin e6 complex was then coated with 3-mercaptopropionic acid for application in a combined therapy involving radiation of X-ray and PDT for chondrosarcoma treatment. Following exposure of chondrosarcoma cells to the QDs, there was a notable reduction in cell viability by around 40%, demonstrating the potential of X-rays in activating the quantum dot complex for cancer treatment. This innovative combination therapy could offer a promising treatment strategy for chondrosarcoma. Studies by Orlova and co-workers[209] have revealed that $Cd_xZn_{1-x}Se_yS_{1-y}$/ZnS QDs, featuring a thick gradient semiconductor shell, can reduce the probability of Förster resonance energy transfer (FRET) or electron transfer, thereby suppressing the photoluminescence of the QDs. The nanostructures formed by combining superparamagnetic iron oxide nanoparticles (SPIONs) with these QDs exhibit excellent stability, are effectively internalized by HeLa cells, and do not exhibit significant cytotoxicity at concentrations up to 25 nM. Furthermore, the authors developed a water-soluble nano-composite by incorporating chitosan (CS)-passivated hydrophobic tetraphenylporphyrin (TPP) molecules with CdSe/ZnS QDs.[210] Spectroscopic analysis confirmed the coexistence of TPP in both monomeric and aggregated forms within the nanocomposite. Due to the FRET within the composite, the nanocomposite demonstrated a significantly enhanced singlet oxygen generation compared to free TPP at an equivalent concentration in CS solution, with an average FRET efficiency of 45%. Owing to the synergistic effects derived from the introduction of QDs and the FRET from QDs to TPP monomers, this nanocomposite exhibits excellent stability and highly efficient singlet oxygen production. Therefore, this system represents a promising candidate as an ideal singlet oxygen generator for PDT.

5.5. Other MS QDs

5.5.1. $CuInS_2$ QDs

Being a representative metal chalcogenide semiconductor, $CuInS_2$ (CIS) has garnered significant attention for its remarkable optical and electrochemical properties, high chemical stability, and low toxicity. These attributes make it a promising candidate for biomedical applications. Specifically, $CuInS_2$-based nanostructures are emerging as viable agents for antimicrobial and anticancer therapies, leveraging their ability to generate photodynamic or photothermal effects even under NIR light irradiation. Concurrently, $CuInS_2$ QDs have become a focal point in photocatalysis research due to their strong absorption coefficient, excellent compatibility with solar spectrum, prolonged charge carrier lifetimes, and eco-friendly nature.[211,212] A study by Lv *et al*.[213] featured CuInS/ZnS QDs (ZCIS QDs) as versatile therapeutic nanomedicines (NMs). These ZCIS QDs, with efficient absorption between 650−750 nm, were utilized for multispectral optoacoustic tomography imaging and combined PTT/PDT treatments (Fig. 11). The research revealed that smaller nanomedicines (ZCIS NMs-25) possessed increased tumour retention, higher tumour uptake, and enhanced tumour penetration compared with larger counterparts (ZCIS NMs-80). By subjecting ZCIS QDs to a 660 nm laser (1.0 W cm^{-2}) for 10 min, both

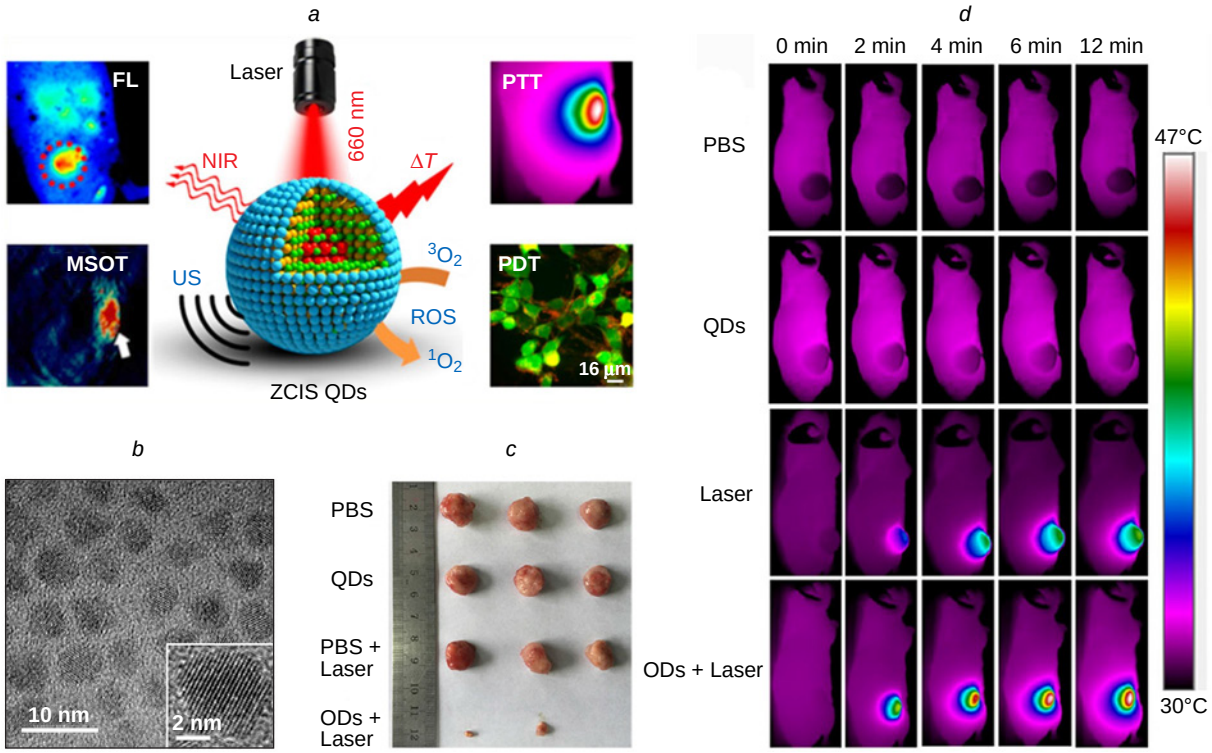

Figure 11. (*a*) Schematic illustrating ZCIS QDs for multispectral optoacoustic tomography imaging and combined PTT/PDT therapy, (*b*) Transmission electron microscopy and high-resolution transmission electron microscopy (insert) visuals of ZCIS QDs, (*c*) Images of tumours of mice in various groups following treatment completion, (*d*) Infrared thermal imaging of 4T1 tumour-carrying mice post intravenous administration of ZCIS NMs-25 and subsequent exposure to 660 nm laser irradiation. Reproduced from Lv *et al*.[213] with permission from the American Chemical Society.

photothermal and photodynamic effects were observed, resulting in a rise in tumour temperature to 46°C and over 95% cell death in 4T1 tumour cells, demonstrating significant therapeutic efficacy against tumours. Overall, the multifunctional ZCIS QDs served as excellent precision therapeutic nanomedicines, showcasing superior therapeutic efficacy and also non-invasive tumour localization through advanced imaging techniques. Mao *et al*.[214] developed biocompatible ZCIS QDs free of toxic heavy metals for use in photothermal nanomedicine. These QDs were modified on the non-optical portion of intraocular lenses (IOLs) through a soaking method following facial activation. When exposed to gentle NIR laser irradiation, the modified IOLs (QDs-IOLs) produced localized warmth, effectively suppressing the growth of lens epithelial cells on their surface. This research offers empirical support for the potential utility of nanotechnology and PTT in addressing posterior capsule opacification. Feng *et al*.[215] introduced CIS/ZnS QDs-ALA conjugates as a new multiphoton-excited PDT PS with a FRET efficiency of 58.49%. The cell survival rates after laser irradiation at 800 nm and 1300 nm were below 40%, suggesting the conjugates possess promising PDT properties for combatting cancer. Tsolekile *et al*.,[216] on the other hand, successfully synthesized large quantities of $CuInS_2$/ZnS QDs *via* aqueous synthesis and linked them with 5,10,15,20-tetrakis(4-hydroxyphenyl) porphyrin. This resulting conjugate exhibited excellent water solubility and stability lasting over 6 months. And the conjugate's ability to generate singlet oxygen highlighted its potential for use in PDT treatments, further emphasizing its importance in the field of cancer therapy.

5.5.2. $AgInS_2$ QDs

$AgInS_2$ (AIS) QDs have a wide bandgap and can emit light in the visible spectrum, specifically in the 600–800 nm range, ideal for medical imaging.[217] In 2020, Hashemkhani *et al*.[218] synthesized $AgInS_2$ QDs coated with glutathione, showing a QY of 21% and long-term stability without a protective inorganic coat. These nano crystals were able to induce a modest increase in temperature, approximately 10°C at 640 nm (300 mW) for 10 min, and 20°C at 808 nm (700 mW) for the same duration. Cell culture experiments revealed good biocompatibility of the coated QDs with various cell lines, including HeLa, HT29, A549, and C2C12, displaying strong intracellular fluorescent signals with minimal cell damage, thus demonstrating their potential for medical imaging. The mild photothermal effect of these nano crystals could potentially be utilized for triggering temperature-dependent drug release. In 2022, the authors used a mixture of polyethyleneimine/2-mercaptosuccinic acid (referred to as AIS-PEI/2MPA) or solely 2-mercaptosuccinic acid (referred to as AIS-2 MPA) as stabilizing agents in order to carry out a simple one-step synthesis of $AgInS_2$ QDs assemblies (referred to as either cationic or anionic AIS QDs assemblies) in as aqueous medium.[219] Both types of AIS QDs were taken up by different cancer cells (including HeLa, HCT116, SW490, and HT29) and displayed strong intracellular luminescence beyond 600 nm (within the optical imaging range) after being stimulated at 488 nm, showcasing their efficacy in medical imaging. Of significant note, these QDs were able to encapsulate the zwitterionic prodrug ALA, thereby increasing the concentration of ALA in tumours and enhancing ALA-mediated porphyrin PDT. The AIS QDs exhibited robust intracellular

photoluminescence, and particularly with the anionic AIS QDs showing excellent biocompatibility and serving as efficient carriers for PDT drugs, indeed highlighting their promising therapeutic potential as QDs.

5.5.3. WS_2 QDs

As a nanostructured transition metal dichalcogenide, WS_2 has shown great potential as a NIR absorber for PTT in cancer treatment. Additionally, the high atomic number of tungsten makes WS_2 a promising radiosensitizer, enhancing the effects of PTT and RT when combined with the treatment.[220,221] Yong *et al.*[20] developed a multifunctional nanomedicine using WS_2 QDs, demonstrating their effectiveness as both radiosensitizers and PTAs for PTT and RT combination therapy. The small-sized WS_2 QDs, generated through a 'green' physical grinding and ultrasonication, exhibited improved CT/PA signals and effectively killed cancer cells with moderate hyperthermia during PTT/RT treatment. *In vivo* studies confirmed the feasibility of using WS_2 QDs for combination therapy through intratumoural administration. *In vitro* experiments showed that the combination therapy of RT/PTT using WS_2 QDs resulted in a significant decrease in cell survival rates compared to using WS_2 QDs alone. The synergistic effects of PTT and RT led to precise tumour localization and complete eradication *in vivo* after intravenous injection of WS_2 QDs. Importantly, WS_2 QDs demonstrated no toxicity in both *in vitro* and *in vivo* studies, indicating their excellent biocompatibility. WS_2 QDs present a novel avenue for the exploration of nanoplatforms for both biomedical imaging and the combined treatment of tumours using RT and PTT. These versatile nanoparticles are essential in enabling the effectiveness of PTT and RT combination therapy,

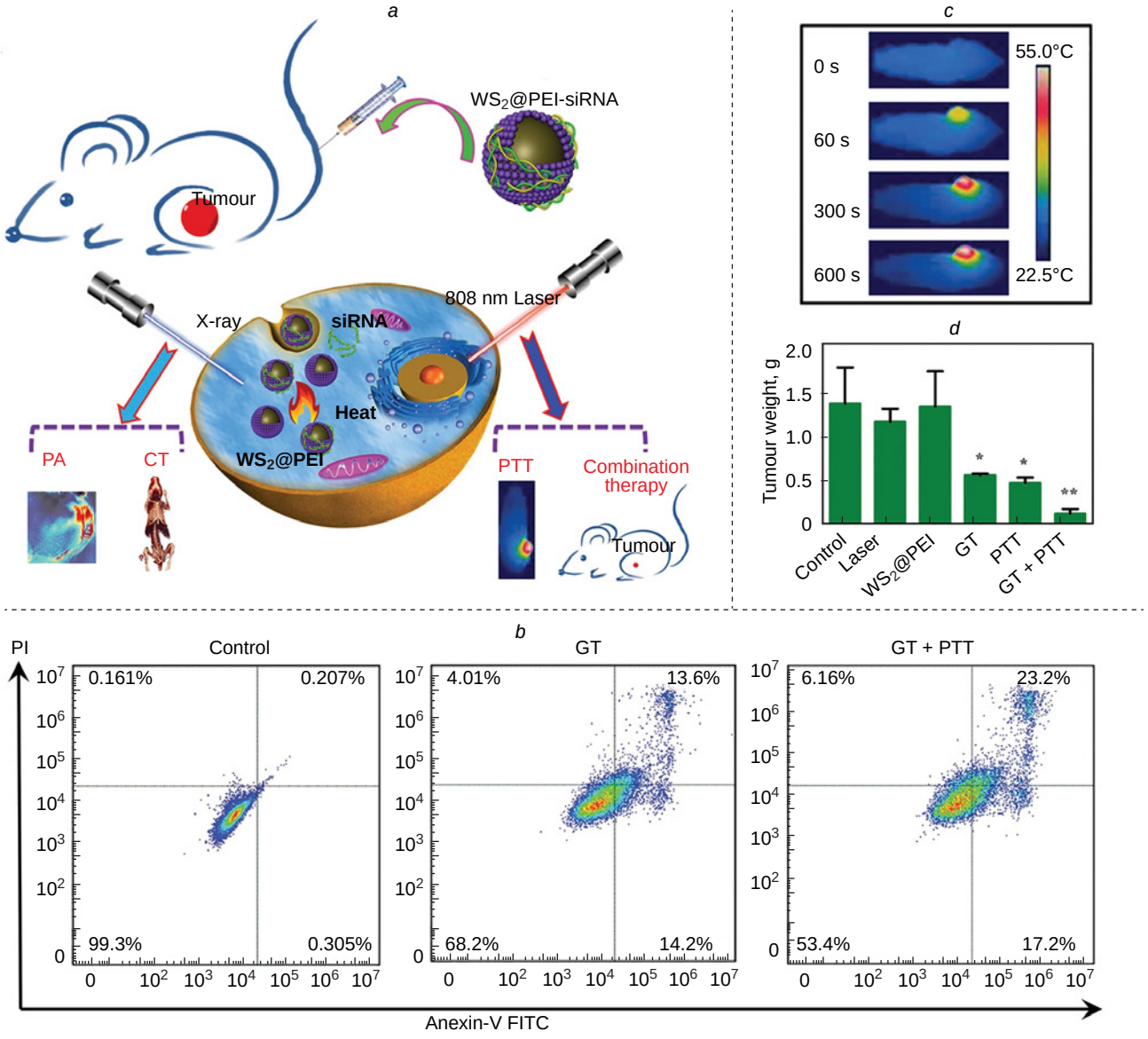

Figure 12. (*a*) Nanoplatforms composed of polyetherimide and WS_2 with versatile functions for the treatment of cancer through a combination of gene-photothermal therapy guided by imaging. (*b*) Flow cytometry analysis of BEL-7402 cells after various treatments for a 24 h, showing representative images. (*c*) Thermal images captured *via* NIR of Balb/c nude mice with BEL-7402 tumours treated intratumourally with WS_2@PEI (40 μg) and subjected to 808 nm laser irradiation at different time points. (*d*) The weight average of tumours harvested from different groups of mice with tumours after diverse treatments. Statistical significance was assessed using one-way ANOVA: $*p < 0.05$ and $**p < 0.01$. Reproduced from Zhang *et al.*[221] with permission from Wiley.

along with facilitating multimodal imaging to enhance treatment outcomes.

In this context, small interfering RNA (siRNA) emerges as a promising carrier to target and inhibit the expression of specific genes, thereby preventing the translation of messenger RNA into proteins. The heat shock response induced by PTT contributes to the thermal resistance observed in cancer cells, which hinders the efficacy of thermal therapy by impeding apoptosis. Through the modulation of gene expression, siRNA can effectively regulate the relevant genes associated with the heat shock response, ultimately increasing the sensitivity of cancer cells to PTT therapy.[222,223] Combining PTT with GT is a strategy aimed at improving the effectiveness of PTT and achieving tumour eradication in sublethal conditions. Zhang *et al*.[221] developed a multifunctional WS_2@polyetherimide (WS_2@PEI) nanoplatform for CT/PA imaging-guided PTT/GT combination therapy (Fig. 12). After 10 min of irradiation with an 808 nm NIR laser at 1.0 W cm^{-2}, the cell viability of BEL-7402 cells treated with WS_2@PEI+GT, WS_2@PEI+PTT, and WS_2@PEI+GT+PTT decreased to 60%, 53.8%, and 13% respectively. In addition, the cell viability of Hela cells decreased to 45%, 41%, and 12.4%, respectively, demonstrating a significant synergistic effect of GT+PTT *in vitro*. Furthermore, laser irradiation of Balb/c nude mice with BEL-7402 tumours resulted in a rapid temperature increase to around 43°C at the tumour site after 10 min of treatment, inducing mild hyperthermia and facilitating the transfection of survivin-siRNA to eliminate cancer cells. By the 12 days post-treatment, the rate of tumour growth inhibition reached 91.7%, indicating not only the suppression of tumour growth but also the effective prevention of tumour recurrence. In summary, the use of WS_2@PEI-siRNA nanocomplexes presents new opportunities for the development of multifunctional nanoplatforms that can enhance tumour PTT through gene therapy in mild conditions.

5.5.4. CoS QDs

Transition metal dichalcogenides, such as cobalt sulfides, are complex compounds with varying crystal phase structures and chemical formulas due to different stoichiometric ratios.[224] CoS is a superior semiconductor material that shows exceptional performance in electrochemistry and as fuel cell catalysts,[225,226] CoS QDs exhibit PTT and CDT effects, ultimately displaying potent anti-cancer properties by enhancing power conversion efficiency and quenching-like activities. Yang *et al*.[227] developed a dual-targeting strategy utilizing a peptide/exosome/cobalt sulfide quantum dots nanocomplex (PEP/Exo/CoS QDs) for efficient PTT and CDT treatment of bladder cancer. The CoS QDs demonstrate dual therapeutic effects, offering a comprehensive approach to managing bladder cancer. In the PEP/Exo/CoS treatment cohort, more than 90% of bladder cancer cells exhibited specific binding and internalization of the PEP/Exo/CoS nanocomplex as indicated by PKH 67 fluorescence. Upon laser irradiation (808 nm, 0.8 W cm^{-2}), the temperature of the Exo/CoS complex could reach 48°C while maintaining it stabile, resulting in a significant apoptosis rate of 93.45%. CoS QDs and exosomes can selectively target cancer cells with minimal impact on healthy tissues, and each exosome is capable of carrying multiple QDs. This innovative study presents a promising strategy for the holistic management of advanced bladder cancer. Zhu *et al*.[228] developed a series of engineered biodegradable CoS_x QDs with sulfur deficiency to enhance the combined PTT and CDT for tumours by regulating PCE and Fenton-like activity. The CoS_x QDs have the ability to induce cancer cell death through multiple mechanisms: (1) catalyzing a Fenton-like reaction to produce more ROS from the body's own H_2O_2, resulting in oxidative stress within cancer cells; (2) disrupting the cellular antioxidant defense system by converting GSH to glutathione disulfide through redox reactions, thereby promoting ROS production; (3) conducting thermal ablation of cancer cells using the photothermal properties of CoS_x QDs; and (4) increasing the rate of Fenton reaction between CoS_x QDs and endogenous H_2O_2 due to the heat generated during the photothermal conversion process. When exposed to NIR laser irradiation (808 nm, 0.8 W cm^{-2}), sulfur-deficient CoS_x QDs demonstrated superior photothermal performance with a PCE of 40.5%. Therefore, following 5 min of laser irradiation, the viability of both 4T1 cells and A431 cells noticeably decreased. After 8 min of laser treatment, the temperature in the tumour region of mice rapidly rose to 52°C. Moreover, the exceptionally small size and biodegradable nature of the QDs facilitated their quick decomposition into ions after the treatment, enabling easy elimination from the body and thereby reducing systemic build-up and potential side effects. These defect-driven CoS_x QDs present as a promising candidate for a personalized multifunctional therapeutic approach against tumours, with adaptable and effective treatment outcomes in the realm of cancer therapy.

5.5.5. Bi_2S_3 QDs

Bismuth is widely recognized for its high biocompatibility and low toxicity levels.[229–231] Bismuth sulfide (Bi_2S_3), an important semiconductor with n-type photoelectric properties, boasts a remarkable absorption coefficient and direct bandgap in the NIR range (1.3–1.7 eV).[232] Various Bi_2S_3 nanomaterials have been created for treating cancer through PDT and PTT.[233–235] Yang and co-workers[236] have successfully developed ultra-small poly-*L*-lysine-coated QDs of bismuth sulfide (PLL-Bi_2S_3 QDs) with an average size of 2.7±0.5 nm. These QDs have proven to enhance cell penetration for combined PDT/PTT therapy, achieving a remarkable PCE of 25.7%. When exposed to 808 nm NIR laser at 0.8 W cm^{-2}, the PLL-Bi_2S_3 QDs can generate ROS and heat, showcasing their efficacy in PDT/PTT combination therapy in both *in vitro* and *in vivo* settings. The apoptosis rates of cells treated solely with PLL-Bi_2S_3 QDs and those treated with a combination of QDs and laser irradiation were 12.7% and 55.3%, respectively. Treatment with PLL-Bi_2S_3 QDs for 24 h followed by 7 min of laser irradiation resulted in significant damage to cancer cells such as MCF-7, HepG2, and HeLa, with over 90% cell death observed at a concentration of 150 μg mL^{-1}. In addition, PLL-Bi_2S_3 QDs demonstrated excellent biocompatibility, highlighting their potential as effective PSs for cancer therapy. Moreover, ultrasound, characterized by outstanding tissue penetration and non-invasive acoustic energy targeting capabilities, holds promise for effectively reaching deep tissues. Sonodynamic therapy is an innovative treatment approach that relies on sonosensitizing agents to absorb ultrasound waves, leading to the stimulation of surrounding oxygen and the generation of ROS to eliminate cancerous cells.[237,238] Meng *et al*.[239] developed a nanoplatform for phototherapy (HA@Bi_2S_{3-x}−Au) that effectively destroyed tumours by combining PPT/PDT guided by NIR-II laser-induced PA imaging. The light that hit the Au NPs on the surface triggered LSPR, allowing HA@

Bi_2S_{3-x}–Au to display outstanding NIR-II optical properties and achieve a high PCE of 43%. The temperature peak of HA@Bi_2S_{3-x}–Au at 1064 nm (1.0 W cm^{-2}) was 55.4°C. Even at a high concentration (800 μg mL^{-1}), cell viability was above 80%, indicating minimal inherent toxicity towards L929, 4T1, and HeLa cells and underscoring the excellent biocompatibility of HA@Bi_2S_{3-x}–Au for *in vivo* therapy. The synergy of PTT/PDT/SDT led to a significant drop in cell viability of 4T1 and HeLa cells to 7.65% and 7.45%, respectively, during simultaneous treatment with 1064 nm laser irradiation and ultrasound (3.0 W cm^{-2}). In mice injected with HA@Bi_2S_{3-x}–Au intravenously, tumour site temperatures rose to approximately 55ºC after just 5 min of laser exposure, enough to trigger the photothermal effect essential for tumour destruction. The tumour growth inhibition rate was an impressive 92.3% after 14 days. Given its outstanding photothermal properties, HA@Bi_2S_{3-x}–Au emerges as a promising nanocomposite material for eradicating tumour cells. Dou *et al*.[240] developed a nanocomposite material (PVP–rGO/Bi_2S_3) functionalized with polyvinylpyrrolidone (PVP) using Bi_2S_3 nanoparticles for chemophotothermal synergistic cancer treatment. These nanocomposites showed a high capacity for drug loading (500% for doxorubicin (DOX)) and exhibited excellent performance in the NIR spectrum (47.83% PCE). When combined with laser irradiation in the NIR range, PVP–rGO/Bi_2S_3@DOX complexes were utilized to combat liver cancer cells (including Hela, MCF-7, and HepG2 cells) as well as BEL-7402 tumour-bearing mice. PVP–rGO/Bi_2S_3 nanocomposites exhibit promising potential as therapeutic tools for dual-mode imaging-guided chemophotothermal combination therapy for cancer and advocate for further exploration and innovation of such multifunctional nanocarriers for imaging-directed therapeutics within the realm of biomedical research.

5.5.6. FeS QDs

Iron is a crucial element found in the human body, and also the magnetic resonance (MR) contrast agents with iron as the base are known for their biocompatibility.[241] Indeed, nanoparticles composed of FeS not only have the ability for MR imaging but also demonstrate increased absorbance in the NIR region, with the capability to convert absorbed NIR light into heat.[242] Thus, these nanoparticles can serve as the dual-modal imaging agents for tumour diagnosis aiding in tumour PTT. Yang *et al*.[243] successfully synthesized FeS QDs with a small size of 3.0 nm that were well dispersed (FeS@BSA QDs). The PCE of FeS@BSA QDs was measured at 30.04%. Even at a concentration of 1000 μg mL^{-1}, the viability of DC2.4 cells and 4T1 cells remained above 80% after 24 and 48 h of exposure, demonstrating the excellent biocompatibility of FeS@BSA QDs. The colour of tumour lesions darkened five hours post intravenous administration of deep green FeS@BSA QDs, indicating a high accumulation of the nanoparticles in the tumour. Following irradiation with a 660 nm laser (2.0 W cm^{-2}) for 10 min at the tumour site of balb/c mice bearing 4T1 tumours and treated with FeS@BSA QDs, there was a rapid increase in tumour temperature from 26 to 57°C. Post imaging and therapeutic procedures, these QDs can be eliminated from the body through urine. FeS@BSA QDs exhibit valuable characteristics like small size, effective longitudinal relaxivity, proficient photothermal conversion, and a high rate of renal clearance, making them a potent agent for T1-weighted MR/PTT/PDT applications.

6. PTT/PDT combination therapy and effect of MS QDs

Although significant progress has been made in utilizing MS QDs for tumour treatment via combined PTT/PDT, their overall therapeutic efficacy remains suboptimal and requires further improvement. To enhance their effectiveness, researchers have explored various strategies, including tuning the physical properties of MS QDs, modifying their surfaces, and increasing their multifunctionality. Additionally, efforts have been directed toward alleviating tumour hypoxia, suppressing the expression of heat shock proteins, and integrating MS QDs with other therapeutic modalities to achieve synergistic effects.

6.1. Modulation of physical properties of MS QDs

The physical characteristics of MS QDs can be adjusted to boost their optoelectronic performance and light absorption capacity by controlling synthesis techniques, reaction conditions, and other factors. Yu *et al*.[244] fabricated the CuS QDs embedded in chitosan (CuS–CS) utilizing a straightforward and eco-friendly co-precipitation method. $CuCl_2 \cdot 2H_2O$ was dissolved in an acidic chitosan aqueous solution, with dropwise addition of Na_2S solution, and pH adjustment with dilute ammonia. Stirring the mixture at 70°C in a water bath for 6 h, centrifugation and washing afforded a deep green precipitate of CuS-CS QDs. Folate was utilized for surface modification of CuS-CS QDs to introduce targeting capabilities. The strong optical absorption of CuS-CS-FA in the NIR-II range was exploited, and CuS-CS-FA (Cu: 0.06–0.3 g L^{-1}) solutions was subjected to 1064 nm laser irradiation (1.0 W cm^{-2}) for 540 seconds, leading to swift temperature elevation across the CuS-CS-FA QDs solutions. Notably, with an increase in Cu concentration from 0 to 0.3 g L^{-1}, the temperature escalated from 5.1 to 36.2°C rapidly. Ultimately, a peak PCE of 47.0% was attained for CuS-CS-FA QDs. Liu *et al*.[245] demonstrated that upon exposure to an 808 nm laser (1.0 W cm^{-2}) for 10 min, the temperature of MoS_2 QDs, MoS_2 NFs, and MoS_2 NSs experienced a significant increase, reaching 10.4, 21.1, and 30.8°C, respectively. It is evident that MoS_2 nanospheres displayed the highest PCE, achieving a heating rate of 5.83°C min^{-1}. In order to further enhance PCE, PS IR820 was modified using PEI to create MoS_2@PEI@IR820 MPI. BSA plays a critical role as a polymeric ligand in both the synthesis and stabilization of nanomaterials.[246] Celikbas *et al*.[247] devised a strategy to load Hemi-Br specifically onto mitochondria-targeting AS QDs conjugated with FA that emit NIR. When irradiated with a 640 nm laser at a power of 215 mW for 20 min, free Hemi-Br, AS-GSH, AS-GSH-FA, and AS-GSH-FA/Hemi-Br demonstrated PCE values of 51.95%, 75.55%, 87.15%, and 93.46%, respectively, in water. Chicken egg white is abundant in proteins featuring numerous active chemical groups (OH, SH, COOH), making it cost-effective, easily accessible, and non-toxic to cells. Zhong *et al*.[190] extracted fresh CEW liquid, which was then stirred and centrifuged, resulting in a clear, transparent, and uniform solution. Subsequently, Cu toke the place of noble metal Ag, and an aqueous solution of $CuCl_2 \cdot 2H_2O$ was added to the CEW solution and stirred at room temperature for 30 min to produce a Cu^{2+} coupled CEW solution. The resulting solution was then heated to 37°C and combined with a $Na_2S \cdot 9H_2O$ solution, leading to a rapid change in colour to black. The mixture was stirred continuously for 6 h at 37°C. Then, upon reaching room temperature, solid samples were obtained through centrifugation and subsequently washed with purified water. This approach

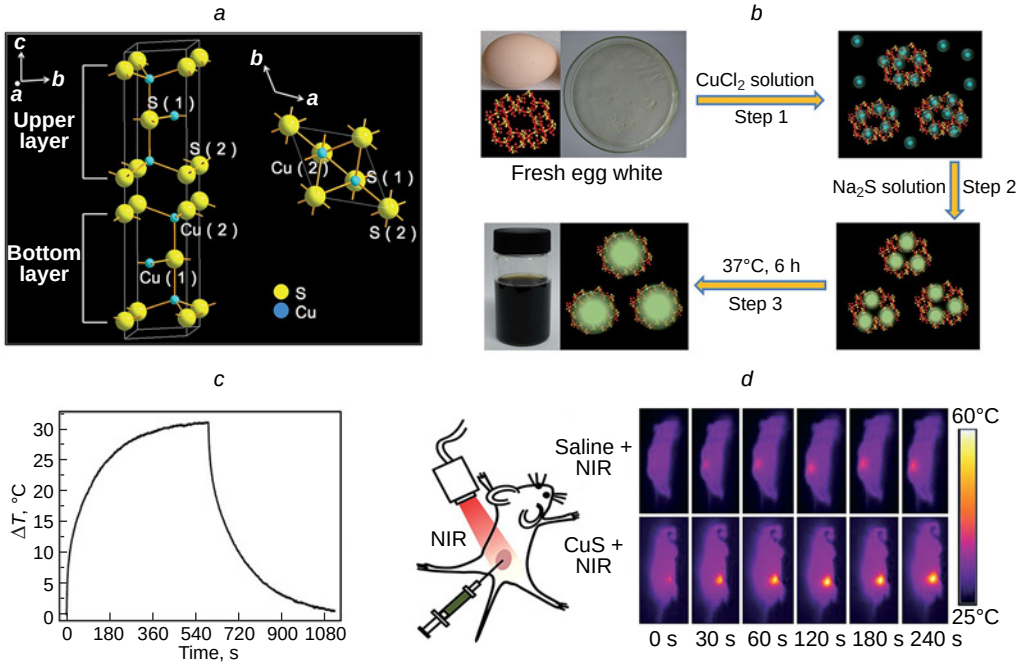

Figure 13. (*a*) Crystal structure of CuS (covellite). (*b*) Schematic illustration of synthesis of CuS QDs. (*c*) Temperature of aqueous dispersion of CuS QDs (0.75 mg mL^{-1}) as a function of time after 980 nm (0.44 W cm^{-2}) laser irradiation for 10 min. (*d*) Thermal images of mice injected with saline or CuS QD solution at different irradiation times with 980 laser (0.44 W cm^{-2}). Reproduced from Zhong *et al.*;[190] copyright (2016) the Royal Society of Chemistry.

facilitated the green synthesis of CuS QDs by using CEW as a surface ligand at the physiological temperature of 37°C (Fig. 13). Upon exposure to 980 nm laser irradiation at a power density of 0.44 W cm^{-2}, the temperature of the CuS QDs aqueous dispersion (with concentrations ranging from 0.25 to 1.0 mg mL^{-1}) increased from 17.2 to 37.4°C within 8 min. Particularly, the highest temperature achieved for the CuS QDs aqueous dispersion at a concentration of 0.75 mg mL^{-1} was 31.2°C at 600 seconds, resulting in a calculated PCE of 47.2%.

6.2. Surface modification and functionalization

By selecting appropriate surface modifiers and functional molecules, targeted interactions between MS QDs and tumour cells or tissues can be achieved, enhancing their selectivity towards tumour cells. One commonly used surface modification method includes coating MS QDs with organic molecules such as carboxylic acids, amines, or polymers. These organic molecules play a crucial role in regulating the stability and solubility of MS QDs. Another prevalent surface modification approach is decorating MS QDs with functional molecules like the targeting ligands, fluorescent labels, or antioxidants. The combination of these functional molecules with MS QDs imparts specific functionalities and applications to the QDs.

Sukhanova *et al.*[248] demonstrated that the smaller the size of QDs, the greater their cytotoxicity *in vitro*. The cytotoxic effect on tumour cells develops more rapidly than on normal cells. Furthermore, QDs with a lower surface negative charge exhibit stronger cytotoxicity compared to those with higher surface negative or positive charges. In addition, the organic coating formed by ligand modification of synthesized QDs can ensure their colloidal stability and biocompatibility. The chemical composition of the QD core has little to no effect on QD cytotoxicity *in vitro*. PF127, a copolymer of poly(ethylene oxide) and poly(propylene oxide) possesses impressive biocompatibility and anti-aggregative properties. It is effective in preventing protein adsorption, tissue adhesion, and recognition by the reticuloendothelial system *in vivo*. PF127 can be tailored with targeting agents and linked with nanomaterials to produce specialized nano-probes for labeling tumours.[249,250] Zhang *et al.*[251] applied an FA-modified version of PF127 onto oil-soluble Ag_2S QDs, resulting in targeted water-soluble nano-probes dubbed as PF127-FA@Ag_2S. When exposed to these nano-probes, HeLa cells exhibited a PA signal comparable to that for cells treated with PF127@Ag_2S, yet notably stronger than A549 cells and HeLa cells treated with PF127@Ag_2S. These findings suggest that FA-conjugated PF127-FA@Ag_2S nano-probes possess enhanced targeting capabilities, ideal for visualizing HeLa tumour cells with elevated FA receptor levels through PA imaging. Research has demonstrated that cyclic RGD peptide (cRGD) is a more potent ligand for targeting tumours compared to linear RGD peptide.[252] In a study by Chen *et al.*[253] the active tumour-targeting tripeptide cRGD was covalently attached to the chemotherapy drug DOX on Ag_2S QDs to create the nano-conjugate Ag_2S-DOX-cRGD. After incubating Ag_2S-DOX and Ag_2S-DOX-cRGD with U87 tumour cells at 37°C, weak fluorescence signals indicated that only a small amount of Ag_2S-DOX entered into U87 tumour cells. The fluorescence signals detected after incubation of U87 tumour cells with Ag_2S and Ag_2S-cRGD for 2 h were significantly stronger than those of Ag_2S-DOX-treated U87 cells (Fig. 14*a*–*d*), which demonstrated that cRGD enhances the affinity of Ag_2S QDs to tumour cells which are expressing high levels of integrin $\alpha_v\beta_3$. Lu *et al.*[254] employed a gentle water-soluble strategy to produce PEGylated silver sulfide QDs (Ag_2S-PEG-R) for *in vivo* cancer imaging. Ag_2S-PEG-R displayed a consistent quasi-spherical shape (2.30±0.19 nm) with a hydrodynamic size of 10.5 nm. It exhibited intense emission at around 1050 nm and a fluorescence quantum efficiency of around 2.33% in aqueous solution. Following injection into

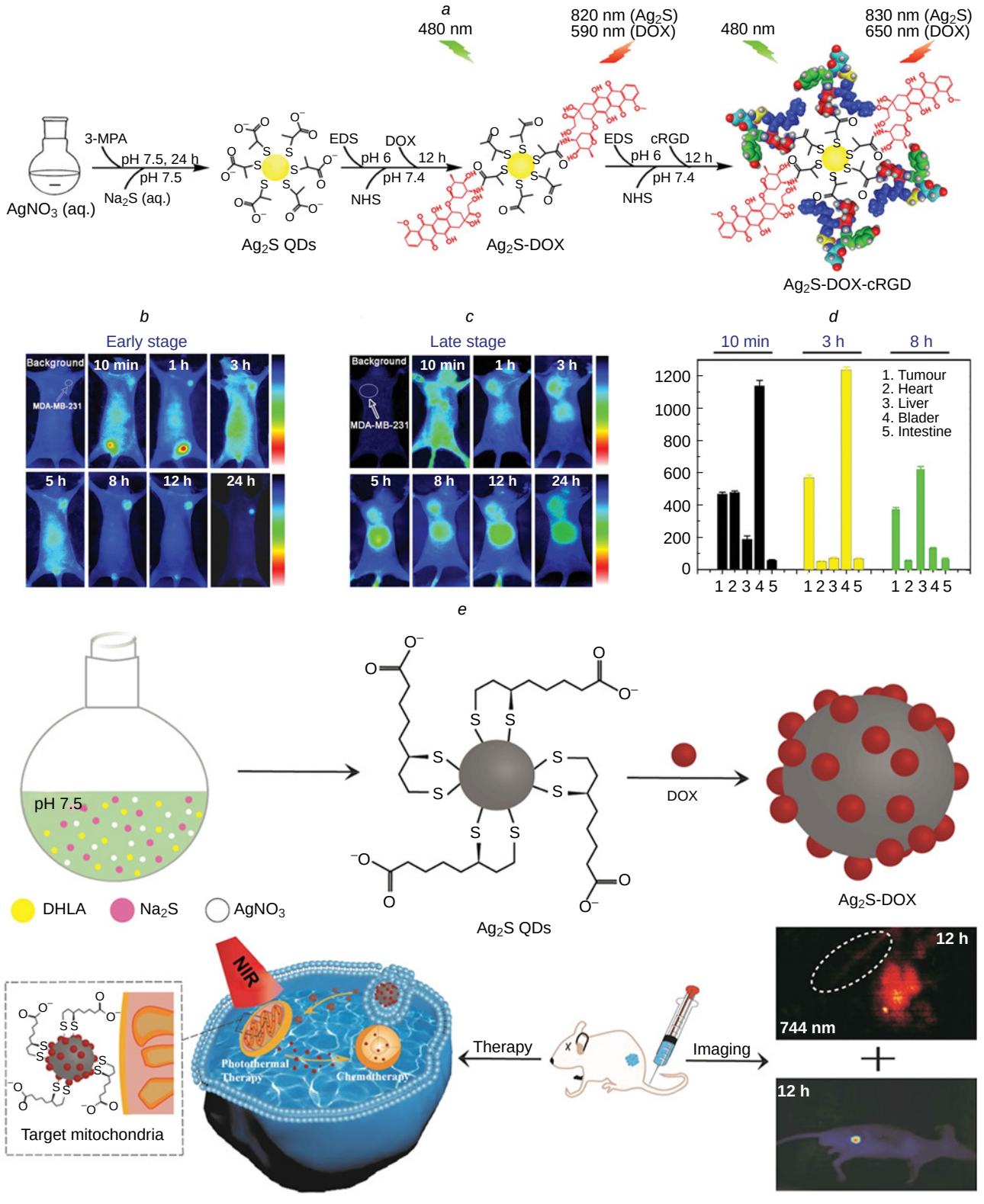

Figure 14. (*a*) The procedure for creating the nano-conjugate (Ag_2S-DOX-cRGD) was synthesized. Fluorescence imaging of Ag_2S-cRGD was conducted *in vivo* in various MDA-MB-231 tumour-bearing mice at both (*b*) early stage and (*c*) late stage. (*d*) Following injection of the probe, fluorescence intensity from the tumour and key organs (such as the heart, liver, bladder, and intestine) was analyzed using Scion Image software. Reproduced (*a*–*d*) from Chen *et al*.;[253] copyright (2014) the Royal Society of Chemistry. (*e*) Illustration of the preparation process of mitochondria-targeted Ag_2S-DOX and the application for dual-modal fluorescence imaging/photoacoustic imaging and chemo-photothermal combined therapy of tumour. Reproduced from Xuan *et al*.[259] with permission from the American Chemical Society.

mice's veins, Ag_2S-PEG-R demonstrated enhanced efficiency in targeting tumours compared to the original Ag_2S-PEG. The NIR-II fluorescence at the tumour location was notable at 2 h post-injection and persisted even after 24 h. It was noticed that in live mice, small vessels with a diameter of 0.20 mm were identifiable, indicating the high resolution achieved through

NIR-II imaging, while not achievable with usual NIR-I imaging methods. Distinct vascular branching was observed after 2 h, and main blood vessels in the hind limbs were still visible at 4 h. Following this, the signal from blood vessels vanished, and nanoparticle accumulation in the tumour peaked at 6 h. Overall, post PEGylation optimization, the blood flow and tumour-targeting abilities of Ag_2S QDs were significantly enhanced. Chlorotoxin (CTX) is a ligand that attaches specifically to U-87 brain tumour cells. Chen *et al*.[255] introduced a straightforward and harmless thermolysis synthesis approach, yielding QYs of 13% and 41% for AIS and AIS/ZnS QDs, respectively. QD micelles comprised of AIS/ZnS QDs were achieved by encapsulating them with the amphiphilic polymer PLGA-PEG, aiding in the transfer between phases and the bioconjugation of AIS/ZnS QDs, for cellular imaging. Utilization of CTX as a targeting ligand for the conjugated QD micelles indeed facilitated specific internalization into U-87 MG brain tumour cells, as verified through cellular imaging analyses. These QDs' phase transfer and bioconjugation present opportunities for their utilization in identifying endogenous targets present on brain tumour cells or in other broader applications related to cell- or tissue-based diagnostics and therapeutics. Tumour-specific receptors like FA and RGD peptide can serve as targets for intervention and diagnostic imaging. For instance, Deng *et al*.[256] altered ZAIS QDs by incorporating tumour cell-specific targeting ligands like FA and RGD peptide, resulting in the QD-PEG_{2000}-FA probe. Fluorescence imaging revealed that FA modification enhanced the targeted delivery of the probe to the FA receptor-positive tumour cells. In addition, in comparison to the original ZAIS QDs and CH_3O-PEG_{2000}-coated QDs, FA modification enhanced the penetration of the probe into the cellular matrix and its binding to dense regions such as the cell nucleus. PEGylated quaternary QDs exhibit promising applications in tumour cell imaging. Subcellular targeting has recently emerged as a pivotal technique in cancer therapy. Compared to non-targeted chemotherapeutic agents, mitochondria-targeted drugs can reduce toxicity to normal cells while enhancing cytotoxicity against cancer cells, thereby overcoming drug resistance and improving therapeutic efficacy.[257,258] In this context, Xuan *et al*.[259] fabricated novel mitochondria-targeting Ag_2S-DOX QDs using lipoic acid as a ligand (see Fig. 14*e*). These quantum dots exhibit excellent water solubility and biocompatibility. Both *in vitro* and *in vivo* studies demonstrated that the Ag_2S-DOX platform is suitable not only for fluorescent and photoacoustic dual-modal imaging but also for synergistic tumour-targeted CHT and PTT, presenting a promising strategy for cancer treatment.

6.3. Improvement of tumour hypoxia and reduction of heat shock protein expression

Hypoxia is a significant feature of the tumour microenvironment, potentially limiting the efficacy of oxygen-dependent PDT.[260] Novel approaches, such as oxygen delivery systems or the systems of its *in situ* generation, have been devised to address hypoxia, like the production of ROS by MnO_2, that is, MnO_2 nanostructures are able to trigger the decomposition of H_2O_2 existing in the tumour-associated macrophages into water and oxygen *in situ*, leading to an increased quantity of ROS accessible for PDT cancer therapy.[261] Under mild PTT conditions, the elevated expression of heat shock proteins in cancer cells can induce thermal stress tolerance, resulting in the heightened tumour recurrence rate.[262,263] Consequently, a novel strategy could be formulated to reverse hypoxia in PDT and decrease HSP expression in PTT, with the aim of bolstering the phototherapy of NIR PSs by fortifying PDT and PTT. This would render it suitable for clinical cancer management.

Heat shock protein 70 (HSP70) has been shown to play a significant role in regulating multiple cellular processes involved in cancer development.[261] The interactions between HSP70 and these signalling pathways have important implications for understanding the mechanisms underlying cancer progression and potentially identifying new treatment targets. In cancer cells, HSP70 can modulate critical signaling pathways such as the phosphoinositide 3-kinase-Akt pathway, the mitogen-activated protein kinase pathway, and the Janus kinase-signal transducer and activator of transcription pathway. These pathways are involved in regulating cell survival, proliferation, and migration, all of which is process that is dysregulated in cancer. By influencing these pathways, HSP70 can promote tumour growth, metastasis, and resistance to therapy. Cao *et al*.[264] developed a general method to load the NIR plasmonic colloid $Cu_{2-x}S$ *in situ* onto the surface of MnO_2 nanosheet (forming $MnO_2/Cu_{2-x}S$). After that, it was loaded with HSP70 siRNA to obtain $MnO_2/Cu_{2-x}S$-siRNA, which significantly enhanced PTT/PDT synergistic anti-tumour efficacy by inhibiting the heat shock response relieving tumour hypoxia, and at meantime achieved precise multimodal tumour imaging diagnosis. It is noted that in the acidic tumour microenvironment, MnO_2 is converted to Mn^{2+} and initiated the breakdown of endogenous H_2O_2 to produce O_2, thereby facilitating tumour hypoxia and boosting PDT therapy against tumours. Following exposure to 980 nm NIR laser (0.72 W cm^{-2}) for 5 min, cells treated with $MnO_2/Cu_{2-x}S$-siRNA displayed noticeable suppression of HSP70 expression. The siRNA aimed at the HSP70 gene efficiently interrupted the heat shock response in PTT, indicating the excellent HSP70 silencing capabilities of $MnO_2/Cu_{2-x}S$-siRNA, while simultaneously enhancing PDT by reducing hypoxia. With the joint action of PTT/PDT, a substantial therapeutic effect was observed, effectively impeding tumour growth without recurrence. Additionally, $MnO_2/Cu_{2-x}S$-siRNA displayed distinctive SPR bands and photostability within the NIR range, proving to be an ideal contrast agent for MR/PA dual-mode imaging. The application of intelligent multifunctional nanomedicines to regulate tumour cell defense mechanisms and the microenvironment for achieving comprehensive anti-cancer effects has been exhibited enormous promise. Similarly, Hashemkhani *et al*.[265] and colleagues developed a novel approach to create stable small therapeutic diagnostic nanoparticles by combining Ag_2S QDs and MnO_2, incorporating ALA for improved PDT/PTT in combination tumour therapy. The presence of MnO_2 facilitated the conversion of H_2O_2 into O_2, leading to increased ROS generation and enhanced ALA-PDT efficiency by depleting GSH. These ALA/Ag_2S/MnO_2 hybrid nanoparticles effectively addressed tumour hypoxia, efficiently delivered ALA to tumour cells, and enabled NIR tracking to enhance the PDT + PTT combined therapy under short-duration, low-dose long-wavelength co-irradiation.

6.4. Combination with other therapeutic approaches

Metal sulfide QDs have shown great potential in combination therapy with other tumour treatment modalities, such as CHT and RT. By combining MS QDs with these treatments, the overall efficacy of the therapy can be significantly improved. Additionally, this approach has the potential to reduce the negative side effects often associated with traditional treatments.

The synergistic effects of combining MS QDs with other modalities can enhance the body's response to tumour treatment, ultimately leading to better outcomes for patients.

CDT in cells converts endogenous H_2O_2 into toxic ROS through Fenton or Fenton-like reactions activated by the tumour microenvironment, resulting in tumour cell death.[266] He *et al.*[267] designed a protein-based nanosystem (Ag_2S@CAT-Ce6@Oxa) and treated HT29 cells with Ag_2S@CAT-Ce6@Oxa nanoparticles for 4 h to assess PDT efficiency by monitoring singlet oxygen production within the cells. Following cell co-incubation, Ag_2S@CAT-Ce6@Oxa increased $O_2^{\bullet-}$ levels, potentially improving PDT effectiveness in cancer treatment under laser exposure (300 mW cm^{-2}, 10 min). Upon injection into BALB/cHT29 tumour-bearing nude mice and subsequent NIR laser irradiation, the temperature at the tumour site increased significantly (by 29.6°C) within the first 3 min. This temperature remained at 59.5°C after 12 h. This illustrates the nanoparticles' strong ability to elevate local tumour temperature under NIR illumination and showcases its superior in PTTs *in vivo*. Moreover, the BALB/cHT29 tumour-bearing nude mice irradiated with 660 nm laser (300 mW cm^{-2}) for 10 min displayed the smallest tumour size and lowest mass after 14 days. So, the utilization of Ag_2S@CAT-Ce6@Oxa nanoparticles *in vivo* showcased outstanding synergistic PDT/PTT/CDT effects, effectively curtailing tumour growth. Li *et al.*[268] conducted experiments to evaluate the cytotoxic effects of CuS:Ce6@HA:DOX@RGD on MCF-7 cells using PI (dead cells)/calcein-AM (living cells) staining. The group treated with CuS:Ce6@HA:DOX@RGD exhibited the highest rate of cell elimination following two rounds of irradiation. As the concentration of CuS:Ce6@HA:DOX@RGD increased, the viability of MCF-7 cells decreased significantly. Changes in tumour volume were monitored for a period of 14 days post-treatment. The combination therapy of PDT/PTT/CDT resulted in moderate tumour suppression in the group exposed to a single round of irradiation, whereas multiple rounds of irradiation led to maximum inhibition of tumour growth. Conversely, the group treated with CuS:Ce6@HA:DOX@RGD without radiation displayed limited tumour suppression due to reliance solely on CHT. Notably, after 14 days of treatment, the group receiving two rounds of irradiation exhibited the smallest tumour size, volume, and a tumour growth inhibition of 90.3%. The most pronounced morphological changes and necrosis within the tumour were observed in this group, indicating the potent synergistic effect of PDT/PTT/CDT in inhibiting tumour growth and enhancing cancer cell destruction. The nano-complex Co_3S_4-ICG, as reported by Jiang *et al.*,[269] decomposes within the tumour area, producing Co^{2+} that catalyzes the formation of $^{\bullet}OH$ *via* a Fenton-like process, which aids in cancer treatment with CDT. When exposed to NIR laser light, the Co_3S_4-ICG nano-complex stimulates photothermal conversion and generates harmful $O_2^{\bullet-}$, enabling both PTT and PDT concurrently (Fig. 15).

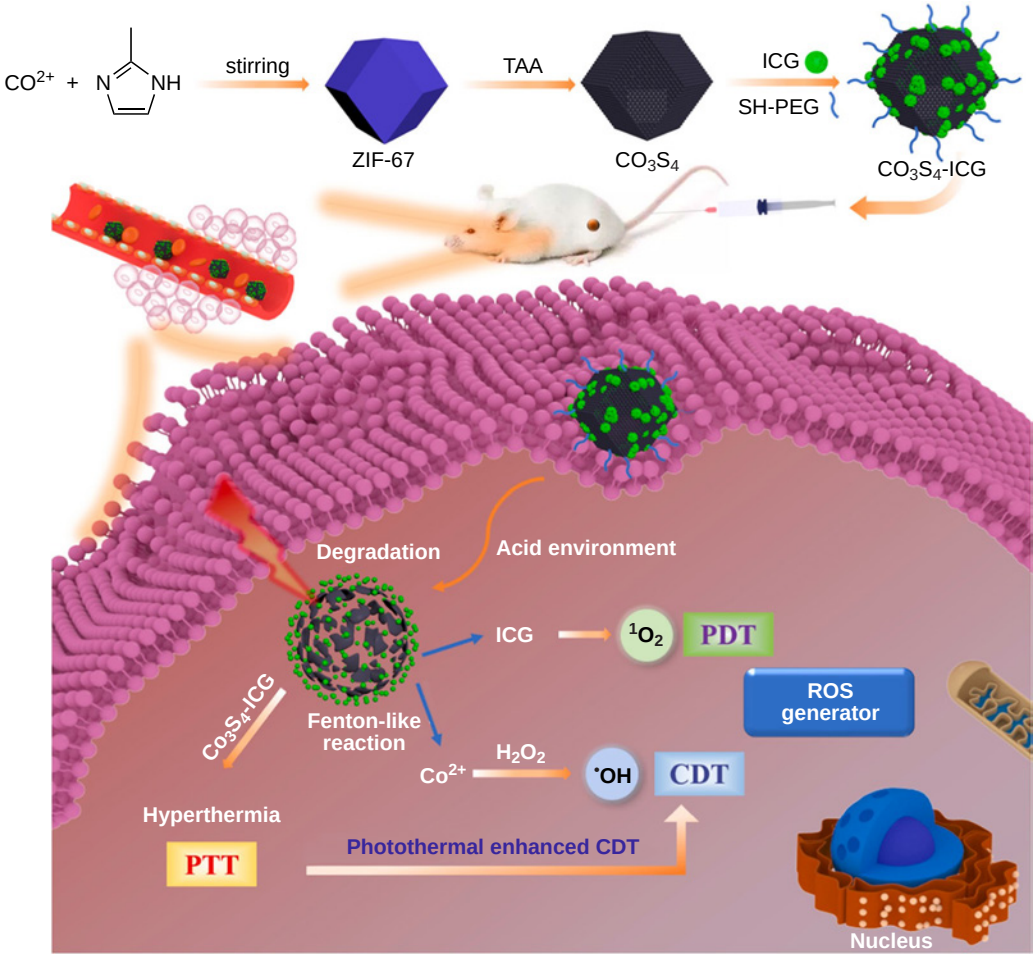

Figure 15. *In vivo* assessment of Co_3S_4-ICG photothermal imaging and its impact on tumour suppression. Reproduced from Jiang *et al.*;[269] copyright (2021) Elsevier.

Moreover, the production of $^{\bullet}OH$ is hastened through thermally-induced Fenton-like reactions, further boosting the CDT efficacy. Co_3S_4-ICG displays remarkable combined effects for tumour treatment through CDT/PDT/PTT strategies.

Furthermore, cancer therapy has also been transformed by immunotherapy, especially through immune checkpoint blockade, which educates the host immune system to improve monitoring and defensive processes for eradicating tumours. Among immunostimulants, unmethylated CpG oligonucleotides are detected by Toll-like receptor 9 in plasmacytoid dendritic cells. This recognition triggers immune responses, leading to the production of helper T cell 1 cells and pro-inflammatory cytokines, such as tumour necrosis factor alpha and interleukin-12. Interleukin-12 is a potent stimulator of cytotoxic T lymphocytes, facilitating their maturation and infiltration into tumour regions. Upon activation, cytotoxic T lymphocytes release interferon gamma to eliminate tumour cells. Tumour cells can resist immune surveillance by inducing CTL exhaustion through the PD-L 1 signaling pathway; however, blocking PD-L 1 (aPD-L 1) will effectively thwart this evasion mechanism.[270–273] Yang *et al*.[274] have developed IR780-ZnS@HSA, which not only triggers the cGAS-STING pathway but also induces immunogenic cell death (ICD) and pyroptosis in cancerous cells. Helper T cells, specifically $CD3^+$ and $CD4^+$ cells, are involved in immune modulation and can be categorized into two distinct subtypes based on their functions: effector T cells ($CD3^+$, $CD4^+$, $FoxP3^-$) and regulatory T cells (Tregs).[275] Effector T cells promote anti-tumour immune responses, whereas Tregs suppress them. The combination of IR780-ZnS@HSA with laser treatment and he aPD-L 1 has been found to boost $CD8^+$ T cell levels in the tumour microenvironment and reduce the presence of $FoxP3^+$ T cells. This combination also significantly increases interferon-gamma and the tumour necrosis factor alpha levels in the bloodstream of mice, showcasing potent immune regulatory effects. In preclinical experiments, IR780-ZnS@HSA demonstrated a remarkable ability to inhibit tumour growth in mice with 4T1 tumours and modify the immunosuppressive tumour microenvironment, ultimately enhancing immune responses. Given its triple-functionality as a photothermal sensitizer for PTT, PDT, and immunotherapy, the IR780-ZnS@HSA holds promise for further investigation in the realm of targeted cancer immunotherapy.

7. Conclusion

In this review, we have provided an overview of the advancements in utilizing MS QDs for combined CDT, PTT and PDT in cancer therapy. Various methods for synthesizing MS QDs have been discussed, including solvent or hydrothermal synthesis and thermal injection approaches, with more sustainable methods that researchers are now focusing on. These novel nanomaterials, known for their exceptional optical properties and biocompatibility, show significant potential for PTT and PDT applications. While investigations on the use of MS QDs for combined PTT and PDT are still limited, prior studies have predominantly concentrated on CuS QDs, Ag_2S QDs, and MoS_2 QDs. Recently, interest has also been stirred up in Bi_2S_3 QDs, FeS QDs, and WS_2 QDs. Despite some encouraging findings, there are persistent challenges associated with the use of MS QDs in cancer therapy, including concerns about toxicity, biocompatibility, regulation of photothermal effects, enhancement of photodynamic effects, tumour targeting and penetration, as well as considerations for clinical translation. The present trajectory in the development of QDs involves efforts to minimize toxic components, create eco-friendly materials, and discover new avenues for application. QD developers are increasingly focusing on advancing the field towards safer and more effective nanomaterials for cancer therapy.

Future research directions in the field of MS QDs may involve enhancing their photovoltaic conversion efficiency, stability, and photosensitivity through structural and design adjustments. Another key area of focus could be improving the selectivity and uptake capacity of MS QDs towards tumour cells by modifying their surfaces and incorporating targeting molecules. Overcoming challenges in producing high-quality MS QDs, such as ensuring uniform size distribution and high QY, should be prioritized in future studies. Additionally, the development of functionalized MS QDs tailored for targeted delivery, therapy, and drug release will present exciting opportunities for exploration. It is essential to further investigate the biocompatibility, toxicity, and tissue penetration of MS QDs to ensure their safety and effectiveness in clinical applications. Moreover, customizing treatment strategies based on individual patient variations and exploring synergistic effects by combining MS QDs with different therapeutic approaches, such as PDT and immunotherapy, may lead to enhanced efficacy in cancer treatment. Ultimately, continuous research into the properties, synthesis, efficacy, and biocompatibility of MS QDs could potentially revolutionize clinical cancer therapy by offering a valuable modality with improved treatment outcomes. By addressing these research areas and challenges, MS QDs has the potential to become a pivotal component in the future of cancer treatment.

Acknowledgements

The authors acknowledge the financial support from National Natural Science Foundation of China (52272287, 22067019, 22367023), Yunnan Provincial Science and Technology Plan Project (202305AF150116), Major Science and Technology project of Yunnan Province (202402AE090006), Yunnan Provincial Science and Technology Department-Yunnan University Joint Special Project (No. 202201BF070001-001).

Conflict of interest

The authors declare that they have no known competing financial interests or personal relationships that could have appeared to influence the work reported in this review.

8. List of abbreviations and designations

ac — acetate,
acac — acerylacetonate,
Ag_2S-PEG-R — PEGylated silver sulfide QDs,
AIS — $AgInS_2$,
AIS-2 MPA — 2-mercaptosuccinic acid,
AIS-PEI/2MPA — polyethyleneimine/2-mercaptosuccinic acid,
ALA — aminolevulinic acid,
BSA — bovine serum albumin,
CB — conduction band,
CDT — chemodynamic therapy,
Ce6 — chlorine E6,
CEW — chicken egg white,
CHT — chemotherapy,
CIS — $CuInS_2$,
CIZS QDs — Cu–In–Zn–S photoluminescent QDs,

cRGD — cyclic RGD peptide,
CT — computerized tomographic (imaging),
CTAB — cetyltrimethylammonium bromide,
CTX — chlorotoxin,
DCB — dichlorobenzene,
DDT — dodecanethiol,
DEA — *N*-alkylalkanolamide,
DOX — doxorubicin,
EDTA — ethylenediaminetetraacetic acid,
EF — Fermi level,
EGFR — epidermal growth factor receptor,
FA — folate,
FRET — Förster resonance energy transfer,
GSH — glutathione,
GT — gene therapy,
Hemi-Br — hemi-branched cysteine bromide,
HSP70 — heat shock protein 70,
IOLs — intraocular lenses,
ICG — indocyanine green,
LSPR — localized surface plasmon resonance,
MoS_2@PANI — MoS_2QDs@polyaniline,
MRI — magnetic resonance imaging,
MSND — mussel-protein-mineralized silver nanodots,
MSOT — multispectral optoacoustic tomography
MS QD — metal sulfide quantum dot,
NIR — near-infrared,
NMP — *N*-methyl-2-pyrrolidone,
NM — nanomedicine,
NP — nanoparticle,
$O_2^{-\bullet}$ — superoxide anions,
$^3O_2$ — triplet-state oxygen,
$^1O_2$ — singlet oxygen,
OA — oleic acid,
OAm — oleylamine,
ODE — 1-octadecene,
OP — oxidized photocatalyst,
PA — photoacoustic,
PCE — photothermal conversion efficiency,
PDT — photodynamic therapy,
PEG — polyethylene glycol,
PEP/Exo/CoS QDs — peptide/exosome/cobalt sulfide quantum dots nanocomplex,
PS — photosensitizer,
PTA — photothermal agent,
PTT — photothermal therapy,
PVP — polyvinylpyrrolidone,
QD — quantum dot,
QDs-IOLs — IOLs modified with QDs,
QY — quantum yield,
ROS — reactive oxygen species,
RP — reduced photocatalyst,
RT — radiation therapy,
RTIL — room temperature ionic liquid,
S-scheme — step-scheme,
SDT — sonodynamic therapy,
SDS — sodium dodecyl sulfate,
SILAR — successive ionic layer adsorption and reaction,
siRNA — small interfering RNA,
SPIONs — superparamagnetic iron oxide nanoparticles,
TAA — thioacetamide,
TAD-NP — tri-anthracene derivative nanoparticle,
TDPA — tetradecylphosphonic acid,
TMS — trimethylsilyl,
TOP — tri-*n*-octylphosphine,
TOPO — tri-*n*-octylphosphine oxide,
TPP — tetraphenylporphyrin,
TSL — thermosensitive liposomes,
Tu — thiourea,
VB — valence band,
UVA/UVB — ultraviolet A/B irradiation.
WS_2@PEI — WS_2@polyetherimide,
ZCIS QDs — CuInS/ZnS QDs.

9. References

1. H.Sung, J.Ferlay, R.L.Siegel, M.Laversanne, I.Soerjomataram, A.Jemal, F.Bray. *CA Cancer J. Clin.*, **71**, 209 (2021); https://doi.org/10.3322/caac.21660
2. C.Holohan, S.Van Schaeybroeck, D.B.Longley, P.G.Johnston. *Nat. Rev. Cancer*, **13**, 714 (2013); https://doi.org/10.1038/nrc3599
3. K.Azuma, A.Tamiya, Y.Adachi, T.Enomoto, S.Kouno, Y.Taniguchi, N.Saijo, K.Okishio, S.Atagi. *Ann. Oncol.*, **30,** xi30 (2019); https:// doi.org/10.1093/annonc/mdz449.037
4. K.Wang, F.M.Kievit, M.Zhang. *Pharmacol. Res.*, **114**, 56 (2016); https://doi.org/10.1016/j.phrs.2016.10.016
5. W.Xu, S.Zhu, Z.Sun, J.Ye, H.Chu. *Acta Pharm. Sin. B*, (2025) (in the press); https://doi.org/10.1016/j.apsb.2025.06.011
6. L.Cheng, C.Wang, L.Feng, KYang, Z.Liu. *Chem. Rev.*, **114**, 10869 (2014); https://doi.org/10.1021/cr400532z
7. L.-x.Zhang, X.-m.Sun, Z.P.Xu, R.-t.Liu. *ACS Appl. Mater. Interfaces*, **11**, 35566 (2019); https://doi.org/10.1021/acsami.9b11746
8. Y.-j.Hou, X.-x.Yang, R.-q.Liu, D.Zhao, C.-n.Guo, A.-c.Zhu, M.-n.Wen, Z.Liu, G.-f.Qu, H.-x.Meng. *Int. J. Nanomed.*, **15**, 6827 (2020); https://doi.org/10.2147/IJN.S269321
9. M.Z.Quazi, J.Park, N.Park. *Technol. Cancer Res. Treat.*, **22**, 15330338231170939 (2023); https://doi.org/10.1177/15330338231170939
10. K.Yang, S.Zhang, G.Zhang, X.Sun, S.-T.Lee, Z.Liu. *Nano Lett.*, **10**, 3318 (2010); https://doi.org/10.1021/nl100996u
11. Z.Wei, P.Liang, J.Xie, C.Song, C.Tang, Y.Wang, X.Yin, Y.Cai, W.Han, X.Dong. *Chem. Sci.*, **10**, 2778 (2019); https://doi.org/10.1039/c8sc04123g
12. P.Agostinis, K.Berg, K.A.Cengel, T.H.Foster, A.W.Girotti, S.O.Gollnick, S.M.Hahn, M.R.Hamblin, A.Juzeniene, D.Kessel. *CA Cancer J. Clin.*, **61**, 250 (2011); https://doi.org/10.3322/caac.20114
13. Z.Fan, X.Dai, Y.Lu, E.Yu, N.Brahmbatt, N.Carter, C.Tchouwou, A.K.Singh, Y.Jones, H.Yu, P.C.Ray. *Mol. Pharm.*, **11**, 1109 (2014); https://doi.org/10.1021/mp4002816
14. Y.Wang, S.Luo, Y.Wu, P.Tang, J.Liu, Z.Liu, S.Shen, H.Ren, D.Wu. *ACS Nano*, **14**, 17046 (2020); https://doi.org/10.1021/acsnano.0c06415
15. M.Qiu, D.Wang, W.Liang, L.Liu, Y.Zhang, X.Chen, D.K.Sang, C.Xing, Z.Li, B.Dong, F.Xing, D.Fan, S.Bao, H.Zhang, Y.Cao. *Proc. Natl. Acad. Sci. USA*, **115**, 501 (2018); https://doi.org/10.1073/pnas.1714421115
16. S.Kwiatkowski, B.Knap, D.Przystupski, J.Saczko, E.Kedzierska, K.Knap-Czop, J.Kotlinska, O.Michel, K.Kotowski, J.Kulbacka. *Biomed. Pharmacother.*, **106**, 1098 (2018); https://doi.org/10.1016/j.biopha.2018.07.049
17. X.Li, N.Kwon, T.Guo, Z.Liu, J.Yoon. *Angew. Chem., Int. Ed.*, **57**, 11522 (2018); https://doi.org/10.1002/anie.201805138
18. C.-Y.Han, S.-H.Lee, S.-W.Song, S.-Y.Yoon, J.-H.Jo, D.-Y.Jo, H.-M.Kim, B.-J.Lee, H.-S.Kim, H.Yang. *ACS Energy Lett.*, **5**, 1568 (2020); https://doi.org/10.1021/acsenergylett.0c00638
19. O.Ouellette, A.Lesage-Landry, B.Scheffel, S.Hoogland, F.P.García de Arquer, E.H.Sargent. *Adv. Funct. Mater.*, **30,** 1908200 (2019); https://doi.org/10.1002/adfm.201908200
20. Y.Yong, X.Cheng, T.Bao, M.Zu, L.Yan, W.Yin, C.Ge, D.Wang, Z.Gu, Y.Zhao. *ACS Nano*, **9**, 12451 (2015); https://doi.org/10.1021/acsnano.5b05825

21. S.Aftab, B.Aslam, S.Khan, Z.Baloch. *Russ. Chem. Rev.*, **94** (6) RCR5168 (2025); https://doi.org/10.59761/RCR5168
22. Y.Xia, N.Kapuria, M.He, U.V.Ghorpade, X.Guo, B.Hao, S.W.Shin, Z.Hameiri, X.Hao, M.P.Suryawanshi. *Adv. Powder Mater.*, **4**, 100283 (2025); https://doi.org/10.1016/j.apmate.2025.100283
23. J.Zhang, K.Qi, R.Pitcheri, C.Duan. *J. Photochem. Photobiol., C*, **65**, 100722 (2025); https://doi.org/10.1016/j.jphotochemrev.2025.100722
24. S.K.Arumugasamy, G.Chellasamy, N.Murugan, S.Govindaraju, K.Yun, M.-J.Choi. *Adv. Colloid Interface Sci.*, **331**, 103245 (2024); https://doi.org/10.1016/j.cis.2024.103245
25. R.Li, J.Xu, X.Mu, F.Zeng. *Next Nanotechnol.*, **7**, 100144 (2025); https://doi.org/10.1016/j.nxnano.2025.100144
26. X.Wu, Y.Liu, B.Wang, L.Li, Z.Li, Q.Wang, Q.Cheng, G.Xing, S.Qu. *Acta Phys.-Chim. Sin.*, **41**, 100109 (2025); https://doi.org/10.1016/j.actphy.2025.100109
27. K.Qi, B.Sun, S.-y.Liu, M.Zhang. *Biomed. Pharmacother.*, **165**, 115070 (2023); https://doi.org/10.1016/j.biopha.2023.115070
28. D.Cui, L.Han, W.Jiang, L.Chen, N.Niu. *ACS Appl. Nano Mater.*, **6**, 1303 (2023); https://doi.org/10.1021/acsanm.2c04944
29. W.B.Direrssa, G.Getachew, A.Wibrianto, A.S.Rasal, V.S.Gurav, M.Zakki Fahmi, J.Y.Chang. *J. Colloid Interface Sci.*, **647**, 528 (2023); https:/ doi.org/10.1016/j.jcis.2023.05.099
30. A.Yadav, P.Dogra, P.Sagar, M.Srivastava, A.Srivastava, R.Kumar, S.K.Srivastava. *Spectrochim. Acta Part A: Mol. Biomol. Spectrosc.*, **335**, 126002 (2025); https://doi.org/10.1016/j.saa.2025.126002
31. X.Zhang, YMa, Y.Shi, L.Jiang, L.Wang, H.ur Rashid, M.Yuan, X.Liu. *Biomed. Pharmacother.*, **174**, 116586 (2024); https://doi.org/10.1016/j.biopha.2024.116586
32. P.A.Tarasov, A.A.Grigoriev, E.A.Isaev, G.V.Detkov. *Phys. Atom. Nuclei*, **86**, 2738 (2024);
33. W.Wei, X.Zhang, S.Zhang, G.Wei, Z.Su. *Mater. Sci. Eng.: C*, **104**, 109891 (2019); https://doi.org/10.1016/j.msec.2019.109891
34. P.Wang, B.Chen, Y.Zhan, L.Wang, J.Luo, J.Xu, L.Zhan, Z.Li, Y.Liu, J.Wei. *Pharmaceutics*, **14**, 2279 (2022); https://doi.org/10.3390/pharmaceutics14112279
35. P.P.Sarngan, C.P.Manju, P.adhao, D.Sarkar. *IOP Conf. Ser.: Mater. Sci. Eng.*, **1219**, 012012 (2022); https://doi.org/10.1088/1757-899x/1219/1/012012
36. A.Bucharskaya, G.Maslyakova, G.Terentyuk, A.Yakunin, Y.Avetisyan, O.Bibikova, E.Tuchina, B.Khlebtsov, N.Khlebtsov, V.Tuchin. *Int. J. Mol. Sci.*, **17**, 1295 (2016); https://doi.org/10.3390/ijms17081295
37. A.B.Bucharskaya, N.G.Khlebtsov, B.N.Khlebtsov, G.N.Maslyakova, N.A.Navolokin, V.D.Genin, E.A.Genina, V.V.Tuchin. *Materials*, **15**, 1606 (2022); https://doi.org/10.3390/ma15041606
38. S.Duan, Y.Hu, Y.Zhao, K.Tang, Z.Zhang, Z.Liu, Y.Wang, H.Guo, Y.Miao, H.Du, D.Yang, S.Li, J.Zhang. *RSC Adv.*, **13**, 14443 (2023); https://doi.org/10.1039/d3ra02620e
39. J.-J.Hu, Q.Lei, X.-Z.Zhang. *Prog. Mater. Sci.*, **114**, 100685 (2020); https://doi.org/10.1016/j.pmatsci.2020.100685
40. E.I.Shramova, S.P.Chumakov, V.O.Shipunova, A.V.Ryabova, G.B.Telegin, A.V.Kabashin, S.M.Deyev, G.M.Proshkina. *Light Sci. Appl.*, **11**, 38 (2022); https:/doi.org/10.1038/s41377-022-00729-4
41. S.-S.Long, W.-X.Zhang, L.Ou, W.Liu, F.Deng, K.Zeng, X.-D.Jiang, Y.-W.Lin. *Chin. Chem. Lett.*, 112226 (2025); https://doi.org/10.1016/j.cclet.2025.112226
42. M.Ju, L.Yang, G.Wang, F.Zong, Y.Shen, S.Wu, X.Tang, D.Yu. *Biomater. Sci.*, **12**, 2831 (2024); https://doi.org/10.1039/d4bm00319e
43. H.Tappeiner. *Münch. Med. Wochenschr.*, **47**, 2042 (1903)
44. J.Chen, T.Fan, Z.Xie, Q.Zeng, P.Xue, T.Zheng, Y.Chen, X.Luo, H.Zhang. *Biomaterials*, **237**, 119827 (2020); https://doi.org/10.1016/j.biomaterials.2020.119827
45. M.Chudy, K.Tokarska, E.Jastrzebska, M.Bułka, S.Drozdek, Ł.Lamch, K.A.Wilk, Z.Brzozka. *Biosens. Bioelectron.*, **101**, 37 (2018); https://doi.org/10.1016/j.bios.2017.10.013
46. A.Verger, N.Brandhonneur, Y.Molard, S.Cordier, K.Kowouvi, M.Amela-Cortes, G.Dollo. *Int. J. Pharm.*, **604**, 120763 (2021); https://doi.org/10.1016/j.ijpharm.2021.120763
47. J.Park, Y.K.Lee, I.K.Park, S.R.Hwang. *Biomedicines*, **9**, 85 (2021); https://doi.org/10.3390/biomedicines9010085
48. Y.Wang, H.Shen, Z.Li, S.Liao, B.Yin, R.Yue, G.Guan, B.Chen, G.Song. *J. Am. Chem. Soc.*, **146**, 6252 (2024); https://doi.org/10.1021/jacs.3c14387
49. H.Wang, Z.Yang, K.Zhang, W.Wang, F.Lin, H.Huang, W.Qin, Z.Chi, Z.Yang. *ACS Mater. Lett.*, **6**, 1317 (2024); https://doi.org/10.1021/acsmaterialslett.3c01210
50. S.Yao, Y.Chen, W.Ding, F.Xu, Z.Liu, Y.Li, Y.Wu, S.Li, W.He, Z.Guo. *Chem. Sci.*, **14**, 1234 (2023); https://doi.org/10.1039/d2sc05982g
51. S.Wang, W.Chen, C.Jiang, L.Lu. *Electrophoresis*, **40**, 2204 (2019); https://doi.org/10.1002/elps.201900005
52. H.S.Kim, D.Y.Lee. *Polymers*, **10**, 961 (2018); https://doi.org/10.3390/polym10090961
53. Q.An, S.Su, W.Hu, Y.Wang, T.Liang, X.Li, C.Li. *Nanoscale*, **15**, 19815 (2023); https://doi.org/10.1039/d3nr05219b
54. C.Wu, D.Li, L.Wang, X.Guan, Y.Tian, H.Yang, S.Li, Y.Liu. *Acta Biomater.*, **53**, 631 (2017); https://doi.org/10.1016/j.actbio.2017.01.078
55. F.Liu, J.Lin, Y.Luo, D.Xie, J.Bian, X.Liu, J.Yue. *Biomater. Sci.*, **11**, 4009 (2023); https://doi.org/10.1039/d3bm00339f
56. J.Tian, L.Ding, H.-J.Xu, Z.Shen, H.Ju, L.Jia, L.Bao, J.-S.Yu. *J. Am. Chem. Soc.*, **135**, 18850 (2013); https://doi.org/10.1021/ja408286k
57. L.Au, Q.Zhang, C.M.Cobley, M.Gidding, A.G.Schwartz, J.Chen, Y.Xia. *ACS Nano*, **4**, 35 (2010); https://doi.org/10.1021/nn901392m
58. J.Zeng, Y.Xuan. *Appl. Energy*, **212**, 809 (2018); https://doi.org/10.1016/j.apenergy.2017.12.083
59. W.Liu, Y.Yu, W.Cheng, X.Wang, M.Zhou, B.Xu, P.Wang, Q.Wang. *Adv. Healthcare Mater.*, **12**, 2203303 (2023); https://doi.org/10.1002/adhm.202203303
60. C.-W.Hsiao, E.-Y.Chuang, H.-L.Chen, D.Wan, C.Korupalli, Z.-X.Liao, Y.-L.Chiu, W.-T.Chia, K.-J.Lin, H.-W.Sung. *Biomaterials*, **56**, 26 (2015); https://doi.org/10.1016/j.biomaterials.2015.03.060
61. Y.Wang, K.Wang, J.Zhao, X.Liu, J.Bu, X.Yan, R.Huang. *J. Am. Chem. Soc.*, **135**, 4799 (2013); https://doi.org/10.1021/ja312221g
62. S.Zhou, X.Jiao, Y.Jiang, Y.Zhao, P.Xue, Y.Liu, J.Liu. *Appl. Surf. Sci.*, **552**, 149498 (2021); https://doi.org/10.1016/j.apsusc.2021.149498
63. B.Li, L.Sun, T.Li, Y.Zhang, X.Niu, M.Xie, Z.You. *J. Mater. Chem. B*, **9**, 1138 (2021); https://doi.org/10.1039/d0tb02410d
64. J.Chen, R.Zhang, C.Tao, X.Huang, Z.Chen, X.Li, J.Zhou, Q.Zeng, B.Zhao, M.Yuan, M.Ma, Z.Wu. *Nanotoxicology*, **14**, 774 (2020); https:/doi.org//10.1080/17435390.2020.1759727
65. S.Weng, L.Pan, D.Jiang, W.Xie, Z.Zhang, C.Shi, B.Liang, S.Wu. *Mater. Des.*, **230**, 112008 (2023); https://doi.org/10.1016/j.matdes.2023.112008
66. K.Hayashi, M.Nakamura, H.Miki, S.Ozaki, M.Abe, T.Matsumoto, T.Kori, K.Ishimura. *Adv. Funct. Mater.*, **24**, 503 (2014); https://doi.org/10.1002/adfm.201301771
67. T.Oka, H.Mizuno, M.Sakata, H.Fujita, T.Yoshino, Y.Yamano, K.Utsumi, T.Masujima, A.Utsunomiya. *Sci. Rep.*, **8**, 14979 (2018); https://doi.org/10.1038/s41598-018-33175-7
68. H.Zhu, P.Cheng, P.Chen, K.Pu. *Biomater. Sci.*, **6**, 746 (2018); https://doi.org/10.1039/c7bm01210a
69. B.Yang, Z.Dai, G.Zhang, Z.Hu, X.Yao, S.Wang, Q.Liu, X.Zheng. *Adv. Healthcare Mater.*, **9**, 1901634 (2020); https://doi.org/10.1002/adhm.201901634
70. J.Lin, S.Wang, P.Huang, Z.Wang, S.Chen, G.Niu, W.Li, J.He, D.Cui, G.Lu, X.Chen, Z.Nie. *ACS Nano*, **7**, 5320 (2013); https://doi.org/10.1021/nn4011686
71. L.Zhang, H.Forgham, X.Huang, A.Shen, T.Davis, R.Qiao, B.Guo. *Mater. Today Adv.*, **14**, 100226 (2022); https://doi.org/10.1016/j.mtadv.2022.100226
72. W.W.Tong, G.H.Tong, Y.Liu. *Int. J. Oncol.*, **53**, 469 (2018); https://doi.org/10.3892/ijo.2018.4417

73. A.C.Midgley, Y.Wei, Z.Li, D.Kong, Q.Zhao. *Adv. Mater.*, **32**, e1805818 (2020); https://doi.org/10.1002/adma.201805818
74. B.Thienpont, J.Steinbacher, H.Zhao, F.D'Anna, A.Kuchnio, A.Ploumakis, B.Ghesquiere, L.Van Dyck, B.Boeckx, L.Schoonjans, E.Hermans, F.Amant, V.N.Kristensen, K.Peng Koh, M.Mazzone, M.Coleman, T.Carell, P.Carmeliet, D.Lambrechts. *Nature*, **537**, 63 (2016); https://doi.org/10.1038/nature19081
75. Z.Zhou, J.Song, L.Nie, X.Chen. *Chem. Soc. Rev.*, **45**, 6597 (2016); https://doi.org/10.1039/c6cs00271d
76. A.J.Dixon, S.J.Anderson, M.P.Dixon, J.B.Dixon. *J. Plast. Reconstr. Aesthet. Surg.*, **68**, e28 (2015); https://doi.org/10.1016/j.bjps.2013.02.002
77. A.P.Alivisatos. *Science*, **271**, 933 (1996); https:/doi.org//10.1126/science.271.5251.933
78. R.D.Harris, S.Bettis Homan, M.Kodaimati, C.He, A.B.Nepomnyashchii, N.K.Swenson, S.Lian, R.Calzada, E.A.Weiss. *Chem. Rev.*, **116**, 12865 (2016); https://doi.org/10.1021/acs.chemrev.6b00102
79. R.Rossetti, S.Nakahara, L.E.Brus. *J. Chem. Phys.*, **79**, 1086 (1983); https://doi.org/10.1063/1.445834
80. C.B.Murray, D.J.Norris, M.G.Bawendi. *J. Am. Chem. Soc.*, **115**, 8706 (2002); https://doi.org/10.1021/ja00072a025
81. X.Gao, Y.Cui, R.M.Levenson, L.W.K.Chung, S.Nie. *Nat. Biotechnol.*, **22**, 969 (2004); https://doi.org/10.1038/nbt994
82. D.D.Sarma, P.V.Kamat. *ACS Energy Lett.*, **8**, 5149 (2023); https://doi.org/10.1021/acsenergylett.3c02390
83. L.M.Liz-Marzan, N.Artzi, S.Bals, J.M.Buriak, W.C.W.Chan, X.Chen, M.C.Hersam, I.D.Kim, J.E.Millstone, P.Mulvaney, W.J.Parak, A.Rogach, R.E.Schaak. *ACS Nano*, **17**, 19474 (2023); https://doi.org/10.1021/acsnano.3c09671
84. S.Kargozar, S.J.Hoseini, P.B.Milan, S.Hooshmand, H.W.Kim, M.Mozafari. *Biotechnol. J.*, **15**, 2000117 (2020); https://doi.org/10.1002/biot.202000117
85. A.A.Rempel, O.V.Ovchinnikov, I.A.Weinstein, S.V.Rempel, Y.V.Kuznetsova, A.V.Naumov, M.S.Smirnov, I.Y.Eremchev, A.S.Vokhmintsev, S.S.Savchenko. *Russ. Chem. Rev.*, **93** (4), RCR5114 (2024); https://doi.org/10.59761/RCR5114
86. S.-Y.Li, L.He. *Front. Phys.*, **17**, 33201 (2021); https://doi.org/10.1007/s11467-021-1125-2
87. F.Ahmed, C.Awada, S.A.Ansari, A.Aljaafari, A.Alshoaibi. *R. Soc. Open Sci.*, **6**, 191444 (2019); https://doi.org/10.1098/rsos.191444
88. K.Hagiwara, S.Horikoshi, N.Serpone. *Chem. – Eur. J.*, **27**, 9466 (2021); https://doi.org/10.1002/chem.202100823
89. P.S.Samokhvalov, P.A.Linkov, M.AZvaigzne, A.V.Kosmynceva, I.O.Petrova, V.A.Krivenkov, A.V.Sukhanova, I.R.Nabiev. *KnE Energy*, **3**, 449 (2018); https://doi.org/10.18502/ken.v3i2.1850
90. V.Pilla, S.R.de Lima, A.A.Andrade, A.C.A.Silva, N.O.Dantas. *Chem. Phys. Lett.*, **580**, 130 (2013); https://doi.org/10.1016/j.cplett.2013.07.007
91. J.Song, Y.Zhang, Y.Dai, J.Hu, L.Zhu, X.Xu, Y.Yu, H.Li, B.Yao, H.Zhou. *ACS Appl. Mater. Interfaces*, **11**, 9884 (2019); https://doi.org/10.1021/acsami.9b00121
92. V.Biju, T.Itoh, A.Anas, A.Sujith, M.Ishikawa. *Anal. Bioanal. Chem.*, **391**, 2469 (2008); https://doi.org/10.1007/s00216-008-2185-7
93. F.Ranjbari, F.Fathi. *Anti-Cancer Agents Med. Chem.*, **24**, 733 (2024); https://doi.org/10.2174/0118715206295598240215112910
94. K.J.Noel, M.S.Umashankar, D.Narayanasamy. *Cureus*, **16**, e67869 (2024); https://doi.org/10.7759/cureus.67869
95. L.Liao, J.Qi, J.Gao, X.Qu, Z.Hu, B.Fu, F.Wu. *ACS Appl. Mater. Interfaces*, **16**, 42632 (2024); https://doi.org/10.1021/acsami.4c07741
96. Y.Liu, J.Zhang, Y.Shen, J.Yan, Z.Hou, C.Mao, W.Zhao. *RSC Adv.*, **7**, 54638 (2017); https://doi.org/10.1039/c7ra09300d
97. E.Kontareva, E.Pershikova, A.Sizikov, A.Mutali, M.Pustovalova, S.Leonov, Y.Merkher. *J. Photochem. Photobiol., A*, **465,** 116359 (2025); https://doi.org/10.1016/j.jphotochem.2025.116359
98. A.Alsuraifi, M.M.Mouzan, A.Algzaare, Z.Aqeel, U.I.Al-Essa, N.A.R.Mohammed, A.Ayad. *J. Fluoresc.*, **11**, 625 (2025); https://doi.org/10.1007/s10895-025-04452-2
99. C.J.Lightdale, S.K.Heier, N.E.Marcon, J.S.McCaughan, H.Gerdes, B.F.Overholt, M.V.Sivak, G.V.Stiegmann, H.R.Nava. *Gastrointest. Endosc.*, **42**, 507 (1995); https://doi.org/10.1016/s0016-5107(95)70002-1
100. P.R.Jethwa, J.C.Barrese, A.Gowda, A.Shetty, S.F.Danish. *Oper. Neurosurg.*, **71**, ons133 (2012); https://doi.org/10.1227/NEU.0b013e31826101d4
101. C.Tian, X.Chen, J.Cao, L.Yang. *Oncol. Lett.*, **15**, 5760 (2018); https://doi.org/10.3892/ol.2018.8056
102. H.Cai, Y.-x.Wang, J.-C.Zheng, P.Sun, Z.-y.Yang, Y.-l.Li, X.-y.Liu, Q.Li, W.Liu. *Lasers Med. Sci.*, **30**, 1505 (2015); https://doi.org/10.1007/s10103-015-1754-1
103. X.Hu, Y.He, L Lin, X.Li, X.Luo, L.Wang, C.Xu. *Photodiagn. Photodyn. Ther.*, **41**, 103259 (2023); https:/doi.org/10.1016/j.pdpdt.2022.103259
104. Q.Zhang, Y.Jiang, K.Chen, X.Fu, M.Wang, N.Zhang. *Photodiagn. Photodyn. Ther.*, **45**, 103982 (2024); https://doi.org/10.1016/j.pdpdt.2024.103982
105. X.Wu, S.Xie, H.Zhang, Q.Zhang, B.F.Sels, Y.Wang. *Adv. Mater.*, **33**, 2007129 (2021); https://doi.org/10.1002/adma.202007129
106. X.Wan, M.Liu, M.Ma, D.Chen, N.Wu, L.Li, Z.Li, G.Lin, X.Wang, G.Xu. *Front. Pharmacol.*, **10**, 141 (2019); https://doi.org/10.3389/fphar.2019.00141
107. J.Fu, Q.Xu, J.Low, C.Jiang, J.Yu. *Appl. Catal. B*, **243**, 556 (2019); https://doi.org/10.1016/j.apcatb.2018.11.011
108. B.Zhu, C.Jiang, J.Xu, Z.Zhang, J.Fu, J.Yu. *Mater. Today*, **82**, 251 (2025); https://doi.org/10.1016/j.mattod.2024.11.012
109. F.Xu, Y.He, J.Zhang, G.Liang, C.Liu, J.Yu. *Angew. Chem., Int. Ed.*, **64**, e202414672 (2025); https://doi.org/10.1002/anie.202414672
110. M.Gu, J.Zhang, I.V.Kurganskii, A.S.Poryvaev, M.V.Fedin, B.Cheng, J.Yu, L.Zhang. *Adv. Mater.*, **37**, 2414803 (2024); https://doi.org/10.1002/adma.202414803
111. Z.Meng, J.Zhang, H.Long, H.García, L.Zhang, B Zhu, J.Yu. *Angew. Chem., Int. Ed.*, **64**, e202505456 (2025); https://doi.org/10.1002/anie.202505456
112. S.Wang, B.Cheng, K.Qi. *Chin. J. Catal.*, **78**, 1 (2025); https://doi.org/10.1016/s1872-2067(25)64810-8
113. K.Qi, Z.Wei, H.Wang, H.Liang, D.Ma, J.-W.Shi, Y.Li, X.Xiang, Y.Chen, B.Yu, C.Wang, Z.Xing, C.Imparato, A.Bifulco, D.A.Lukyanov, E.V.Alekseeva, O.V.Levin, M.I.Chebanenko, V.I.Popkov, T.Zhang, J.Li, G.Liu, W.Li, L.Song, R.Ren, Z.Wang, J.Ma. *Chin. Chem. Lett.*, **37**, 111661 (2026); https:/doi.org//10.1016/j.cclet.2025.111661
114. X.Yao, R.Zhang, M.Zhu, D.Zhang, X.Pu, J.Liu, H.Li, P.Cai. *Appl. Surf. Sci.*, **645**, 158890 (2024); https://doi.org/10.1016/j.apsusc.2023.158890
115. H.Jiang, J.Sun, F.Liu, Y.Zhao, X.Chen, C.Dai, Z.Wen. *J. Nanobiotechnol.*, **22**, 123 (2024); https://doi.org/10.1186/s12951-024-02391-x
116. A.J.Houtepen, E.H.Sargent, I.Infante, J.S.Owen, P.B.Green, R.D.Schaller, S.Bals, S Zeiske, T.Stöferle, Z Hens. *Nat. Rev. Methods Primers*, **5**, 42 (2025); https://doi.org/10.1038/s43586-025-00413-y
117. V.K.LaMer, R.H.Dinegar. *J. Am. Chem. Soc.*, **72**, 4847 (1950); https:/doi.org/10.1021/ja01167a001
118. E.J.Luber, M.H.Mobarok, J.M.Buriak. *ACS Nano*, **7**, 8136 (2013); https://doi.org/10.1021/nn4034234
119. W.Ostwald. *Z. Phys. Chem.*, **22**, 289 (1897); https://doi.org/10.1515/zpch-1897-2233
120. P.Reiss, M.Carrière, C.Lincheneau, L.Vaure, S.Tamang. *Chem. Rev.*, **116**, 10731 (2016); https://doi.org/10.1021/acs.chemrev.6b00116
121. D.C.Onwudiwe, C.A.Strydom. *Spectrochim. Acta Part A: Mol. Biomol. Spectrosc.*, **135**, 1080 (2015); https://doi.org/10.1016/j.saa.2014.08.004
122. N.Pradhan, B.Katz, S.Efrima. *J. Phys. Chem. B*, **107**, 13843 (2003); https://doi.org/10.1021/jp0357951

123. S.Shen, Y.Zhang, L.Peng, B.Xu, Y.Du, M.Deng, H.Xu, Q.Wang. *CrystEngComm*, **13**, 4572 (2011); https://doi.org/10.1039/c0ce00982b
124. P.Jiang, Z.Chen. *New J. Chem.*, **41**, 5707 (2017); https://doi.org/10.1039/c7nj01049d
125. J.Zhu, X.Yan, J.Cheng. *Nanoscale Res. Lett.*, **13**, 19 (2018); https://doi.org/10.1186/s11671-017-2421-1
126. A.Malankowska, D.Kulesza, J.Sowik, O.Cavdar, T.Klimczuk, G.Trykowski, A.Zaleska-Medynska. *Catalysts*, **10**, 403 (2020); https://doi.org/10.3390/catal10040403
127. Y.Wang, Y.Hu, Q.Zhang, J.Ge, Z.Lu, Y.Hou, Y.Yin. *Inorg. Chem.*, **49**, 6601 (2010); https://doi.org/10.1021/ic100473e
128. Q.Lu, J.Hu, K.Tang, Y.Qian, G.Zhou, X.Liu. *Inorg. Chem.*, **39**, 1606 (2000); https://doi.org/10.1021/ic9911365
129. X.Wang, X.Liu, D.Yin, Y.Ke, M.T.Swihart. *Chem. Mater.*, **27**, 3378 (2015); https://doi.org/10.1021/acs.chemmater.5b00618
130. C.Yan, E.Gu, F.Liu, Y.Lai, J.Li, Y.Liu. *Nanoscale*, **5**, 1789 (2013); https://doi.org/10.1039/c3nr33268c
131. Z.Luo, H.Zhang, J.Huang, X.Zhong. *J. Colloid Interface Sci.*, **377**, 27 (2012); https://doi.org/10.1016/j.jcis.2012.03.074
132. X.L.Han, Q.Li, H.Hao, C.Liu, R.Li, F.Yu, J.Lei, Q.Jiang, Y.Liu, J.Hu. *RSC Adv.*, **10**, 9172 (2020); https://doi.org/10.1039/c9ra09840b
133. S.Peng, S.Zhang, S.G.haisalkar, S.Ramakrishna. *Phys. Chem. Chem. Phys.*, **14**, 8523 (2012); https://doi.org/10.1039/c2cp40848a
134. S.Peng, L.Li, Y.Wu, L.Jia, L.Tian, M.Srinivasan, S.Ramakrishna, Q.Yan, S.G.Mhaisalkar. *CrystEngComm*, **15**, 1922 (2013); https://doi.org/10.1039/c2ce26593a
135. X.Zhang, G.Guo, C.Ji, K.Huang, C.Zha, Y.Wang, L.Shen, A.Gupta, N.Bao. *Sci. Rep.*, **4**, 5086 (2014); https:/ doi.org/10.1038/srep05086
136. A.Dalui, A.H.Khan, B.Pradhan, J.Pradhan, B.Satpati, S.Acharya. *RSC Adv.*, **5**, 97485 (2015); https://doi.org/10.1039/c5ra18157g
137. C.Yan, C.Huang, J.Yang, F.Liu, J.Liu, Y.Lai, J.Li, Y.Liu. *Chem. Commun.*, **48**, 2603 (2012); https://doi.org/10.1039/c2cc16972j
138. M.Chylii, L.Loghina, A.Kaderavkova, S.lang, P.Svec, J.Rodriguez Pereira, B.Frumarova, D.Cizkova, A.Bezrouk, M.Vlcek. *Mater. Chem. Phys.*, **284**, 126060 (2022); https://doi.org/10.1016/j.matchemphys.2022.126060
139. R.Zeng, T.Zhang, G.Dai, B.Zou. *J. Phys. Chem. C*, **115**, 3005 (2011); https://doi.org/10.1021/jp111288h
140. R.Zeng, R.Shen, Y.Zhao, Z.Sun, X.Li, J.Zheng, S.Cao, B.Zou. *CrystEngComm*, **16**, 3414 (2014); https://doi.org/10.1039/c3ce42273a
141. Y.Vahidshad, R.Ghasemzadeh, A.Irajizad, S.M.Mirkazemi. *J. Nanostruct.*, **3**, 145 (2013); https://doi.org/10.7508/jns.2013.02.003
142. C.Deng, B.Fu, Y.Wang, L.Yang. *Nano*, **13**, 1850114 (2018); https://doi.org/10.1142/s179329201850114x
143. L.Liu, H.Li, Z.Liu, Y.-H.Xie. *Mater. Design*, **149**, 145 (2018); https://doi.org/10.1016/j.matdes.2018.04.015
144. T.Koyanagi, G.Kapil, Y.Ogomi, K.Yoshino, Q.Shen, T.Toyoda, T.N.Murakami, H.Segawa, S.Hayase. *J. Nanopart. Res.*, **22**, 69 (2020); https://doi.org/10.1007/s11051-020-04787-w
145. A.Wang, X.Yan, MZhang, S.Sun, M.Yang, W.Shen, X.Pan, P.Wang, Z.Deng. *Chem. Mater.*, **28**, 8132 (2016); https://doi.org/10.1021/acs.chemmater.6b01329
146. Z.M.Hu, G.T.Fei, L.D.Zhang. *J. Lumin.*, **208**, 18 (2019); https://doi.org/10.1016/j.jlumin.2018.12.023
147. T.Omata, H.Asano, S.Tsukuda, M.Kita. *J. Lumin.*, **232,** 117876 (2021); https://doi.org/10.1016/j.jlumin.2020.117876
148. A.Sánchez-Solís, D.Esparza, A.Orona-Navar, A.Torres-Castro, J.M.Rivas, N.Ornelas-Soto, T.López-Luke. *J. Lumin.*, **235**, 118025 (2021); https://doi.org/10.1016/j.jlumin.2021.118025
149. R.Kottayi, V.Murugadoss, P.Panneerselvam, R.Sittaramane, S.Angaiah. *Int. J. Energy Res.*, **45**, 13563 (2021); https://doi.org/10.1002/er.6685
150. S.-K.Ming, R.A.Taylor, P.D.McNaughter, D.J.Lewis, P.O'Brien. *New J. Chem.*, **46**, 18899 (2022); https://doi.org/10.1039/d2nj03169h
151. R.Kottayi, V.Ilangovan, R.Sittaramane. *Optik*, **255**, 168692 (2022); https://doi.org/10.1016/j.ijleo.2022.168692
152. V.A.Öberg, X.Zhang, M.B.Johansson, E.M.J.Johansson. *ChemNanoMat*, **4**, 1223 (2018); https://doi.org/10.1002/cnma.201800263
153. M.Srivastava, P.Tiwari, V.K.Mall, S.K.Srivastava, R.Prakash. *Mikrochim. Acta*, **186**, 415 (2019); https://doi.org/10.1007/s00604-019-3525-3
154. X.Li, X.Lv, N.Li, J.Wu, Y.-Z.Zheng, X.Tao. *Appl. Catal. B*, **243**, 76 (2019); https://doi.org/10.1016/j.apcatb.2018.10.033
155. J.Joo, H.B.Na, T.Yu, J.H.Yu, Y.W.Kim, F.Wu, J.Z.Zhang, T.Hyeon. *J. Am. Chem. Soc.*, **125**, 11100 (2003); https://10.1021/ja0357902
156. H.S.Choi, W.Liu, P.Misra, E.Tanaka, J.P.Zimmer, B.Itty Ipe, M.G.Bawendi, J.V.Frangioni. *Nat. Biotechnol.*, **25**, 1165 (2007); https://doi.org/10.1038/nbt1340
157. M.Lotfipour, T.Machani, D.P.Rossi, K.E.Plass. *Chem. Mater.*, **23**, 3032 (2011); https://10.1021/cm1031656
158. Z.Zhuang, X.Lu, Q.Peng, Y.Li. *Chemistry*, **17**, 10445 (2011); https://doi.org/10.1002/chem.201101145
159. A.Tang, Y.Wang, H.Ye, C.Zhou, C.Yang, X.Li, H.Peng, F.Zhang, Y.Hou, F.Teng. *Nanotechnology*, **24**, 355602 (2013); https://doi.org/10.1088/0957-4484/24/35/355602
160. M.B.Sigman, B.A.Korgel. *Chem. Mater.*, **17**, 1655 (2005); https://doi.org/10.1021/cm0478733
161. Y.-J.Yuan, D.-Q.Chen, X.-F.Shi, J.-R.Tu, B.Hu, L.-X.Yang, Z.-T.Yu, Z.-G.Zou. *Chem. Eng. J.*, **313**, 1438 (2017); https://doi.org/10.1016/j.cej.2016.11.049
162. T.Mirkovic, M.A.Hines, P.S.Nair, G.D.Scholes. *Chem. Mater.*, **17**, 3451 (2005); https://10.1021/cm048064m
163. K.Luo, H.Chen, Q.Zhou, Z.Yan, Z.Su, K.Li. *Spectrochim. Acta Part A: Mol. Biomol. Spectrosc.*, **240**, 118563 (2020); https://doi.org/10.1016/j.saa.2020.118563
164. W.Gu, Y.Yan, C.Zhang, C.Ding, Y.Xian. *ACS Appl. Mater. Interfaces*, **8**, 11272 (2016); https://doi.org/10.1021/acsami.6b01166
165. X.Wang, Q.Wu, K.Jiang, C.Wang, C.Zhang. *Sens. Actuators, B*, **252**, 183 (2017); https://doi.org/10.1016/j.snb.2017.05.177
166. H.Huang, C.Du, H.Shi, X.Feng, J.Li, Y.Tan, W.Song. *Part. A: Syst. Charact.*, **32**, 72 (2014); https://doi.org/10.1002/ppsc.201400101
167. M.L.Desai, S.Jha, H.Basu, S.Saha, R.K.Singhal, S.K.Kailasa. *Mater. Sci. Eng., C*, **111**, 110778 (2020); https://doi.org/10.1016/j.msec.2020.110778
168. S.Liu, H.Zhang, Y.Qiao, X.Su. *RSC Adv.*, **2**, 819 (2012); https://doi.org/10.1039/c1ra00802a
169. Y.Jia, H.Wang, Z.Yan, L.Deng, H.Dong, N.Ma, D.Sun. *RSC Adv.*, **6**, 93303 (2016); https://doi.org/10.1039/c6ra14733j
170. J.Chang, E.R.Waclawik. *CrystEngComm*, **15**, 5612 (2013); https://doi.org/10.1039/c3ce40284c
171. S.Sugan, R.Dhanasekaran. *IOP Conf. Ser.: Mater. Sci. Eng.*, **73**, 012147 (2015); https://doi.org/10.1088/1757-899x/73/1/012147
172. Y.Vahidshad, M.N.Tahir, A.I.zad, S.M.Mirkazemi, R.Ghazemzadeh, W.Tremel. *J. Mater. Chem. C*, **3**, 889 (2015); https://doi.org/10.1039/c4tc02516d
173. C.M.Fan, M.D.Regulacio, C.Ye, S.H.Lim, Y.Zheng, Q.H.Xu, A.W.Xu, M.Y.Han. *Chem. Commun.*, **50**, 7128 (2014); https://doi.org/10.1039/c4cc01778a
174. B.Zhou, M.Li, Y.Wu, C.Yang, W.H.Zhang, C.Li. *Chemistry*, **21**, 11143 (2015); https://doi.org/10.1002/chem.201501000
175. H.Jiang, P.Dai, Z.Feng, W.Fan, J.Zhan. *J. Mater. Chem.*, **22**, 7502 (2012); https://doi.org/10.1039/c2jm16870g
176. L.Peng, D.Li, Z.Zhang, K.Huang, Y.Zhang, Z.Shi, R.Xie, W.Yang. *Nano Res.*, **8**, 3316 (2015); https://doi.org/10.1007/s12274-015-0832-9
177. P.Ilaiyaraja, P.S.Mocherla, T.K.Srinivasan, C.Sudakar. *ACS Appl. Mater. Interfaces*, **8**, 12456 (2016); https://doi.org/10.1021/acsami.6b02175
178. L.Tan, Y.Liu, B.Mao, B.Luo, G.Gong, Y.Hong, B.Chen, W.Shi. *Inorg. Chem. Front.*, **5**, 258 (2018); https://doi.org/10.1039/c7qi00607a

179. X.Han, F.Yu, J.Lei, J.Zhu, H.Fu, J.Hu, X.L.Yang. *Front. Chem.*, **10**, 821392 (2022); https://doi.org/10.3389/fchem.2022.821392
180. Y.Jia, H.Wang, L.Xiang, X.Liu, W.Wei, N.Ma, D.Sun. *J. Mater. Sci. Technol.*, **34**, 942 (2018); https://doi.org/10.1016/j.jmst.2017.07.014
181. S.Das, P.Mahanandia. *Mater. Chem. Phys.*, **281**, 125878 (2022); https://doi.org/10.1016/j.matchemphys.2022.125878
182. Y.Nicolau. *Appl. Surf. Sci.*, **22-23**, 1061 (1985); https://doi.org/10.1016/0378-5963(85)90241-7
183. P.Kumar, H.-Y.Peng, Y.-H.Yang, U.Kumar, Z.-Y.Deng, K.-L.Chen, M.-W.Lee, C.-H.Wu. *J. Alloys Compd.*, **967**, 171688 (2023); https://doi.org/10.1016/j.jallcom.2023.171688
184. Y.Suchikova, S.Kovachov, I.Bohdanov, E.Popova, A.Moskina, A.Popov. *Coatings*, **13**, 639 (2023); https://doi.org/10.3390/coatings13030639
185. A.Bora, L.P.L.Mawlong, R.Das, P.K.Giri. *J. Colloid Interface Sci.*, **561**, 519 (2020); https://doi.org/10.1016/j.jcis.2019.11.027
186. L.-H.Cheng, U.Kumar, Z.-Y.Deng, C.-H.Wu. *ACS Appl. Nano Mater.*, **6**, 9506 (2023); https://doi.org/10.1021/acsanm.3c01181
187. X.Fu, P.Ilanchezhiyan, G.Mohan Kumar, H.D.Cho, L.Zhang, A.S.Chan, D.J.Lee, G.N.Panin, T.W.Kang. *Nanoscale*, **9**, 1820 (2017); https://doi.org/10.1039/c6nr09022b
188. T.Chen, Y.Xu, L.Wang, W.Jiang, W.Jiang, Z.Xie. *Chemistry*, **24**, 16407 (2018); https://doi.org/10.1002/chem.201803548
189. X.Tan, X.Pang, M.Lei, M.Ma, F.Guo, J.Wang, M.Yu, F.Tan, N.Li. *Int. J. Pharm.*, **503**, 220 (2016); https://doi.org/10.1016/j.ijpharm.2016.03.019
190. R.Zhong, C.Peng, L.Chen, N.Yu, Z.Liu, M.Zhu, C.He, Z.Chen. *RSC Adv.*, **6**, 40480 (2016); https://doi.org/10.1039/c5ra26801j
191. Y.Zhao, M.Song, X.Yang, J.Yang, C.Du, G.Wang, J.Yi, G.Shan, D.Li, L.Liu, D.Yan, Y.Li, X.Liu. *Chem. Eng. J.*, **399**, 125777 (2020); https://doi.org/10.1016/j.cej.2020.125777
192. Y.Zhang, B.Jiang, C.Guo, L.Liu, J.Xu, Y.Wang, C.Shen, J.Zhu, G.Shen, H.Jiang, J.Zhu, J.Tao. *Biomater. Sci.*, **9**, 4086 (2021); https://doi.org/10.1039/d1bm00373a
193. Q.Zhu, J.Nie, Y.Li, L.Ni, X.Kong, H.Zhou, J.Wu. *J. Mater. Chem. B*, **13**, 10836 (2025); https://doi.org/10.1039/d5tb01249j
194. C.Lu, G.Chen, B.Yu, H.Cong. *Adv. Eng. Mater.*, **20**, 1700940 (2018); https://doi.org/10.1002/adem.201700940
195. J.Gao, C.Wu, D.Deng, P.Wu, C.Cai. *Adv. Healthcare Mater.*, **5**, 2437 (2016); https://doi.org/10.1002/adhm.201600545
196. D.H.Zhao, J.Yang, R.X.Xia, M.H.Yao, R.M.Jin, Y.D.Zhao, B.Liu. *Chem. Commun.*, **54**, 527 (2018); https://doi.org/10.1039/c7cc09266k
197. D.H.Zhao, X.Q.Yang, X.L.Hou, Y.Xuan, X.L.Song, Y.D.Zhao, W.Chen, Q.Wang, B.Liu. *J. Mater. Chem. B*, **7**, 2484 (2019); https://doi.org/10.1039/c8tb03043j
198. M.Gao, H.Zhao, Z.Wang, Y.Zhao, X.Zou, L.Sun. *Adv. Powder Technol.*, **32**, 1972 (2021); https://10.1016/j.apt.2021.04.011
199. M.Hashemkhani, G.Demirci, A.Bayir, A.Muti, A.Sennaroglu, L.Mohammad Hadi, E.Yaghini, M.Loizidou, A.J.MacRobert, H.Yagci Acar. *Nanoscale*, **13**, 14879 (2021); https://doi.org/10.1039/d1nr03507j
200. M.S.Kim, I.H.Nam, H.J.Cha, Y.K.Jo. *J. Nanobiotechnol.*, **23**, 541 (2025); https://doi.org/10.1186/s12951-025-03619-0
201. H.Fang, X.Sun, D.Su, L.Tang, J.Gong, H.Xin. *Chin. Chem. Lett.*, 112212 (2025); https://doi.org/10.1016/j.cclet.2025.112212
202. H.Dong, S.Tang, Y.Hao, H.Yu, W.Dai, G.Zhao, Y.Cao, H.Lu, X.Zhang, H.Ju. *ACS Appl. Mater. Interfaces*, **8**, 3107 (2016); https://doi.org/10.1021/acsami.5b10459
203. J.Wang, X.Tan, X.Pang, L.Liu, F.Tan, N.Li. *ACS Appl. Mater. Interfaces*, **8**, 24331 (2016); https://doi.org/10.1021/acsami.6b08391
204. L.Liu, J.Wang, X.Tan, X.Pang, Q.You, Q.Sun, F.Tan, N.Li. *J. Mater. Chem. B*, **5**, 2286 (2017); https://doi.org/10.1039/c6tb03352k
205. P.Li, L.Liu, Q.Lu, S.Yang, L.Yang, Y.Cheng, Y.Wang, S.Wang, Y.Song, F.Tan, N.Li. *ACS Appl. Mater. Interfaces*, **11**, 5771 (2019); https://doi.org/10.1021/acsami.8b18924
206. N.Irmania, K.Dehvari, J.Y.Chang. *J. Biomater. Appl.*, **36**, 1617 (2022); https://doi.org/10.1177/08853282211068959
207. Y.J.Choi, Y.J.Kim, J.W.Lee, Y.Lee, Y.-b.Lim, H.W.Chung. *J. Nanosci. Nanotechnol.*, **12**, 2160 (2012); https://doi.org/10.1166/jnn.2012.5781
208. N.B.Mohsenian, A.Shanei, S.J.Alavi, M.Kheirollahi, A.H.Nia, M.B.Tavakoli. *IET Nanobiotechnol.*, **13**, 387 (2019); https://doi.org/10.1049/iet-nbt.2018.5387
209. A.A.Matiushkina, A.S.Bazhenova, I.K.Litvinov, T.N.Belyaeva, E.S.Kornilova, A.Y.Dubavik, A.O.Orlova. *J. Phys.: Conf. Ser.*, **1866**, 012003 (2021); https://doi.org/10.1088/1742-6596/1866/1/012003
210. F.A.Sewid, K.I.Annas, A.Dubavik, A.V.Veniaminov, V.G.Maslov, A.O.Orlova. *RSC Adv.*, **12**, 899 (2022); https://doi.org/10.1039/d1ra08148a
211. J.Zhang, A.Bifulco, P.Amato, C.Imparato, K.Qi. *J. Colloid Interface Sci.*, **638**, 193 (2023); https://doi.org/10.1016/j.jcis.2023.01.107
212. J.Zhang, Y.Zhao, K.Qi, S.-y.Liu. *J. Mater. Sci. Technol.*, **172**, 145 (2024); https://doi.org/10.1016/j.jmst.2023.06.042
213. G.Lv, W.Guo, W.Zhang, T.Zhang, S.Li, S.Chen, A.S.Eltahan, D.Wang, Y.Wang, J.Zhang, P.C.Wang, J.Chang, X.-J.Liang. *ACS Nano*, **10**, 9637 (2016); https://doi.org/10.1021/acsnano.6b05419
214. Y.Mao, S.Yu, Y.Kang, D.Zhang, S.Wu, J.Zhang, Y.Xiong, M.Li, J.Zhang, J.Wang, K.Wang, X.Wan. *Exp. Eye Res.*, **202**, 108282 (2021); https://doi.org/10.1016/j.exer.2020.108282
215. Y.Feng, L.Liu, S.Hu, Y.Liu, Y.Ren, X.Zhang. *RSC Adv.*, **6**, 55568 (2016); https://doi.org/10.1039/c6ra06937a
216. N.Tsolekile, V.Ncapayi, S.Parani, E.H.M.Sakho, M.C.Matoetoe, S.P.Songca, O.S.Oluwafemi. *MRS Commun.*, **8**, 398 (2018); https://doi.org/10.1557/mrc.2018.60
217. F.Yang, B.Yang, X.Gu, M.Li, K.Qi, Y.Yan. *Spectrochim. Acta Part A: Mol. Biomol. Spectrosc.*, **301**, 122985 (2023); https://doi.org/10.1016/j.saa.2023.122985
218. M.Hashemkhani, A.Muti, A.Sennaroglu, H.Yagci Acar. *J. Photochem. Photobiol., B*, **213**, 112082 (2020); https://doi.org/10.1016/j.jphotobiol.2020.112082
219. M.Hashemkhani, M.Loizidou, A.J.MacRobert, H.Yagci Acar. *Inorg. Chem.*, **61**, 2846 (2022); https://doi.org/10.1021/acs.inorgchem.1c03298
220. Y.Yong, L.Zhou, Z.Gu, L.Yan, G.Tian, X.Zheng, X.Liu, X.Zhang, J.Shi, W.Cong, W.Yin, Y.Zhao. *Nanoscale*, **6**, 10394 (2014); https://doi.org/10.1039/c4nr02453b
221. C.Zhang, Y.Yong, L.Song, X.Dong, X.Zhang, X.Liu, Z.Gu, Y.Zhao, Z.Hu. *Adv. Healthcare Mater.*, **5**, 2776 (2016); https://doi.org/10.1002/adhm.201600633
222. K.Kumar, B.Maiti, P.Kondaiah, S.Bhattacharya. *Mol. Pharmaceutics*, **12**, 351 (2015); https://doi.org/10.1021/mp500620e
223. B.K.Wang, X.F.Yu, J.H.Wang, Z.B.Li, P.H.Li, H.Wang, L.Song, P.K.Chu, C.Li. *Biomaterials*, **78**, 27 (2016); https://doi.org/10.1016/j.biomaterials.2015.11.025
224. Z.Wu, X.Yuan, H.Wang, Z.Wu, L.Jiang, H.Wang, L.Zhang, Z.Xiao, X.Chen, G.Zeng. *Appl. Catal. B*, **202**, 104 (2017); https://doi.org/10.1016/j.apcatb.2016.08.064
225. M.Que, W.Guo, X.Zhang, X.Li, Q.Hua, L.Dong, C.Pan. *J. Mater. Chem. A*, **2**, 13661 (2014); https://doi.org/10.1039/c4ta02052a
226. X.Chen, Y.Zhuang, Q.Shen, X.Cao, W.Yang, P.Yang. *Sol. Energy*, **226**, 236 (2021); https://doi.org/10.1016/j.solener.2021.08.053
227. J.Yang, Q.Wang, T.Xing, X.Wang, G.Li, Z.Shang, J.Wu, W.Chen, T.Ou. *J. Drug Delivery Sci. Technol.*, **83**, 104441 (2023); https://doi.org/10.1016/j.jddst.2023.104441
228. H.Zhu, S.Huang, M.Ding, Z.Li, J.Li, S.Wang, D.T.Leong. *ACS Appl. Mater. Interfaces*, **14**, 25183 (2022); https://doi.org/10.1021/acsami.2c05170
229. M.Aresti, M.Saba, R.Piras, D.Marongiu, G.Mula, F.Quochi, A.Mura, C.Cannas, M.Mureddu, A.Ardu, G.Ennas, V.Calzia, A.Mattoni, A.Musinu, G.Bongiovanni. *Adv. Funct. Mater.*, **24**, 3341 (2014); https://doi.org/10.1002/adfm.201303879

230. Z.Li, Y.Hu, K.A.Howard, T.Jiang, X.Fan, Z.Miao, Y.Sun, F.Besenbacher, M.Yu. *ACS Nano*, **10**, 984 (2016); https://doi.org/10.1021/acsnano.5b06259
231. Y.Cheng, H.Zhang. *Chemistry*, **24**, 17405 (2018); https://doi.org/10.1002/chem.201801588
232. Y.Yu, C.H.Jin, R.H.Wang, Q.Chen, L.M.Peng. *J. Phys. Chem. B*, **109**, 18772 (2005); https://doi.org/10.1021/jp051294j
233. Z.Xiao, C.Xu, X.Jiang, W.Zhang, Y.Peng, R.Zou, X.Huang, Q.Liu, Z.Qin, J.Hu. *Nano Res.*, **9**, 1934 (2016); https://doi.org/10.1007/s12274-016-1085-y
234. Z.Guo, S.Zhu, Y.Yong, X.Zhang, X.Dong, J.Du, J.Xie, Q.Wang, Z.Gu, Y.Zhao. *Adv. Mater.*, **29**, 1704136 (2017); https://doi.org/10.1002/adma.201704136
235. S.Yang, S.Wang, Y.Zhang, Y.Wang, J.Yuan, Y.Jiang, X.He, L.Liu, J.Song, L.Chen, H.Yang. *Colloids Surf., B*, **222**, 113106 (2023); https://doi.org/10.1016/j.colsurfb.2022.113106
236. H.Yang, Y.Zhang, J.Song, M.Wang, S.Yu, L.Chen, X.Li, S.Yang, L.Yang. *Chem. Eng. J.*, **375**, 121941 (2019); https://doi.org/10.1016/j.cej.2019.121941
237. J.Fu, T.Li, Y.Zhu, Y.Hao. *Adv. Funct. Mater.*, **29**, 1906105 (2019); https://doi.org/10.1002/adfm.201906195
238. X.Qian, Y.Zheng, Y.Chen. *Adv. Mater.*, **28**, 8097 (2016); https://doi.org/10.1002/adma.201602012
239. N.Meng, P.Xu, C.Wen, H.Liu, C.Gao, X.C.Shen, H.Liang. *J. Colloid Interface Sci.*, **644**, 437 (2023); https://doi.org/10.1016/j.jcis.2023.04.108
240. R.Dou, Z.Du, T.Bao, X.Dong, X.Zheng, M.Yu, W.Yin, B.Dong, L.Yan, Z.Gu. *Nanoscale*, **8**, 11531 (2016); https://doi.org/10.1039/c6nr01543c
241. J.Lin, M.Wang, H.Hu, X.Yang, B.Wen, Z.Wang, O.Jacobson, J.Song, G.Zhang, G.Niu, P.Huang, X.Chen. *Adv. Mater.*, **28**, 3273 (2016); https://doi.org/10.1002/adma.201505700
242. Z.Meng, F.Wei, W.Ma, N.Yu, P.Wei, Z.Wang, Y.Tang, Z.Chen, H.Wang, M.Zhu. *Adv. Funct. Mater.*, **26**, 8231 (2016); https://doi.org/10.1002/adfm.201603776
243. W.Yang, C.Xiang, Y.Xu, S.Chen, W.Zeng, K.Liu, X.Jin, X.Zhou, B.Zhang. *Biomaterials*, **255**, 120186 (2020); https://doi.org/10.1016/j.biomaterials.2020.120186
244. W.Yu, N.Yu, Z.Wang, X.Li, C.Song, R.Jiang, P.Geng, M.Li, S.Yin, Z.Chen. *J. Colloid Interface Sci.*, **555**, 480 (2019); https://doi.org/10.1016/j.jcis.2019.08.001
245. J.Liu, E.Cui, Q.Zhang, D.Xie. *J. Alloys Compd.*, **970**, 172489 (2024); https://doi.org/10.1016/j.jallcom.2023.172489
246. L.Zhao, R.Liu, X.Zhao, B.Yang, C.Gao, X.Hao, Y.Wu. *Sci. Total Environ.*, **407**, 5019 (2009); https://doi.org/10.1016/j.scitotenv.2009.05.052
247. E.Celikbas, A.Saymaz, H.Gunduz, I.Koc, E.Cakir, A.Sennaroglu, S.Kolemen, H.Yagci Acar, K.Onbasli. *Bioconjugate Chem.*, **34**, 880 (2023); https://doi.org/10.1021/acs.bioconjchem.3c00096
248. A.Sukhanova, S.Bozrova, E.Gerasimovich, M.Baryshnikova, Z.Sokolova, P.Samokhvalov, C.Guhrenz, N.Gaponik, A.Karaulov, I.Nabiev. *Nanomaterials*, **12**, 2734 (2022); https://doi.org/10.3390/nano12162734
249. A.V.Kabanov, E.V.Batrakova, D.W.Miller. *Adv. Drug Delivery Rev.*, **55**, 151 (2003); https://doi.org/10.1016/s0169-409x(02)00176-x
250. Z.Liu, J.Ding, J.Xue. *New J. Chem.*, **33**, 88 (2009); https://doi.org/10.1039/b810302j
251. R.Y.Zhang, Z.Y.Wang, X.Q.Yang, Y.Xuan, K.Cheng, C.Li, X.L.Song, J.An, X.L.Hou, Y.D.Zhao. *Nanotechnology*, **29**, 055101 (2018); https://doi.org/10.1088/1361-6528/aa9acc
252. D.Kaufmann, A.Fiedler, A.Junger, J.Auernheimer, H.Kessler, R.Weberskirch. *Macromol. Biosci.*, **8**, 577 (2008); https://doi.org/10.1002/mabi.200700234
253. H.Chen, B.Li, M.Zhang, K.Sun, Y.Wang, K.Peng, M.Ao, Y.Guo, Y.Gu. *Nanoscale*, **6**, 12580 (2014); https://doi.org/10.1039/c4nr03613a
254. F.Lu, W.Ju, N.Zhao, T.Zhao, C.Zhan, Q.Wang, Q.Fan, W.Huang. *Biochem. Biophys. Res. Commun.*, **529**, 930 (2020); https://doi.org/10.1016/j.bbrc.2020.06.072
255. S.Chen, M.Ahmadiantehrani, N.G.Publicover, K.W.Hunter, X.Zhu. *RSC Adv.*, **5**, 60612 (2015); https://doi.org/10.1039/c5ra11250h
256. D.Deng, J.Cao, L.Qu, S.Achilefu, Y.Gu. *Phys. Chem. Chem. Phys.*, **15**, 5078 (2013); https://doi.org/10.1039/c3cp00046j
257. X.Wu, M.Liu, X.Wang, J.Niu, T.-L.Zhuang, X.Sun, L.Zhu, Q.Zhang, J.Han, R.Guo. *Chin. Chem. Lett.*, 112198 (2025); https://doi.org/10.1016/j.cclet.2025.112198
258. P.Yudaev, Y.Aleksandrova, E.Chugunova, M.Neganova. *Int. J. Mol. Sci.*, **26**, 10733 (2025); https://doi.org/10.3390/ijms2621107331
259. Y.Xuan, Z.Su, M.Guan, Y.Zhao, W.Zhang, Y.Gao, X.Bian, M.Zhang, D.Zhao, S.Zhang. *ACS Appl. Nano Mater.*, **8**, 3737 (2025); https://doi.org/10.1021/acsanm.4c05965
260. D.Li, Z.Zhang, L.Wang. *Biomed. Pharmacother.*, **179**, 117406 (2024); https://doi.org/10.1016/j.biopha.2024.117406
261. G.Yang, L.Xu, Y.Chao, J.Xu, X.Sun, Y.Wu, R.Peng, Z.Liu. *Nat. Commun.*, **8**, 902 (2017); https://doi.org/10.1038/s41467-017-01050-0
262. X.Tang, L.Tan, K.Shi, J.Peng, Y.Xiao, W.Li, L.Chen, Q.Yang, Z.Qian. *Acta Pharm. Sin. B*, **8**, 587 (2018); https://doi.org/10.1016/j.apsb.2018.05.011
263. C.Mathieu, S.Messaoudi, E.Fattal, J.Vergnaud-Gauduchon. *Cancer Drug Resist.*, **2**, 381 (2019); https://doi.org/10.20517/cdr.2019.26
264. Y.Cao, X.Meng, D.Wang, K.Zhang, W.Dai, H.Dong, X.Zhang. *ACS Appl. Mater. Interfaces*, **10**, 17732 (2018); https://doi.org/10.1021/acsami.8b05050
265. M.Hashemkhani, E.Celikbas, M.Khan, A.Sennaroglu, H.Yagci Acar. *ACS Biomater. Sci. Eng.*, **9**, 4126 (2023); https://doi.org/10.1021/acsbiomaterials.3c00105
266. P.Zhao, Z.Tang, X.Chen, Z.He, X.He, M.Zhang, Y.Liu, D.Ren, K.Zhao, W.Bu. *Mater. Horiz.*, **6**, 369 (2019); https://doi.org/10.1039/c8mh01176a
267. M.He, Z.Cheng, Z.Wang, M.Li, H.Liang, H.Liu, L.Yu, L.Zhao, F.Yu. *Adv. Healthcare Mater.*, **12**, e2300752 (2023); https://doi.org/10.1002/adhm.202300752
268. N.Li, X.Jiang, W.Zhang, W.Xiao, Z.Wu, H.Wang, F.He. *Int. J. Nanomed.*, **18**, 6349 (2023); https://doi.org/10.2147/ijn.S428022
269. Y.Jiang, Y.Lu, L.Lei, S.Zhou, L.Yang, X.Yang, Z.Xu, J.Liu, Y.Liu. *Mater. Sci. Eng., C*, **130**, 112465 (2021); https://doi.org/10.1016/j.msec.2021.112465
270. A.W.Hahn, D.M.Gill, S.K.Pal, N.Agarwal. *Immunotherapy*, **9**, 681 (2017); https://doi.org/10.2217/imt-2017-0024
271. K.Wang, S.Wen, L.He, A.Li, Y.Li, H.Dong, W.Li, T.Ren, D.Shi, Y.Li. *ACS Nano*, **12**, 6398 (2018); https://doi.org/10.1021/acsnano.8b00558
272. A.M.Krieg. *Oncogene*, **27**, 161 (2008); https://doi.org/10.1038/sj.onc.1210911
273. X.Li, C.Shao, Y.Shi, W.Han. *J. Hematol. Oncol.*, **11**, 31 (2018); https://doi.org/10.1186/s13045-018-0578-4
274. J.Yang, W.Guo, R.Huang, J.Bian, S.Zhang, T.Wei, C.He, Z.Hu, J.Li, C.Zhou, M.Lu. *Front. Immunol.*, **14**, 1173487 (2023); https://doi.org/10.3389/fimmu.2023.1173487
275. X.Huang, M.Gao, H.Xing, Z.Du, Z.Wu, J.Liu, T.Li, J.Cao, X.Yang, R.Li, W.Wang, J.Wang, S.Luo. *Small*, **18**, e2202728 (2022); https://doi.org/10.1002/smll.202202728